

Applications of the Global Theoretical Ionospheric Model

Matthew W. Fox

**Boston University
Center for Space Physics
725 Commonwealth Avenue
Boston, MA 02215**

July 1999

Final Report

APPROVED FOR PUBLIC RELEASE; DISTRIBUTION UNLIMITED.

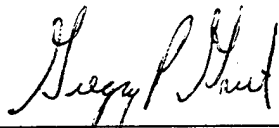


**AIR FORCE RESEARCH LABORATORY
Space Vehicles Directorate
29 Randolph Rd
AIR FORCE MATERIEL COMMAND
Hanscom AFB, MA 01731-3010**

20011120 072

" This technical report has been reviewed and is approved for publication."


KEVIN P. RAY
Contract Monitor


GREGORY P. GINET, Chief
Space Weather Center of Excellence

This report has been reviewed by the ESC Public Affairs Office (PA) and is releasable to the National Technical Information Service (NTIS).

Qualified requestors may obtain additional copies from the Defense Technical Information Center (DTIC). All others should apply to the National Technical Information Service (NTIS).

If your address has changed, if you wish to be removed from the mailing list, or if the addressee is no longer employed by your organization, please notify PL/IM, 29 Randolph Road, Hanscom AFB, MA. 01731-3010. This will assist us in maintaining a current mailing list.

Do not return copies of this report unless contractual obligations or notices on a specific document require that it be returned.

REPORT DOCUMENTATION PAGE				Form Approved OMB No. 0704-0188	
The public reporting burden for this collection of information is estimated to average 1 hour per response, including the time for reviewing instructions, searching existing data sources, gathering and maintaining the data needed, and completing and reviewing the collection of information. Send comments regarding this burden estimate or any other aspect of this collection of information, including suggestions for reducing the burden, to Department of Defense, Washington Headquarters Services, Directorate for Information Operations and Reports (0704-0188), 1215 Jefferson Davis Highway, Suite 1204, Arlington, VA 22202-4302. Respondents should be aware that notwithstanding any other provision of law, no person shall be subject to any penalty for failing to comply with a collection of information if it does not display a currently valid OMB control number.					
1. REPORT DATE (DD-MM-YYYY) July 1999		2. REPORT TYPE Scientific, Final		3. DATES COVERED (From - To) Apr 97-Jul 99	
4. TITLE AND SUBTITLE Applications of the Global Theoretical Ionospheric Model				5a. CONTRACT NUMBER F19628-97-C-0034	
				5b. GRANT NUMBER	
				5c. PROGRAM ELEMENT NUMBER 35160F	
6. AUTHOR(S) Matthew W. Fox				5d. PROJECT NUMBER SMPS	
				5e. TASK NUMBER GL	
				5f. WORK UNIT NUMBER 88	
7. PERFORMING ORGANIZATION NAME(S) AND ADDRESS(ES) Boston University Center for Space Physics 725 Commonwealth Avenue Boston, MA 02215				8. PERFORMING ORGANIZATION REPORT NUMBER	
9. SPONSORING/MONITORING AGENCY NAME(S) AND ADDRESS(ES) Air Force Research Laboratory 29 Randolph Rd Hanscom AFB, MA 01731-3010				10. SPONSOR/MONITOR'S ACRONYM(S)	
				11. SPONSOR/MONITOR'S REPORT NUMBER(S) AFRL-VS-TR-2001-1616	
12. DISTRIBUTION/AVAILABILITY STATEMENT Approved for Public Release; distribution unlimited					
13. SUPPLEMENTARY NOTES					
14. ABSTRACT In this report, we describe a number of ionospheric studies, mostly involving the Air Force Global Theoretical Ionospheric Model. All these studies are ultimately geared towards Air Force objectives of monitoring, understanding, and specifying the ionospheric environment. A new multiple-ion theoretical model has been validated in the topside specification and subsequently utilized to derive ambient space weather conditions using DMSP measurements. In addition, a version of the code has been developed to model geomagnetic disturbances at low latitudes utilizing a new empirical dynamo disturbance drift model. Applications of an empirical profile shape model have been developed to summarize profiles generated by the specification model, PIM; and towards the goal of developing a new slant to vertical TEC conversion. Finally, data analyses have been undertaken to investigate the nature of quiet-time ionospheric variations, using both middle latitude and low latitude information, and using both F region peak and profile summary parameters.					
15. SUBJECT TERMS Theoretical modeling Empirical modeling Ionospheric data analysis					
16. SECURITY CLASSIFICATION OF:			17. LIMITATION OF ABSTRACT UNL	18. NUMBER OF PAGES	19a. NAME OF RESPONSIBLE PERSON Peter Sultan, AFRL/VSBP
a. REPORT UNCL	b. ABSTRACT UNCL	c. THIS PAGE UNCL			19b. TELEPHONE NUMBER (Include area code) (781) 377-1309

TABLE OF CONTENTS

1. INTRODUCTION	1
2. DMSP SATELLITE SIGNATURES	1
2.1 Goals Of The Research	2
2.2 The Approach	2
2.3 SSIES Data	3
2.4 The GTIM	4
3. DMSP DATA/MODEL COMPARISONS	5
3.1 Validation	5
3.2 The Evening Sector	11
3.3 Effects Of Neutral Winds	11
3.4 Effects Of Vertical Drifts	12
3.5 Effects Of Altitude Dependence	18
3.6 Solar Effects	18
4. THE DMSP ALGORITHMS	22
4.1 The Best Density Indicators	23
4.2 Robustness Of The Algorithms	25
4.3 Longitude Dependence	26
4.4 Algorithms And Coefficients	34

4.5 Use Of The Algorithms	38
5. MIDDLE LATITUDE VARIABILITY	40
5.1 Dropouts And Quiet-Time Variations	40
5.2 Modeling Middle Latitude Variability	47
6. LOW LATITUDE VARIABILITY	47
6.1 Dynamo Model Driving	48
6.2 Meridional Neutral Wind Effects	53
7. PROFILE MODEL STUDIES	57
7.1 Parametrizing Model Outputs	58
7.2 Describing Slant TEC	63
TABLE 1	71
TABLE 2	72
TABLE 3	73
APPENDIX A	74

Illustrations

Figure 1. O^+ densities as a function of magnetic latitude as measured on the DMSP satellite F10 during March, June, September and December 1991. The lines are monthly averages and the data have been further averaged by using all observations within 30° of 60°E longitude. The solid line reflects the 2100LT pass, the dotted line, 0900LT.

Figure 2. As in Figure 1, theoretical GTIM O^+ densities for the same four epochs using the monthly averaged solar activity levels.

Figure 3. The upper panel shows daily averaged 2100LT density slices for March 1991 in the 60°E longitude sector. The lower panel shows a range of slices derived from GTIM runs using various vertical drift and neutral wind scalings.

Figure 4. Selected daily average DMSP O^+ densities for March, June, August and December 1991. The thicker solid line in each panel is the monthly average and the thinner lines are selected daily averages that demonstrate a different behavior.

Figure 5. GTIM O^+ densities at selected fieldlines are plotted for a range of wind scaling factors for March 1991 conditions. Different scalings are shown as different symbols and are joined at lower latitudes by different line styles 1.0=plus, solid line, 0.5=asterisk, dotted line, 0.0=diamond, dashed line, and 1.5=triangle, dot-dashed line.

Figure 6. The results of plotting the north/south ratio of wind density as a function of wind scaling for a variety of latitude ranges. Each panel corresponds to a given range of magnetic latitudes that are listed in the subheader.

Figure 7. Examples of the vertical drift scaling effects on density slices for GTIM simulations appropriate to conditions in March 1991 and November 1991. The clear increase in anomaly crests with increasing vertical drift is seen for March 1991 in the upper panel. The lower panel in Figure 7 shows the densities for November 1991 conditions and it clear that a large post-sunset enhancement is required to obtain anomaly crests.

Figure 8. Variations of density ratio parameters with vertical drift scaling are shown. Four panels are used to show the variations in these two parameters for March 1991 and November 1991. The use of a ratio of average anomaly crest density to the equatorial trough density shows a dramatic increase with increasing vertical drift level. GTIM simulations show that below a certain level of vertical drift the ratio of equatorial to wing density correlates well, while above the critical value there is a non-linear relation between the average crest to trough ratio and the effective drift.

Figure 9. An example that reveals the altitude dependent effects of vertical drifts on GTIM density slices. This was runs for conditions approximating September 1991, and shows an overplot of density slices for altitude cutoff values of roughly 19000km (plus signs), 12000km (asterisks), 6000km (diamonds) and 3000km (triangles).

Figure 10. GTIM densities for O^+ (left panels) and H^+ (right panels) at each of 2100LT (upper panels) and 0900LT (lower panels). This was a March 1991 run, with a variety of daily solar fluxes applied. The first panel reveals a strong correlation in equatorial 840km O^+ density with the daily solar flux. The second panel shows that H^+ densities are anticorrelated. The lower two panels reveal that the correlation is not as strong in the morning sector.

Figure 11. Average DMSP densities obtained for June 1991 in six different longitude zones (60E, 120E, 180E, 240E, 300E and 360E). Each panel shows the average density versus latitude pattern for the month for O^+ at both 2100LT (solid line) and 0900LT (dotted line) passes.

Figure 12. As in Figure 11, but shows the results for November 1991, and this shows changes even in the morphology of the variations based solely on longitude.

Figure 13. An example of the longitude-based density variations predicted by the GTIM. The panels in the figure correspond to different longitude sectors (60E, 120E, 300E, 360E). Each panel shows the predicted O^+ density slices for June 1991.

Figure 14. The calibrations between density ratio and effective wind levels for December 1991 results are shown.

Figure 15. As in Figure 14, but here the calibrations are shown for three effective drift levels (0, 1 and 2) for September 1991.

Figure 16. An example of the calibrations between the density ratios defined in the text and effective vertical drift scaling levels. Panels for each of six longitude sectors shows the GTIM variations of the crest/trough ratio (plus symbols) and equator/wing ratio (solid line) for September 1991 conditions.

Figure 17. An example of fitting annual Fourier coefficients to the GTIM variations of effective-wind parameters are plotted for the 240E longitude sector. The six panels correspond to the two linear-fit coefficients (left to right), and the three effective drift levels (top to bottom). The solid lines are the derived GTIM values for each month and drift level and the dashed lines show the first-order modified Fourier fit.

Figure 18. An example showing the nature of the annual variations of effective drift coefficients. There are six panels, corresponding to the parameters defined in the text excluding the critical effective drift parameter. The panels show the GTIM-derived variations of each parameter for the 60E longitude, double effective wind level runs, where the solid lines show the fitted coefficients and the dashed lines the results of the second-order modified Fourier fit.

Figure 19. An example of the annual variations in the critical effective drift parameter, for the same 60E longitude, but showing the results from all three effective wind level runs. The seasonal variations here are very recognizable in that the values of effective drift at which equatorial anomaly crests first appear are lower at equinoxes and higher at solstices.

Figure 20. An example of data from a sample of European stations from several days in April 1958, showing a consistent drop in diurnal maxima on day 13 from a very normal level in day 12. Each panel in the figure shows the monthly median diurnal variation as a solid line, and the individual hourly values as plus symbols. The histogram-like plots along the bottom of each panel denotes the 3-hourly Kp values that is based on the same vertical scale as the foF2 values.

Figure 21. As in Figure 20, but showing data from the same period and region that reveals no drop in foF2 values.

Figure 22. Examples of the GTIM modeled variability in ionospheric parameters as a function of Local Time and neutral wind speed. Panels to the left correspond to Nmax, while Hmax is seen to the right. Northern hemisphere results are seen in the top row, and Southern in the bottom. Each panel shows the fractional standard deviation of each parameter as a function of local time and the magnitude of the random neutral wind component in ms^{-1} .

Figure 23. The results of modeling the low latitude ionospheric response for the case study described in the text. The top panel of this figure shows the drift history over a three-day period where the dotted line is the quiet-time pattern and the dashed line shows the model disturbance drifts. Storm onset is evident in the middle of the first day. The middle panel shows a contour plot in local time and magnetic latitude of the changes in Nmax derived using the GTIM with the drifts in the top panel. The changes are plotted as

percentage changes in N_{\max} compared to the quiet-time values, the contours being spaced at 10% change levels, and where dotted lines show negative phase and solid lines show positive phase. The bottom panel shows the results for the three subsequent days.

Figure 24. As in Figure 23, but showing the results when thermospheric disturbance effects were included in the model run.

Figure 25. Equatorial GTIM TEC results seen as a function of neutral wind surge speed. There are three panels, each of which shows the variations in TEC plotted against local time and magnetic latitude in the US sector for October 1996 conditions. The top panel is the GTIM climatological estimate, the middle panel has added a (peak) 50ms^{-1} (northward) neutral wind, the bottom panel has added a (peak) 100ms^{-1} (northward) neutral wind.

Figure 26. Modeled electron density profiles are contrasted. The panels in left and right columns, respectively, correspond to magnetic latitudes of $+16^\circ$ and -16° , at the anomaly peak. Reading from top to bottom, the profiles are taken from of 1900LT, 2000LT, 2100LT and 2200LT. Within each panel the solid line corresponds to densities based on simulations including the climatological HWM winds, while the dotted and dashed lines comes from simulations that included evening surges of 100ms^{-1} north and 100ms^{-1} south, respectively.

Figure 27. Contours of electron density as a function of horizontal distance (from -20° to $+20^\circ$ at 300E) and altitude. The top panel is the output from a run of PIM, version 1.7. The middle panel shows the electron densities fit using a model profile at each location along the path. The bottom panel shows the reconstructed electron densities when each of the six fitted profile parameters are further fit along the horizontal path using a simple polynomial.

Figure 28. A display of GPS TEC results. The first panel shows the track on an all-sky plot. The second panel shows a close-up of the track, with different symbols plotted for the location on each day in the period showing the day to day consistency of the tracks. The third and fourth panels show overplots of slant TEC for each day in the period, plotted against elevation and azimuth, respectively.

Figure 29. This figure shows overplots of all GPS tracks obtained over Arequipa for March, June, September and December 1996 (reading down), in the four named UT sectors. We note that the sectors in which data are available are typically well-sampled in terms of elevation and azimuth, but sampling in UT is uneven.

Figure 30. GPS TEC data as measured from Arequipa from January 1996. Four panels across are binned according to UT, and panels downward group the data according to the maximum elevation angle. Within each panel, a dial plot shows all tracks of sufficient length that appeared in at least two consecutive days in the month. The different line styles are used to discriminate tracks.

Figure 31. Slant GPS TEC data taken from each track displayed in Figure 30. The panels are defined in the same sense and the line styles correspond directly. The x-axis here is simply an index that orders the data.

Figure 32. As in Figure 31, but showing climatological model estimates of slant TEC. A comparison of the two figures provides a quick visual test of the ability of the model to reproduce observed TEC variations.

1. INTRODUCTION

In the original proposal for the current Air Force contract with the Center for Space Physics at Boston University, a modeling study was included whereby satellite signatures could be interpreted in terms of ambient physical conditions. Specifically, the model is the new multiple-ion Global Theoretical Ionospheric Model (GTIM), the data are in situ ion density measurements made from the Defense Meteorological Satellite Program (DMSP), and the physical parameters sought are scaling factors (relative to climatology) of vertical $\mathbf{E} \times \mathbf{B}$ drifts and neutral meridional winds. These latter parameters are used to driving the Ionospheric Forecast Model (IFM) currently in use in Air Force systems. This project is described in Sections 2, 3 and 4 of this report.

The issue of ionospheric variability is investigated in Sections 5 and 6. Section 5 considers variability at middle latitudes, summarizing the observed variability in key ionospheric parameters, as well as performing a modeling study to examine likely causes. Section 6 describes both a new means of modeling disturbed conditions at low latitudes, and the predicted effects of neutral meridional wind surges on the equatorial anomaly region. Finally, Section 7 describes new applications of a recently developed analytic electron density profile model.

2. DMSP SATELLITE SIGNATURES

In this section, a summary of both the theoretical ionospheric model (GTIM) and the database used for validation and comparisons is given.

The essential assumptions being made here are

(1) that the GTIM provides a realistic description of the topside ionosphere (the DMSP orbit is nominally around 840km)

(2) that the average behavior of topside ion densities measured by the Special Sensor Electron Ion Scintillations (SSIES) can be described by the GTIM

(3) that daily departures from the average behavior of the ion densities are due to variation in the ambient neutral wind and vertical drift fields, and can be summarized by effective wind and drift scaling parameters.

2.1 Goals Of The Research

The ultimate goal of this study is to produce a series of simple algorithms that can be used with future SSIES DMSP observations to derive effective levels of meridional neutral wind and vertical ($\mathbf{E} \times \mathbf{B}$) drift. These parameters are of immediate application in driving the IFM.

2.2 The Approach

Initially, the GTIM ion densities must be validated with respect to the DMSP observations in both magnitude and morphology. Runs of the GTIM are made over a wide range of L values, from L=3.0 down to a sample of low fieldlines at L=1.026. Around 20 fieldlines are required to adequately sample densities at 840km over a good range of latitudes. The variation of ion density at 840 km with latitude will be referred to hereafter as a density "slice". The runs are assumed to be converged within four model days (in the context of the model this is valid at 840km, although not at higher altitudes).

Validation of the model is performed by comparisons of observed and modeled densities over a range of conditions. It must be demonstrated that the model when run over a range of effective vertical drift and neutral wind levels can span the range of observations within any given month. The month has been taken as the unit of time to define the

“climate” i.e. the characteristic variations of the season.

Following validation of the model in this manner, the effects of variations in the levels of vertical drifts and neutral winds on the shapes of density slices can be determined by performing a grid of model runs over a range of values of each parameter. This determination should include both a physical description of the nature of the correlation, and the specification of a numerical relation that defines it.

It will be generally assumed that derivations of effective wind and drift levels from this study will be valid for each day (but will be allowed to vary with longitude); this is primarily based in the nature of the model runs in which different levels of winds and drifts are used but that these remain constant over the day. Prior modeling tests have demonstrated that the effective drift level derived corresponds most with a local time period starting roughly two hours prior to the local time of the observation and analysis. With neutral winds the effects depend variously on the strength of the effect, the duration and the ambient direction of the winds at the time of the effect, and thus no general comments can be made on the effective sampling time of the neutral wind scaling factor, as sampled by an evening pass of DMSP. A daily average value will be taken to represent the “weather” in this case.

2.3 SSIES Data

The SSIES instrument provides in situ data that can subsequently be analyzed to yield both the O^+ density and the non- O^+ density (generally taken to be H^+). Although there is no mass spectrometer aboard the SSIES, assumptions about the mass of the dominant species are used to infer the dominant species density from the total electron density. At solar maximum, the situation is simpler because it is anticipated (and has been observed in the SSIES dataset) that O^+ is the dominant ion. Overall, in a modeling sense,

the effects of neutral wind and vertical drifts upon O^+ are better understood from long experience of F-region modeling using the GTIM. To first order, the H^+ density should be dictated by the same factors that influence O^+ (the latter being the dominant source of the former via resonant charge exchange) but transport and diffusion considerations become more important for the lighter ion.

The data used in this study came from Dr. F. Rich of the Air Force Research Laboratories (AFRL), at Hanscom AFB. Dr. Rich is also responsible for having derived ion densities from the raw SSIES dataset. The majority of the data is in the form of daily averages. This means that the raw data from individual passes of the satellite have been averaged for all passes (either within a specific longitude sector, or over all longitudes) for each UT day. This smooths the steeper and more rapid fluctuations that could be due to either the data analysis or plasma depletions, and it should be stressed here that the smoothing is an important step in the interpretation of the density slice morphology in terms of vertical drift and neutral wind effects.

A list of the dataset provided to Boston University is given in Table 1.

2.4 The GTIM

The newest version of the GTIM solves the equations of continuity and momentum for up to three ion species, O^+ , H^+ and He^+ (typically He^+ is a minor constituent). The thermospheric specification comes from MSIS-90 and the NASA HWM, and ion and electron temperatures are numerical descriptions (ensuring smooth variations in all dimensions) based upon tabulated values of Brace and Theis. The GTIM can thus be described as a model that determines the ionospheric species ion densities within a specified thermosphere. It is thus well-suited to studies such as this where the ionospheric effects of changing one of the so-called “drivers” of the system on the theoretically derived densities.

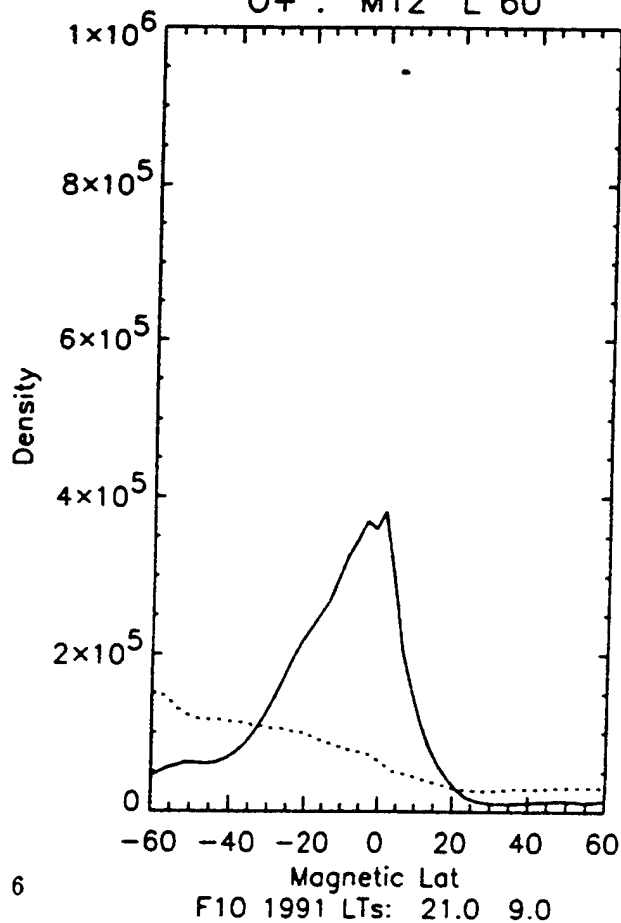
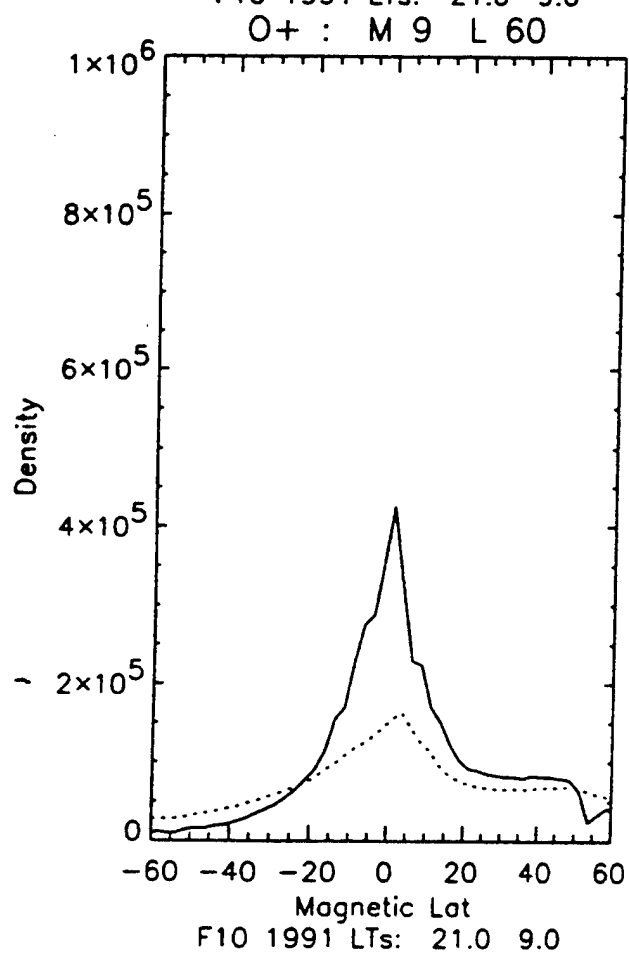
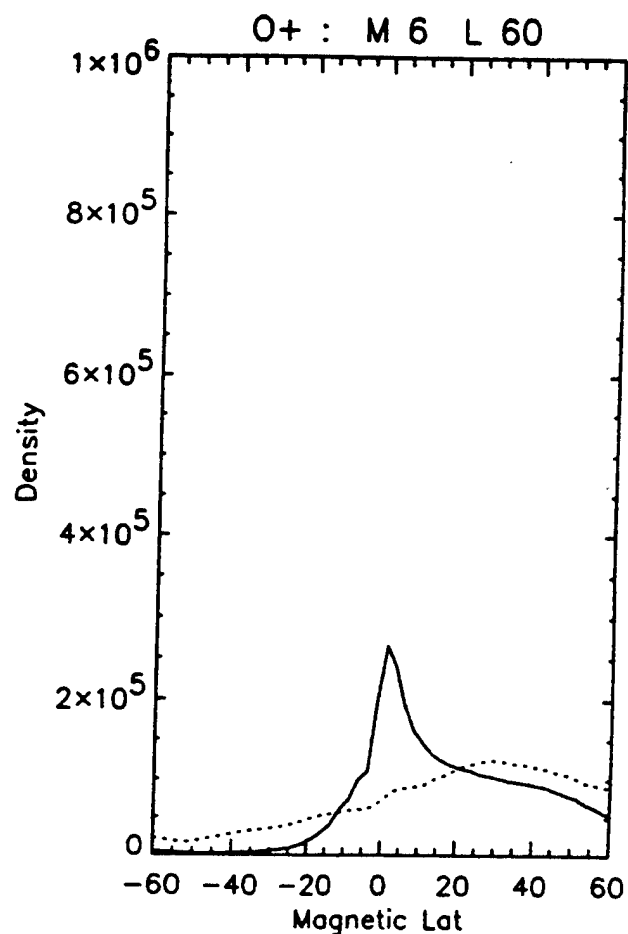
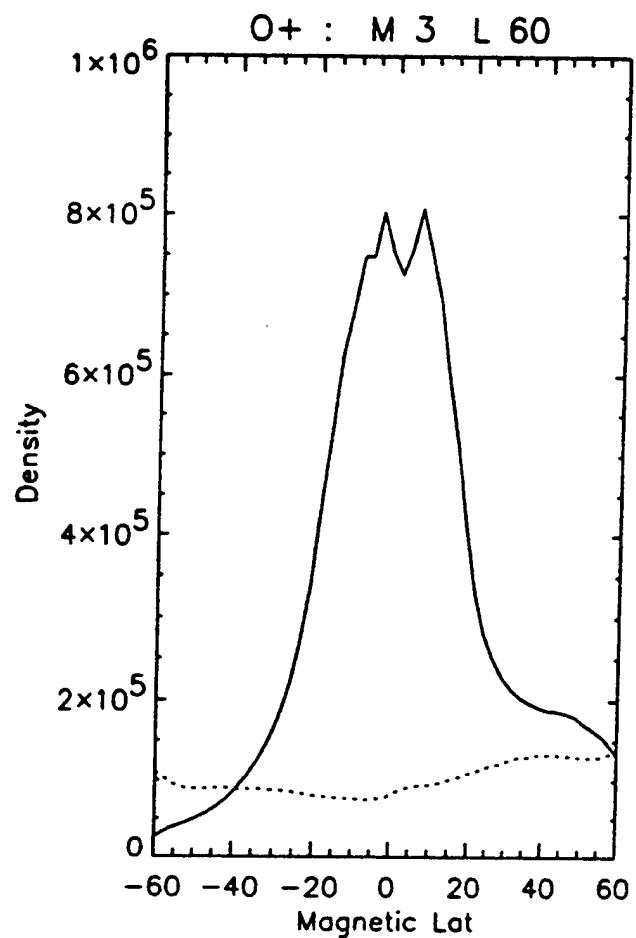
Vertical ion drifts can either be input directly from a file (when performing case studies of situations when measured drifts are available), or can be taken from climatology. This latest set of GTIM runs has been based upon a drift model provided by Dr. R. E. Daniell of CPI, Boston that fully utilizes recently published AE-based drift measurements of Fejer et al. This model contains a Fourier representation of the annual variations and thus is available at all months with smooth transtions between the characteristic diurnal variations at each season, and also containing a smooth longitude variation.

3. DMSP DATA/MODEL COMPARISONS

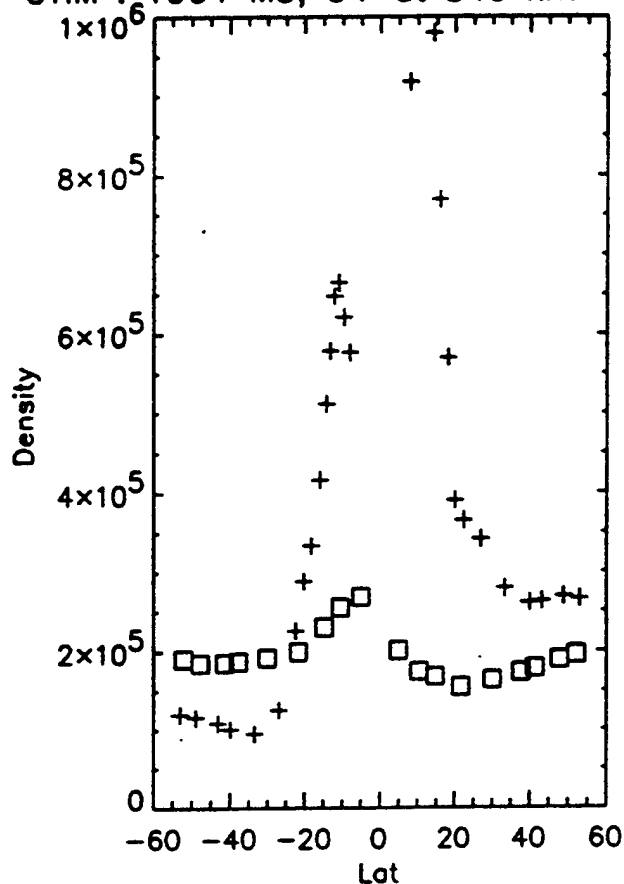
This section describes in detail the results of comparisons between SSIES ion density slices and those derived in the GTIM. The analysis includes a discussion of the basis of the apparent correlations, highlighting the individual influences of neutral winds and vertical ion drifts.

3.1 Validation

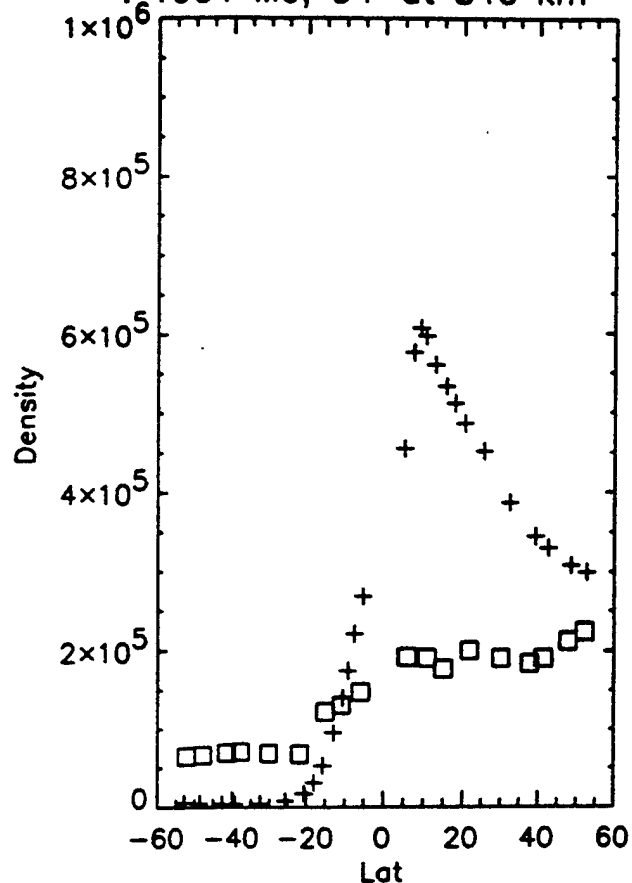
We refer now to the question of model validation, the first of the points listed above. Figure 1 shows O^+ densities as a function of (magnetic) latitude as measured on the DMSP satellite F10 during March, June, September and December 1991. The advantage of solar maximum studies is that the determination of ion species is more clear cut (O^+ dominates). The lines are monthly averages and the data have been further averaged by using all observations within 30° of 60°E longitude. The solid line reflects the 2100LT pass, the dotted line 0900LT data. Next, Figure 2 shows GTIM O^+ densities for the same four epochs using the monthly averaged solar activity levels, at 60°E longitude and using the same vertical scale. A comparison of the two figures reveals a high degree of correlation in both qualitative and quantitative senses. It can also be shown that the range of daily



GTIM : 1991 M3, O+ at 840 km

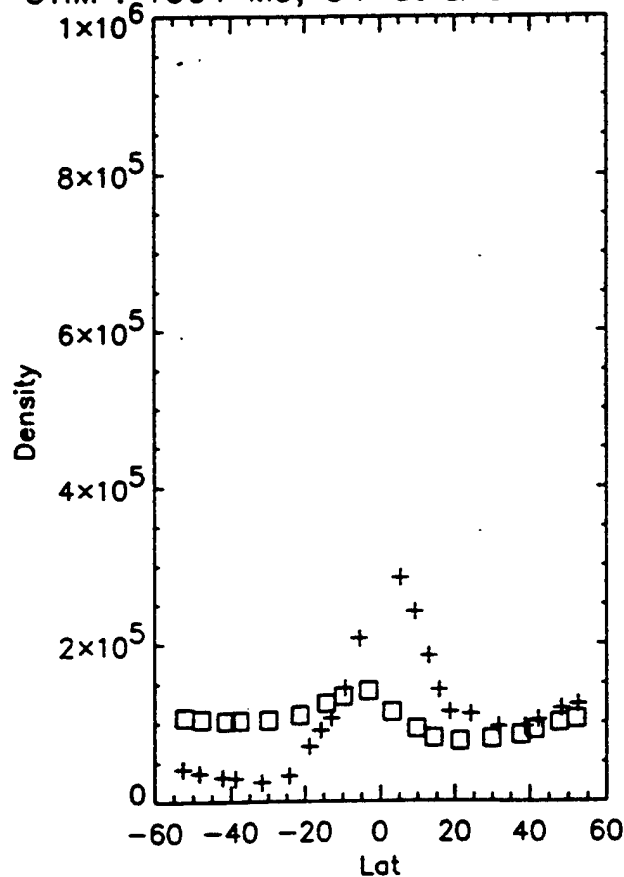


: 1991 M6, O+ at 840 km



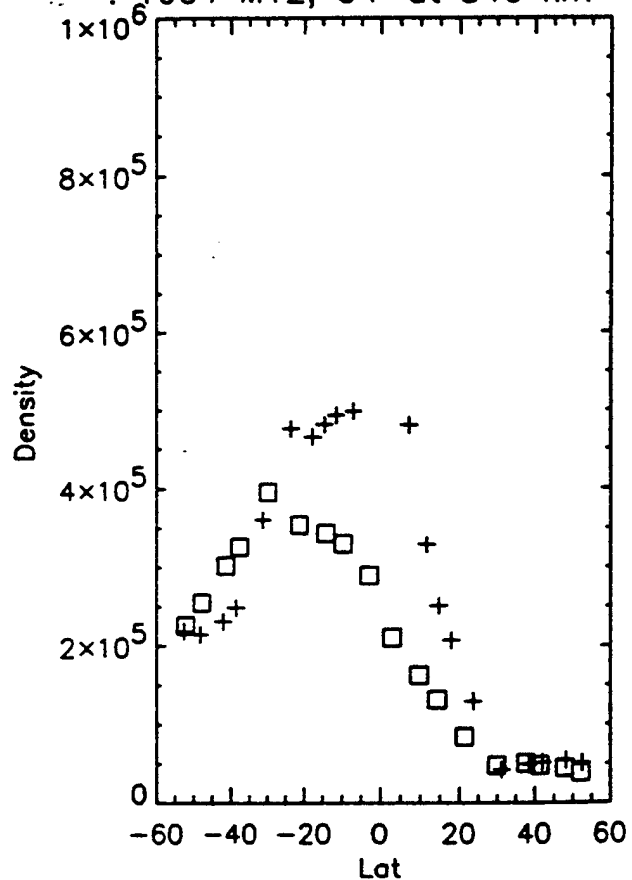
DMSP F10 : 21.00 9.00 (LTs)

GTIM : 1991 M9, O+ at 840 km



DMSP F10 : 21.00 9.00 (LTs)

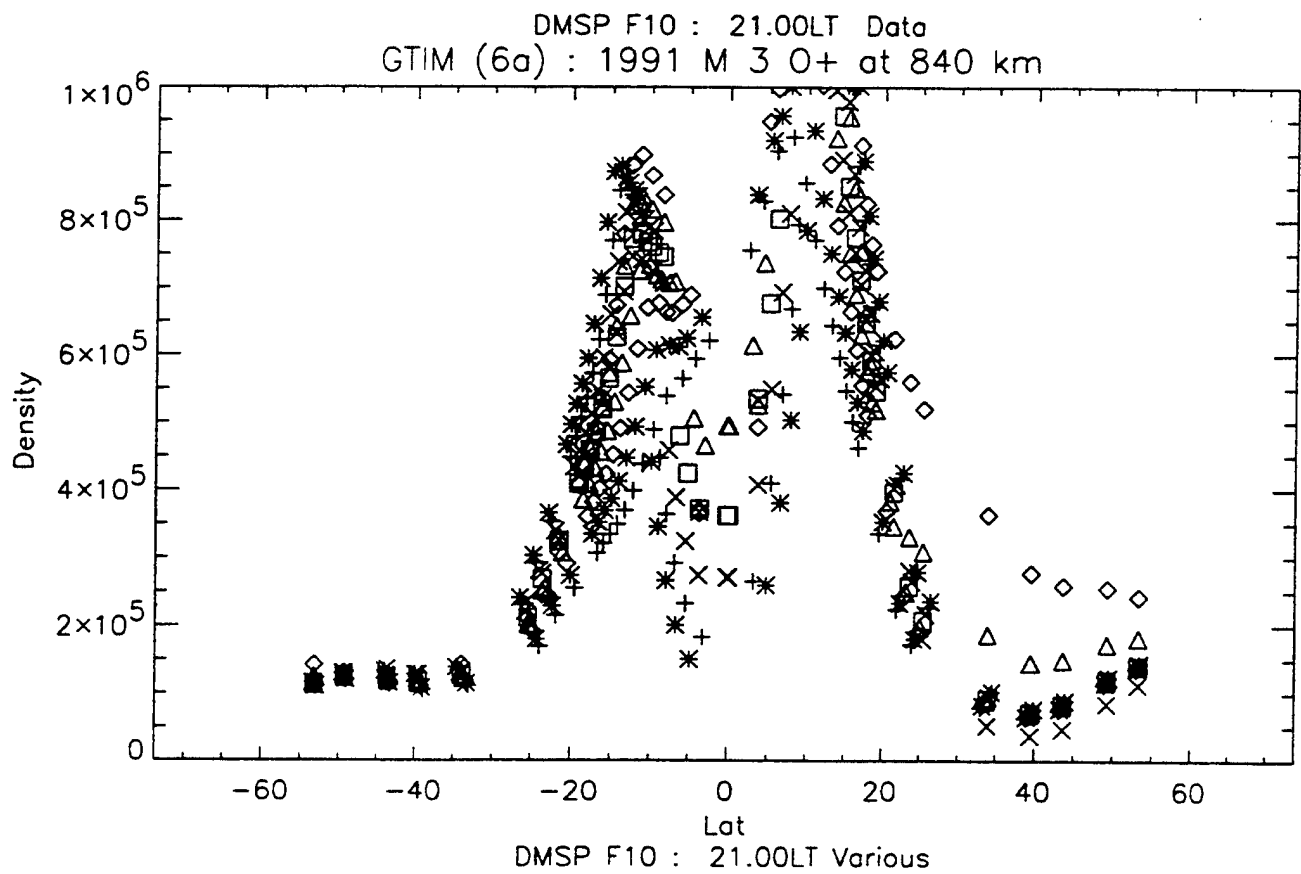
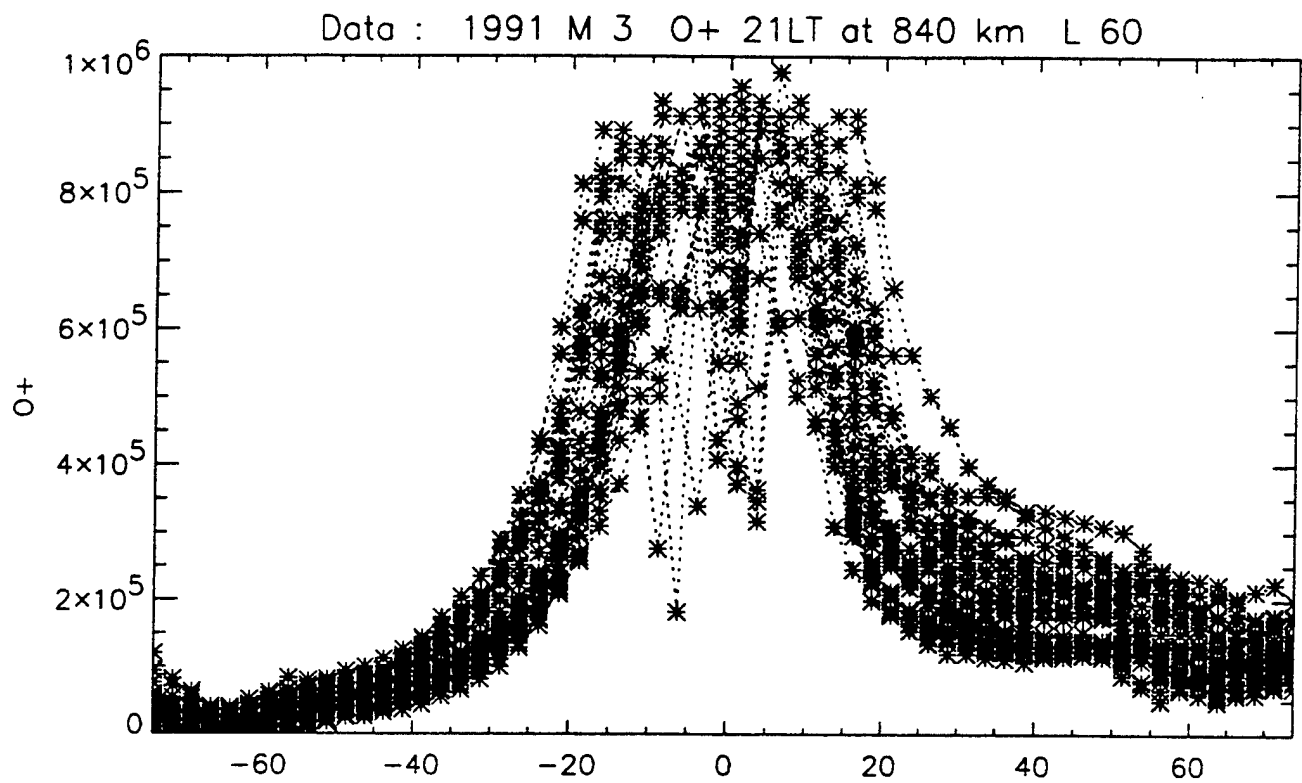
: 1991 M12, O+ at 840 km

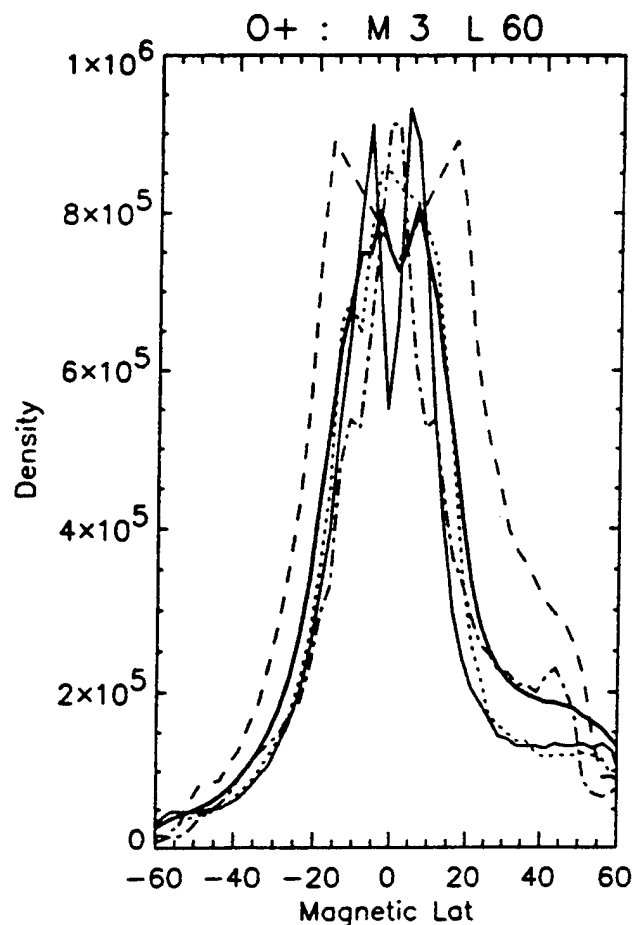


DMSP F10 : 21.00 9.00 (LTs)

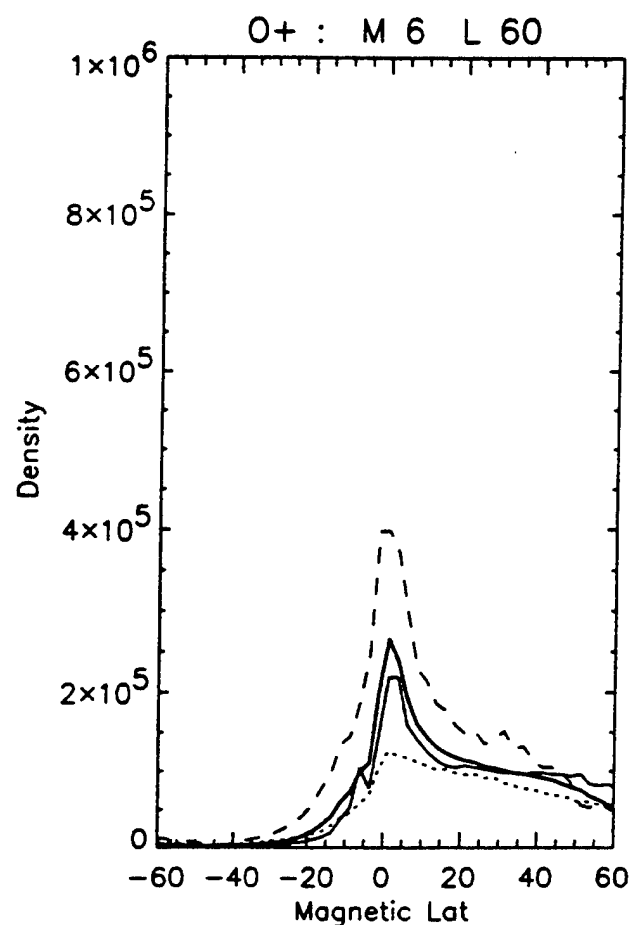
(sector-averaged) values could be spanned by a grid of GTIM runs that include a range of neutral wind and vertical drift scalings. A comparison of this type is shown in Figure 3 where the upper panel shows daily averaged 2100LT density slices for March 1991 in the 60°E longitude sector, and the lower panel shows a range of slices derived from GTIM runs using various vertical drift and neutral wind scalings. Consideration of the daily averaged data from DMSP is important here, because it became evident that the monthly average slices had shapes that did not necessarily occur on any individual day. It should be noted here that the grid of models in the lower panel covered either variations in neutral wind or vertical drift, and thus would not be expected to fully span the observations; however, the level of coverage is good.

Figure 4 shows another type of figure useful in this analysis. Within each panel (one per month), the thicker solid line is the monthly average and the thinner lines are selected daily averages that demonstrate a different shape of slice (the actual days are listed in the panel subheaders). March observations reveal one case where the average variation was not observed in any individual day; the anomaly crests either being larger and wider than the average or not present at all. The first important step in this study was to establish that the GTIM can provide a reasonable description of density variations such as these. A series of model runs were performed over an initially small grid of months (those taken to be typical of seasons) and only one longitude (60°E) in order to validate the GTIM. A summary of the results is found in the following subsections.

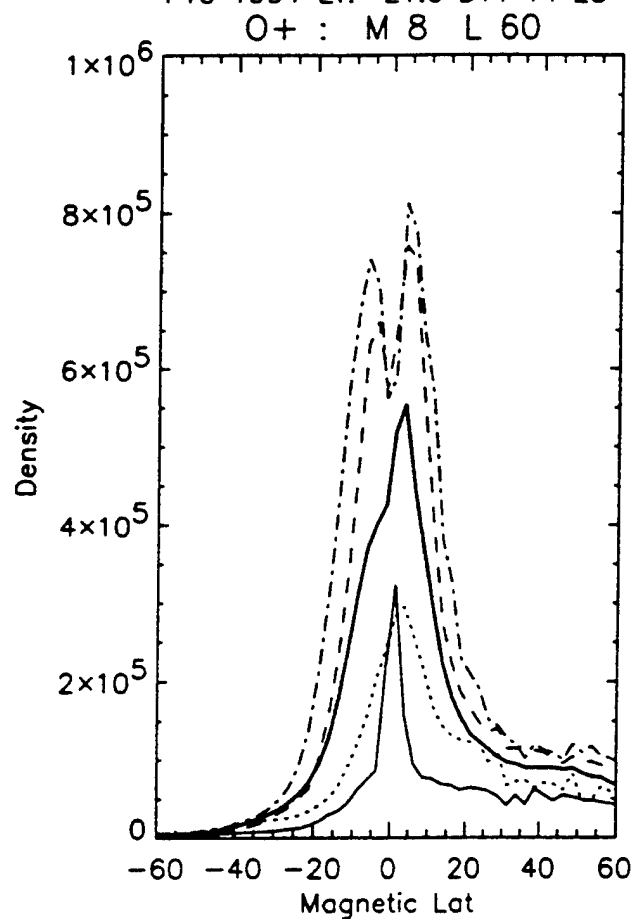




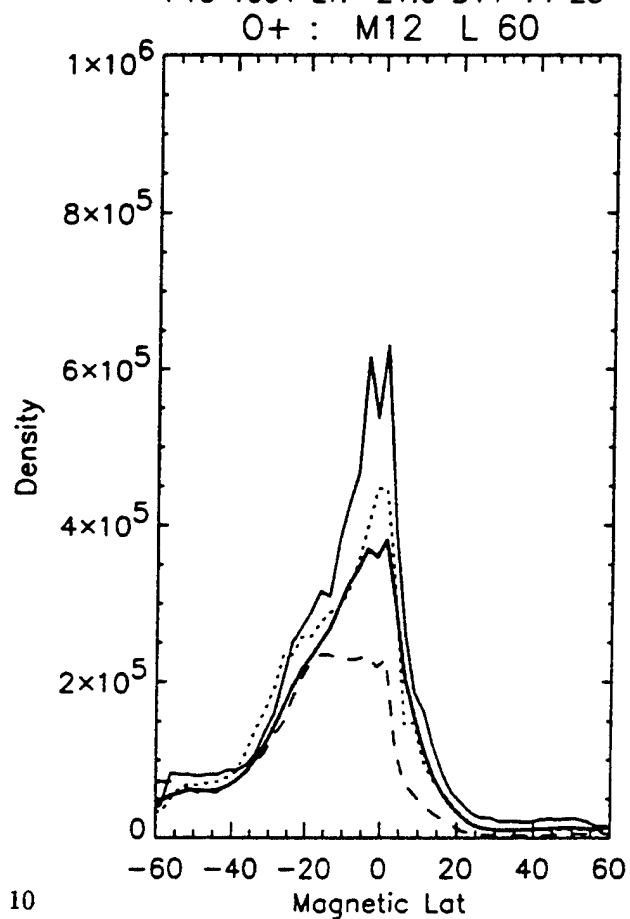
F10 1991 LT: 21.0 D11 14 23



F10 1991 LT: 21.0 D11 14 23



F10 1991 LT: 21.0 D11 14 23



F10 1991 LT: 21.0 D11 14 23

3.2 The Evening Sector

Overall, the results corresponding to the evening sector are easier to interpret than those of the morning sector. Firstly, there is the sensitivity of evening sector (2100LT crossings for F10) densities to the the post-sunset enhancement in vertical drifts that is especially strong at solar maximum conditions. There is a second factor, also vertical-drift related. The climatological drift patterns from Jicamarca, say, typically show a downward surge in drifts in the hour or so immediately prior to sunrise. In the GTIM, this has the effect of lowering the plasma prior to the rise in O^+ production that occurs at sunrise. Because of this, the model (O^+) plasma is at lower altitudes (and lower loss) when production happens, and the GTIM densities in the post-sunrise sector tend to be too high. This is seen in the 0900LT DMSP pass comparisons. For these reasons, the analyses that follow are concerned with the 2100LT passes (of both F10 and F12). It also follows that future comparisons/analyses would work better for 2100LT passes, even over 1930LT passes, for the simple reason that the vertical drifts (that are frequently dominated by the post-sunset enhancement feature) have more time to have influenced the ion densities and thus have a clearer signature in 2100LT data.

There was no equivalent dominant feature in the diurnal variations of neutral wind, and thus neutral wind signatures can equally well be determined from data/model comparisons at any local time. For simplicity, the 2100LT pass has again been selected.

3.3 Effects of Neutral Winds

We now consider the effects of neutral winds, specifically on the density slices being considered in this study. It was expected that the neutral meridional wind would manifest itself most dramatically in the hemispheric asymmetry of the in situ density values, and this was seen to be the case in the GTIM results. Indeed, a simple linear fit proved to be

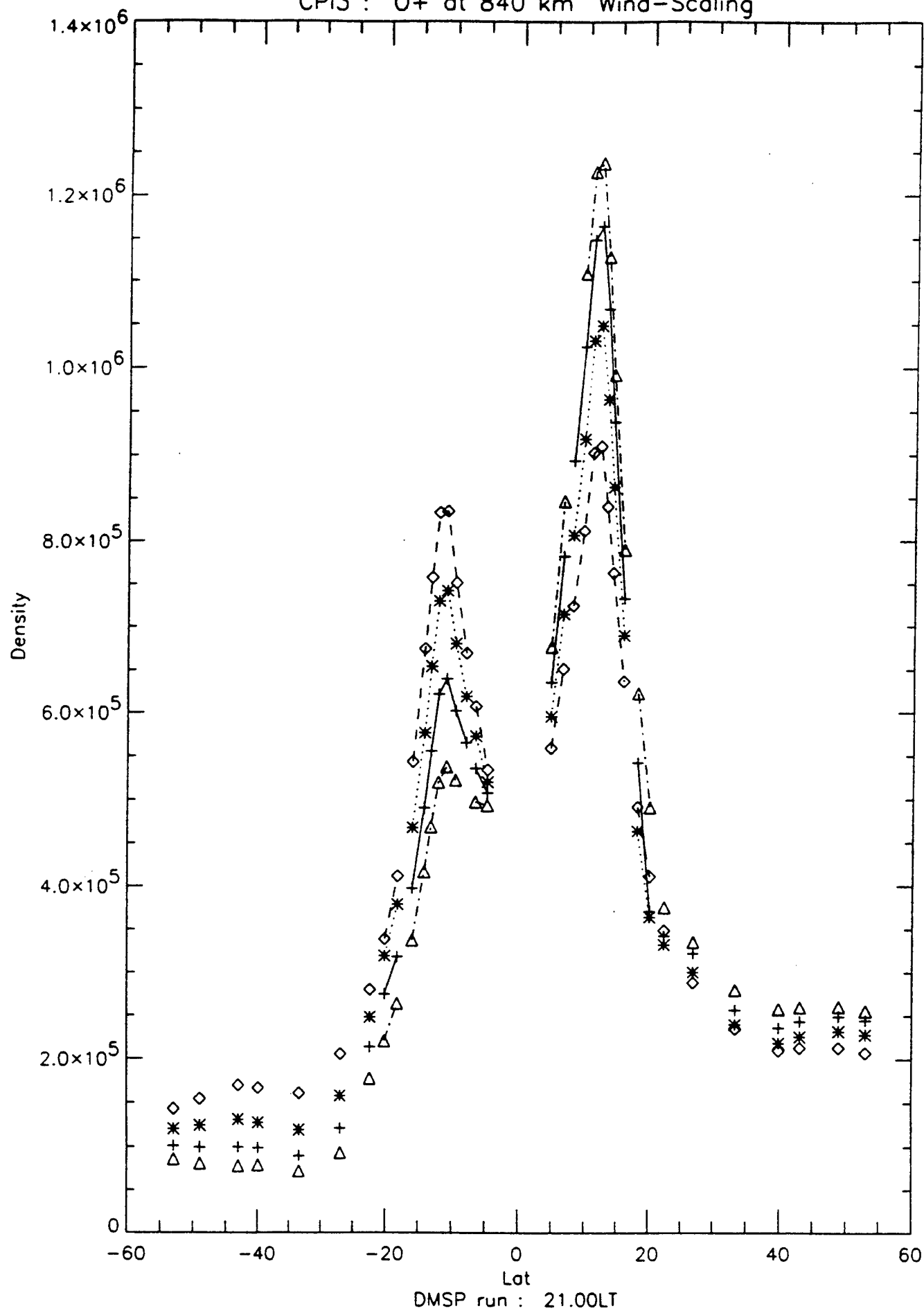
sufficient to describe the numerical relationship between the neutral wind scaling value and the north-south density ratio (or south-north; the ratio to be used is whichever is greater than 1.0).

Let us examine the GTIM results as a function of the neutral wind scaling factor. GTIM O^+ densities at selected fieldlines for a sample of wind-scalings are shown in Figure 5 for model runs made for March 1991. Different scalings are shown as different symbols and joined at lower latitudes by different line styles (1.0=plus, solid line) (0.5=asterisk, dotted) (0.0=diamond, dashed) (1.5=triangle, dot-dashed). As a first attempt at a wind-scaling proxy we consider the ratio of the average densities in the wings at northern and southern latitudes. In principle, this should avoid the vertical drift effects that are concentrated at lower latitudes. There is next the issue of what latitudes to use to define the middle latitude wings. Figure 6 shows the results of plotting the north/south ratio of wind density as a function of wind scaling for a variety of latitude ranges for the results in Figure 5. Each panel in Figure 6 corresponds to a given range of magnetic latitudes that are listed in the subheader. The diamonds in each panel show the desired smooth increase in density ratio as a function of wind scaling. The plus symbols were included to show how the average (of the two hemispheres) density varies with wind scaling where the densities have been normalized to the wind=0.0 average value. The dependence of the average ratio on latitude range is seen to be less than 10% over this fairly large range of wind scaling factors.

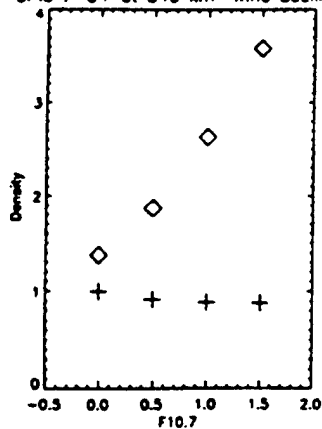
3.4 Effects of Vertical Drifts

In this section of the report we consider the effects of vertical drifts on the shape of ion density slices. The anticipated effect would be an increased development of ionospheric anomaly crests and an equatorial trough at the DMSP altitude.

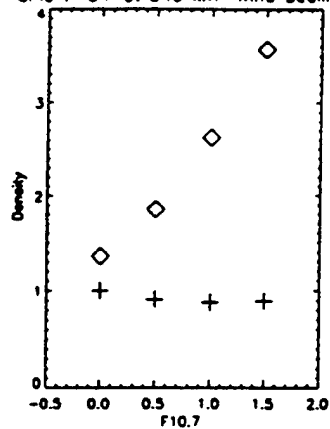
Some examples of the vertical drift scaling effects on density slices are seen in



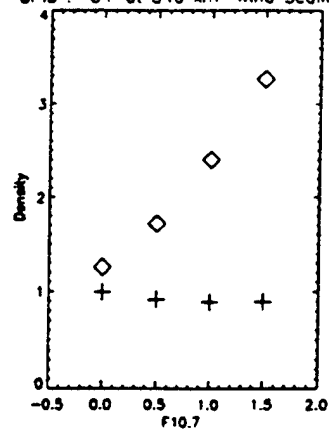
CP13 : 0+ at 840 km Wind Scalings



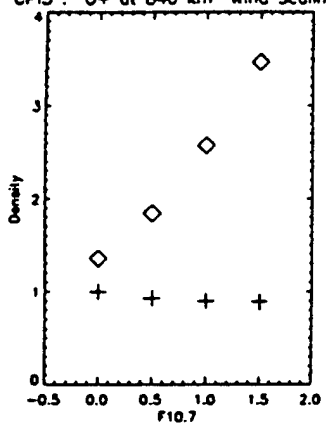
CP13 : 0+ at 840 km Wind Scalings



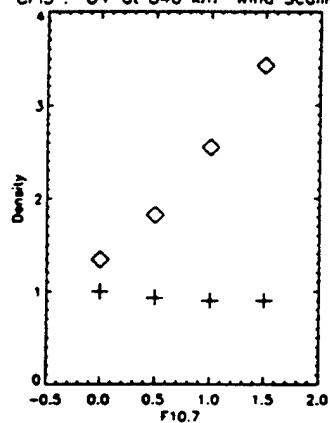
CP13 : 0+ at 840 km Wind Scalings



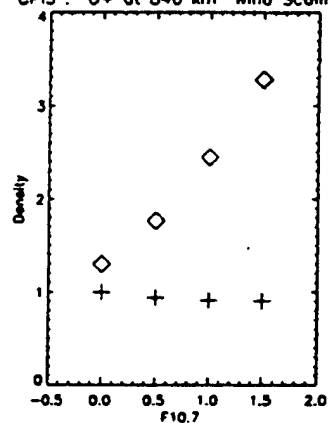
21LT - ave N/S ratio between 26 42
CP13 : 0+ at 840 km Wind Scalings



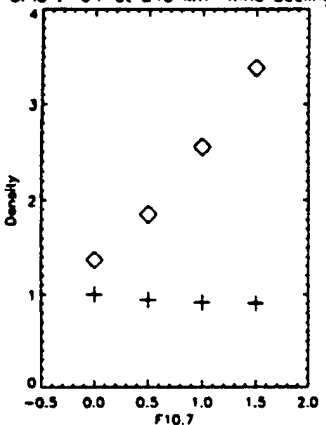
21LT - ave N/S ratio between 30 42
CP13 : 0+ at 840 km Wind Scalings



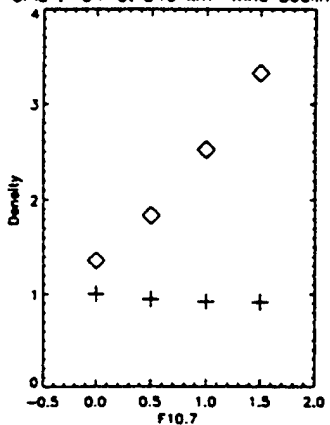
21LT - ave N/S ratio between 34 42
CP13 : 0+ at 840 km Wind Scalings



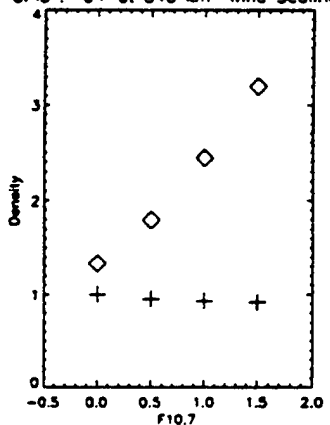
21LT - ave N/S ratio between 26 50
CP13 : 0+ at 840 km Wind Scalings



21LT - ave N/S ratio between 30 50
CP13 : 0+ at 840 km Wind Scalings



21LT - ave N/S ratio between 34 50
CP13 : 0+ at 840 km Wind Scalings



21LT - ave N/S ratio between 26 56

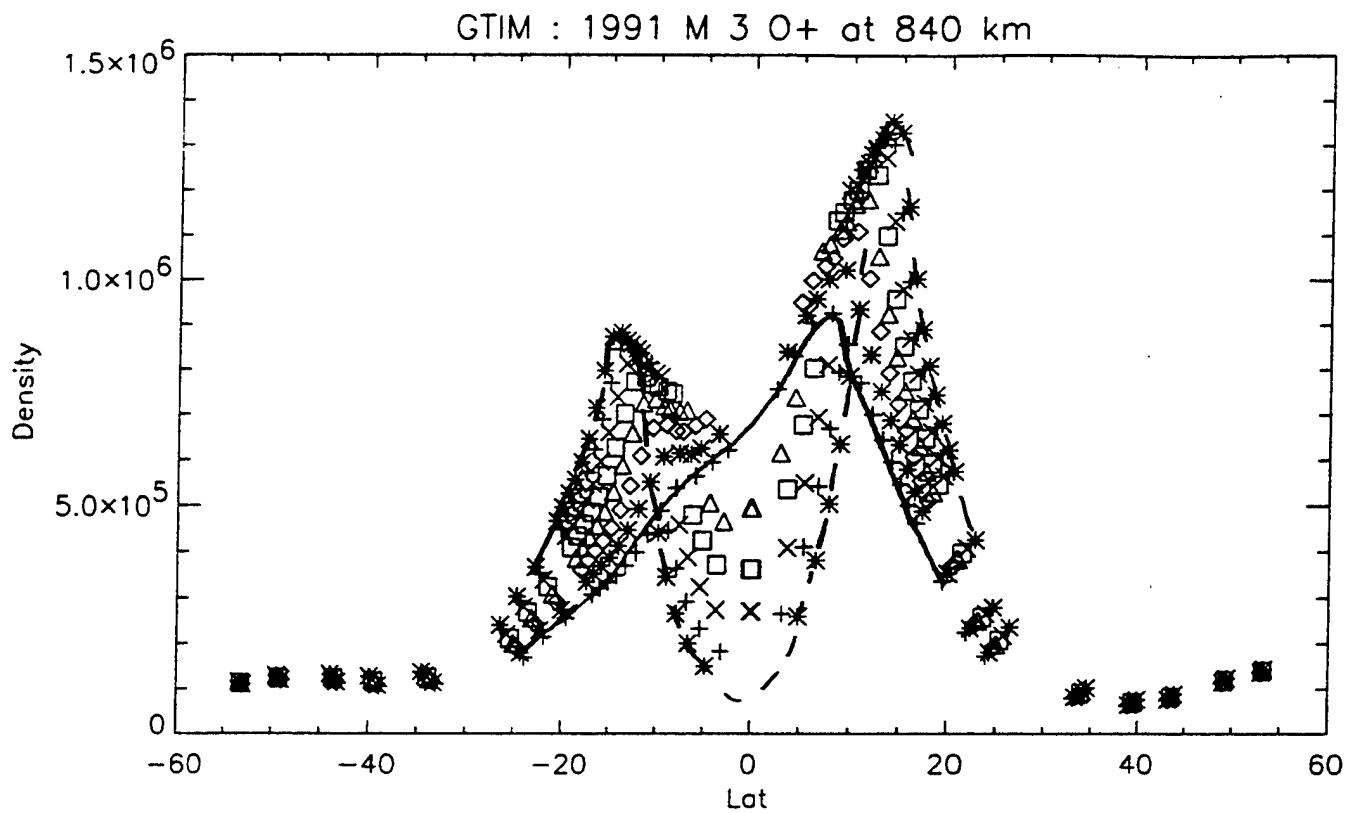
21LT - ave N/S ratio between 30 56

21LT - ave N/S ratio between 34 56

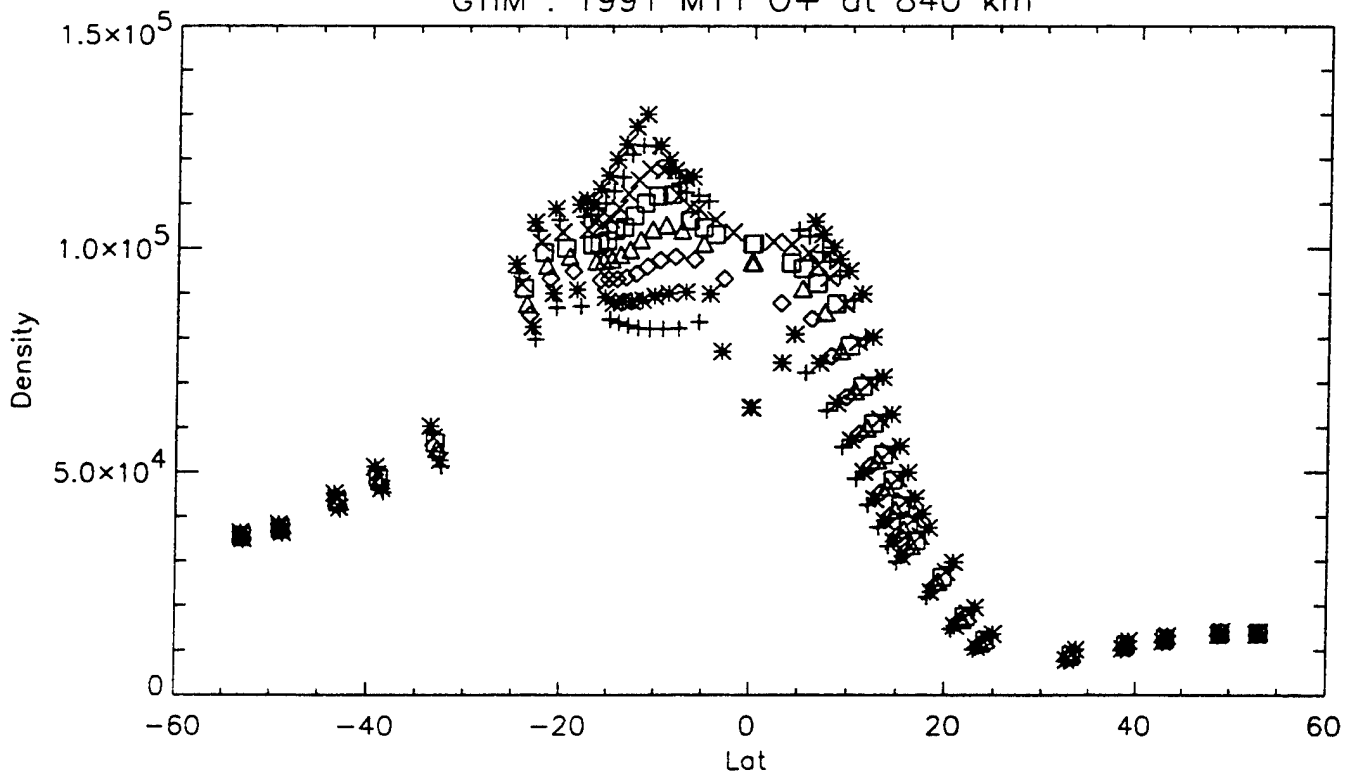
Figure 7, for GTIM simulations appropriate to conditions in March 1991 and November 1991. The clear increase in anomaly crests with increasing vertical drift is seen for March 1991, in the first panel. With a minimal post-sunset vertical drift enhancement (the plus symbols, joined for clarity) there is no evidence of anomaly crests or equatorial trough, whereas a larger vertical drift (asterisks, also joined for clarity), demonstrates clear (asymmetric) crests and a deep trough.

There is another factor to consider in the derivation of effective vertical drifts using DMSP-derived density slices; there are not always crests in SSIES measurements at 840km, especially at solstitial months when pre-reversal enhancements are typically small or at lower solar activity levels when the enhancements are absent. The lower panel in Figure 7 shows the November simulations, where only a large post-sunset enhancement results in anomaly crests. To derive effective drifts at lower drift levels/seasons, a new parameter was defined- the ratio of the equatorial density to the average density in the wings (defined at a middle latitude range). Both parameters are consistent with the concept that as vertical drifts are scaled upwards, that because all post-sunset drifts are upwards, that more plasma will be seen at lower latitudes, until the higher drift levels when anomaly crests and the equatorial trough develop at DMSP altitudes.

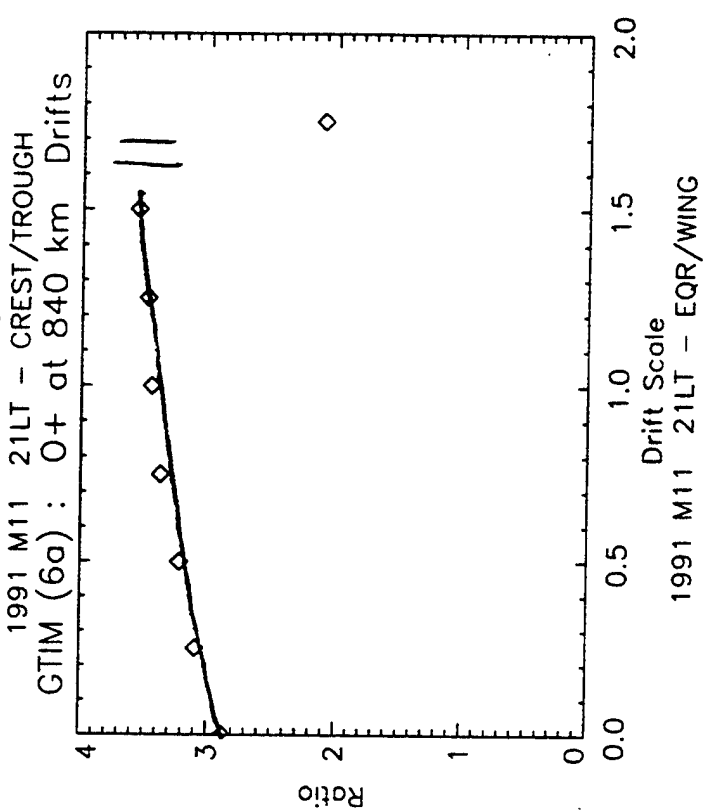
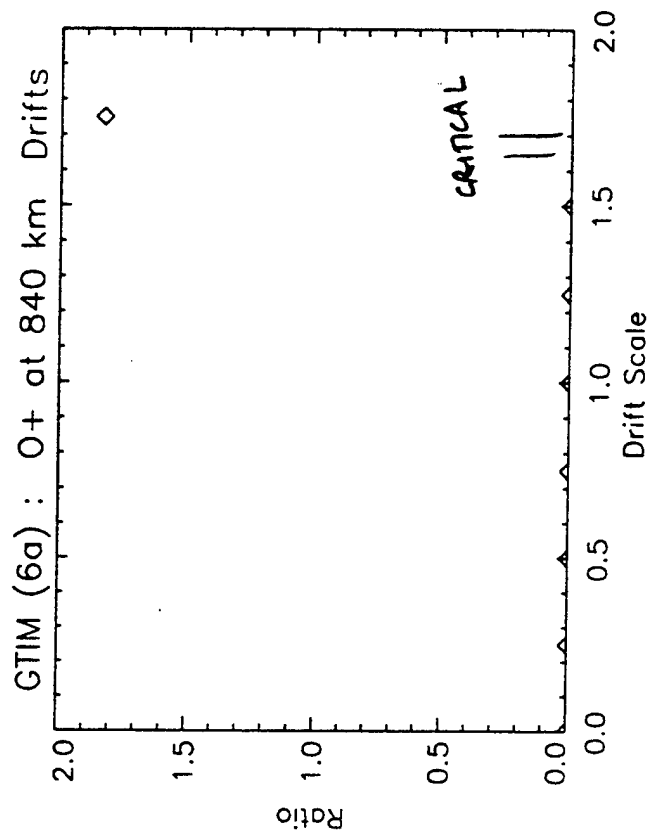
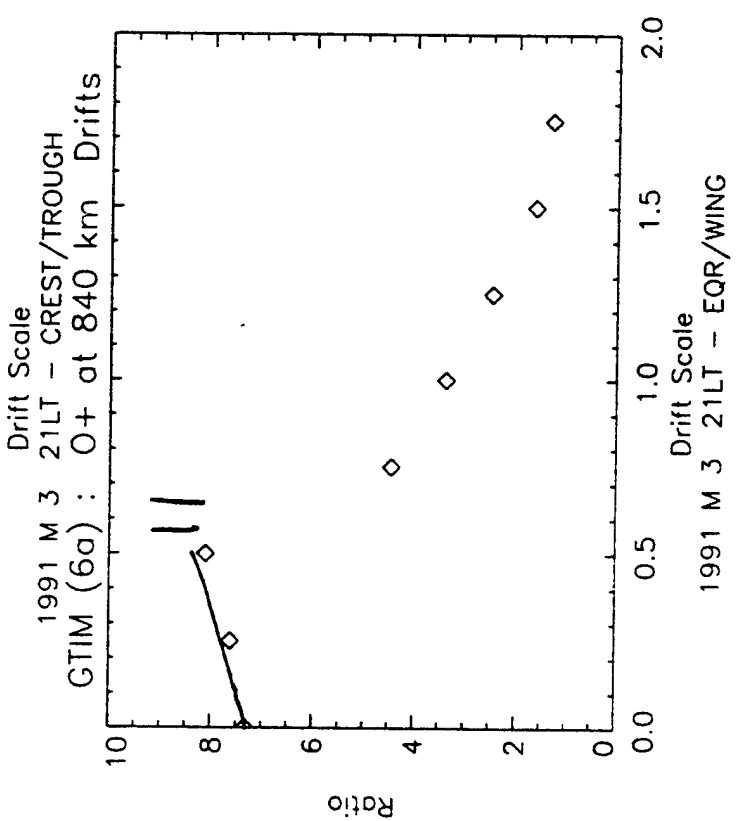
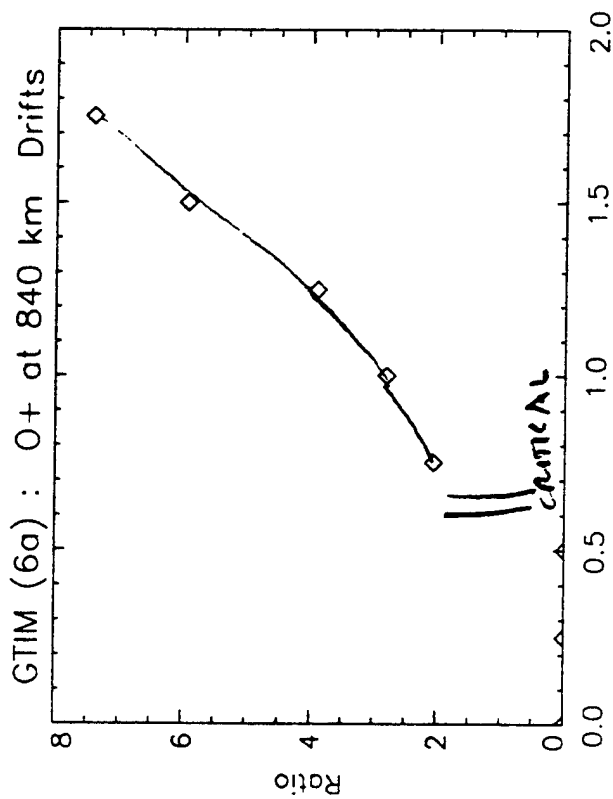
An example of the variations of these parameters with vertical drift scaling is seen in Figure 8. In this figure, four panels are used to show the variations in these two parameters for same two months in Figure 7, March and November 1991. The use of a ratio of average (of north and south) anomaly crest density to the equatorial trough density showed a clear and dramatic increase with increasing vertical drift level although a linear relationship was not sufficient. The important point to make about this figure is that the GTIM simulations show that below a certain level of vertical drift (that varies from month to month) the ratio of equatorial density to average wing density correlates well, while above the critical value



DMSP F10 : 21.00LT Drift-PRE Scaling
GTIM : 1991 M11 O+ at 840 km



DMSP F10 : 21.00LT Drift-PRE Scaling



there is a non-linear relation between the average crest to trough ratio and the drift scaling factor. Some notes have been added to Figure 8 to highlight these points.

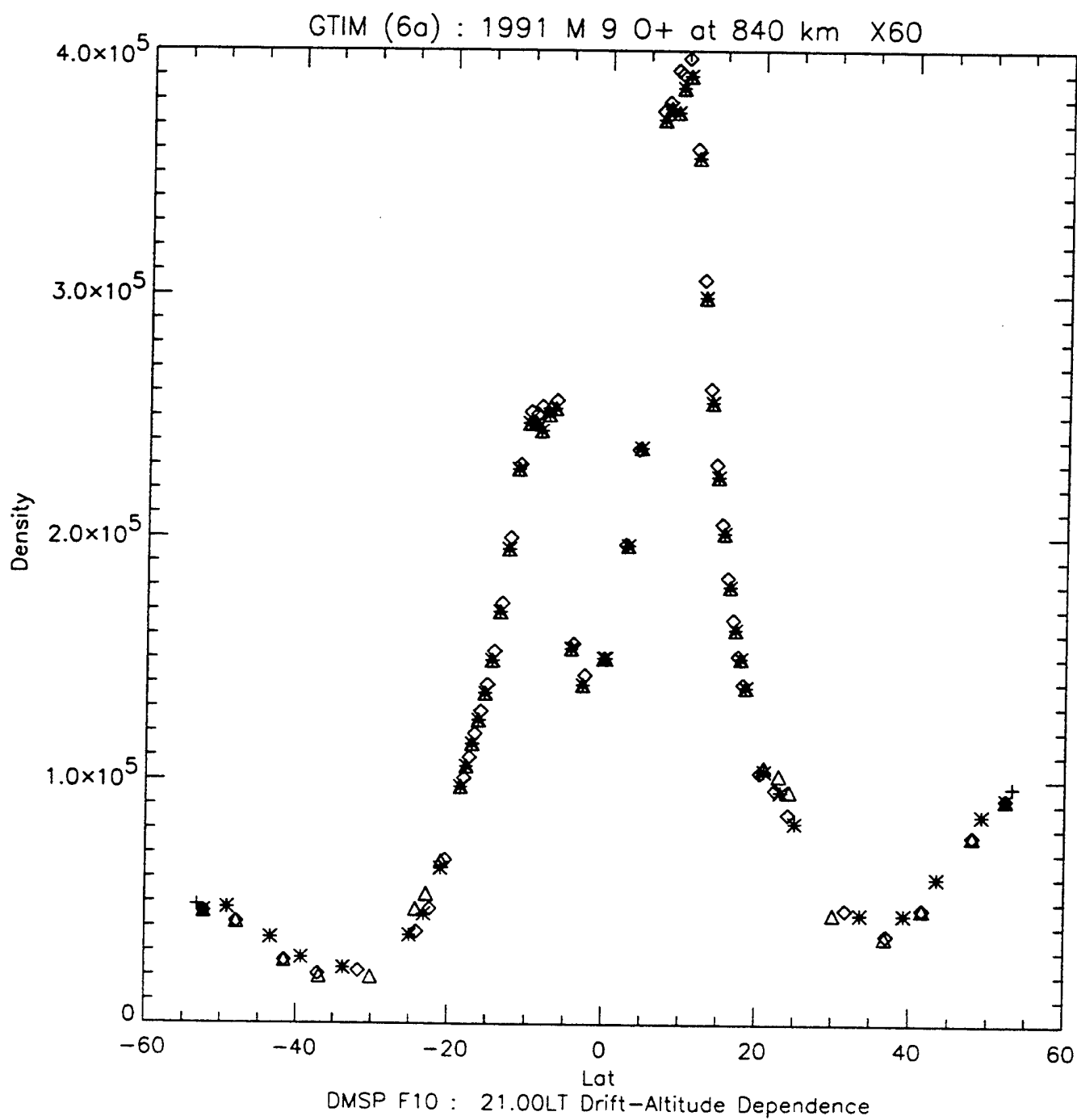
3.5 Effects of Altitude Dependence

An additional grid of model runs was performed at selected conditions to investigate the effects of altitude-dependence of vertical drifts on these DMSP-like density slices. The motivation for this was that as the altitude dependence of vertical drifts is little understood at present, and that the GTIM can be used to estimate the effects in order to ultimately make the algorithms produced by this study robust with respect to variations of this type. There have been indications in recent years that there is some dropoff in the magnitude of vertical drifts with altitude.

An example that reveals the altitude dependent effects on GTIM density slices is given in Figure 9. This was runs for conditions approximating September 1991, and shows an overplot of density slices for altitude cutoff values of roughly 19000km (plus signs), 12000km (asterisks), 6000km (diamonds) and 3000km (triangles). What is apparent with comparisons of this type is that there is little discernible effect on crest magnitudes, but in some situations there can be a change in the crest location. Specifically, lowering the altitude cutoff can lower the (absolute) latitudes of the anomaly crests. Thus, robustness with respect to the latter type of variation can be achieved through the use of feature-specific (i.e. the density value at the crest) rather than location-specific (i.e. the density at a fixed latitude) quantities.

3.6 Solar Effects

A recent result from AFRL demonstrated that there is a high degree of correlation between density measurements made in situ aboard DMSP satellites and the daily value

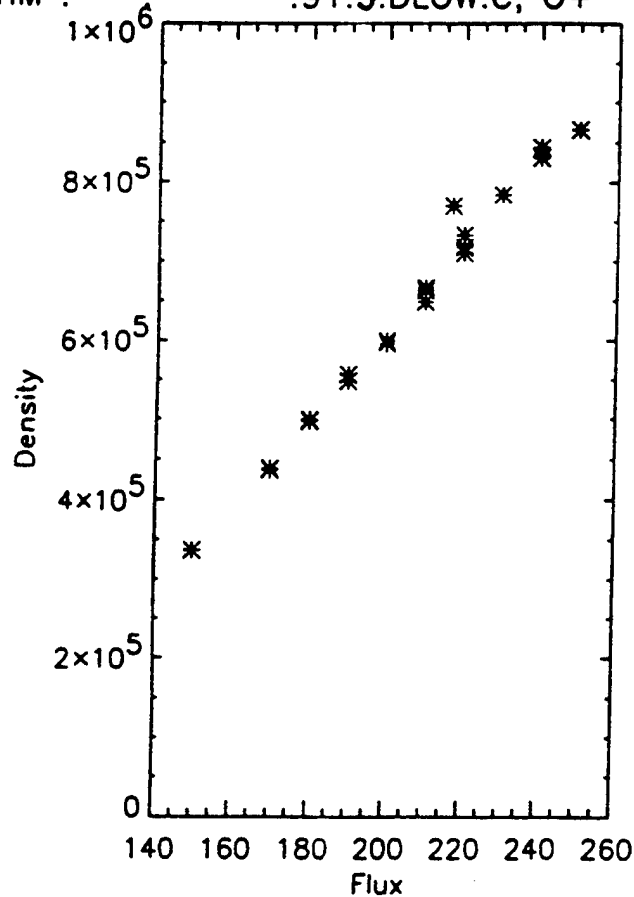


of the F10.7cm solar flux, especially at solar maximum conditions. This was an interesting result, and contrasted with earlier studies that have shown no such correlation between the daily solar flux and either the F region peak density, N_{max} , or the total electron content, TEC.

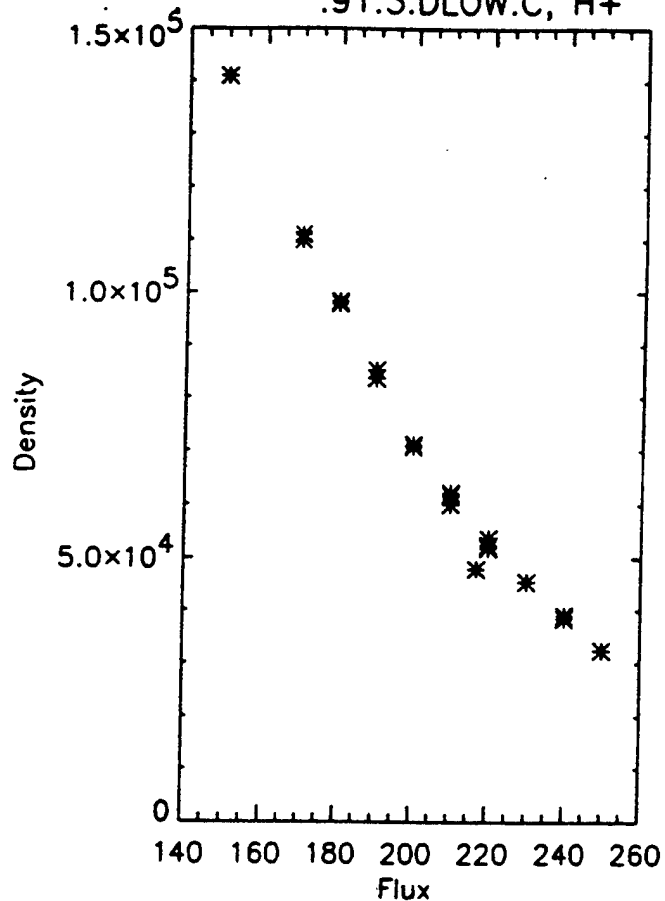
This empirical correlation has been reproduced with the GTIM, using two distinct methodologies. In the first, the model was run to convergence at DMSP altitudes using a given average value of daily flux for the month, but with various individual current daily values of daily flux. In the second, the model is run to convergence as above using average monthly conditions, and then continued for a large number of additional days using randomly generated daily flux values. Both types of run were applied over a wide variety of conditions and both revealed a high degree of correlation between topside densities and daily solar flux. This result applied to the densities at any local time. Within the GTIM it has been determined that the daily solar flux drives the neutral atmospheric temperature specified by the MSIS model, that is in turn an important influence on neutral (and therefore ionized) oxygen densities in the F region topside.

An example of the second type of model test is seen in Figure 10. Results are shown for GTIM densities for both O^+ (left panels) and H^+ (right) at each of 2100LT (upper) and 0900LT (lower). This was a solar maximum (1991), March run, with a variety of daily solar fluxes applied (implicit in the x-axis). The first panel reveals a strong correlation in equatorial 840km O^+ density with the daily solar flux. The second panel shows that H^+ densities are anticorrelated. The lower two panels reveal that the correlation is not as strong at the morning pass (0900LT). It is worth noting too, that the correlation and anticorrelation seen with O^+ and H^+ respectively, would be consistent with the observational trend of a clear correlation at solar maximum (where O^+ dominates) and no clear trend at solar minimum (where either ion can dominate and the effects are in an opposing sense).

GTIM : .91.3.DLOW.C, O+

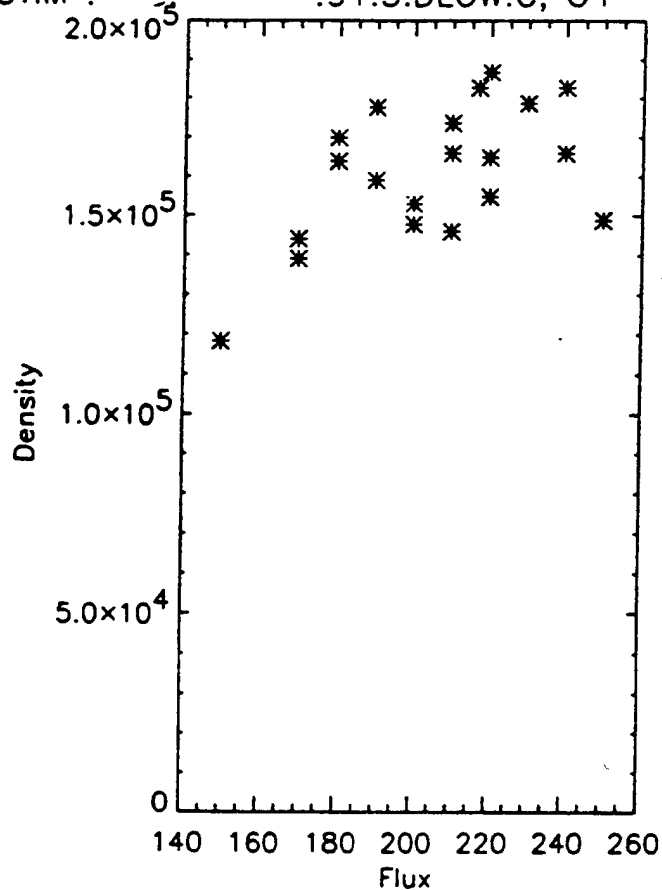


.91.3.DLOW.C, H+



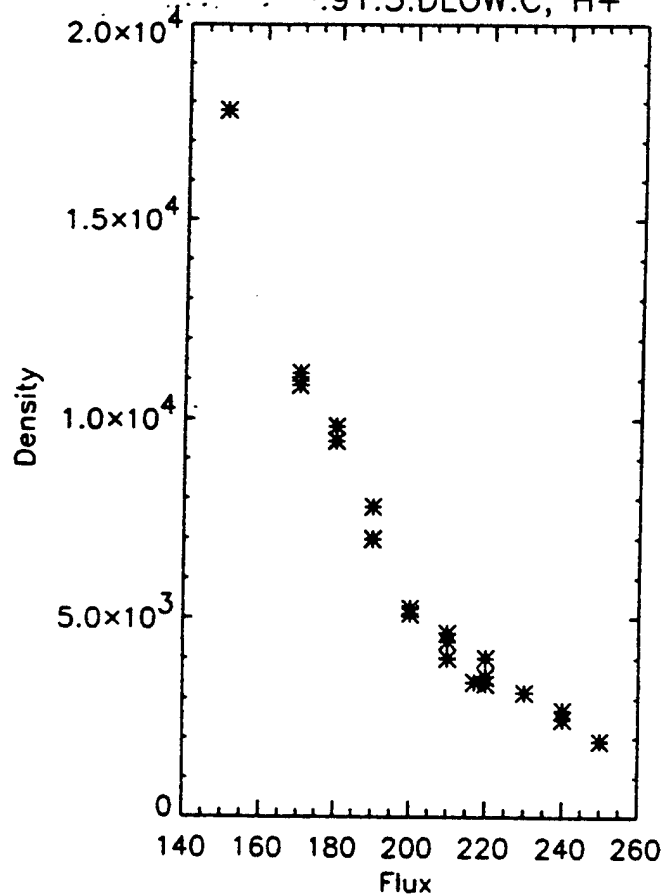
DMSP F10 : 21.00LT, near Lat= 0

GTIM : .91.3.DLOW.C, O+



DMSP F10 : 21.00LT, near Lat= 0

.91.3.DLOW.C, H+



DMSP F10 : 9.00LT, near Lat= 0 21

DMSP F10 : 9.00LT, near Lat= 0

No specific correlations were sought with respect to daily variations in solar-geomagnetic activity. Here it is assumed that magnetic activity will be one factor that induces changes in the daily effective neutral wind and vertical drift level. Future studies may reveal what changes in winds and/or drifts are related in an average climatological sense to a geomagnetic index such as Ap.

4. THE DMSP ALGORITHMS

This section of the report is concerned with outlining all the specific details of the algorithms that can be used to derive effective neutral wind and vertical drift levels from DMSP-based in situ density measurements. The specifics include:

- processing of the raw data
- details of the in situ density parameters that are best correlated with winds and drifts
- how robustness is built into the parameters/algorithms
- how the algorithms are used in an applications sense.

Generally, the process of determining algorithms for wind and drift scaling factors is as follows:

- isolate a quantity that can be identified with each of the neutral wind scaling and vertical drift scaling
- show that in the GTIM, this quantity is largely determined by one process (robust to changes in the other)
- show that the range of values of this parameter in the data and model are the same (that the data can be spanned by a model grid)

- quantify the GTIM scaling factor dependence using the best parameter determined for each case.

4.1 The Best Density Indicators

This section outlines the parameters available from DMSP density slices that provide the clearest signatures of vertical drift and neutral wind levels.

Let us first consider the effects of meridional neutral winds on topside densities. Trans-equatorial transport of ions due to different wind levels gives rise to different levels of asymmetry. To make the indicator robust with respect to vertical drift variations, the equatorial region is avoided. At higher magnetic latitudes, topside in situ densities may be low and thus can contain higher uncertainties, leading to unreliable density ratio calculations. A number of (magnetic) latitude ranges were examined to determine which was the most stable both in the modeling and measurement/sampling domains. Overall, $15 - 30^\circ$ magnetic in each hemisphere proved to be the most stable range. To make the determination robust with respect to daily solar flux variations, the quantity used was the ratio of the northern hemisphere average density to the southern hemisphere average density (where the average is derived within the above latitude range).

In summary then, to derive effective meridional neutral winds:

- take the observations for a given slice (density as a function of latitude), and smooth them in latitude
- take the data between magnetic $15 - 35^\circ$ N, and form an average
- take the data between magnetic $15 - 35^\circ$ S, and form an average
- take the ratio of north to south average densities.

We next consider vertical drifts. The upward transport of plasma in the equatorial

region leads to increasing levels of anomaly crests in the SSIES measured densities, and decreasing densities at the magnetic equator. Meridional neutral winds do bring about differing levels of asymmetry in the anomaly crests and an average crest density is used to remove the wind effects to first order. Because altitude dependence in the vertical drifts can give rise to different locations for the crests, the crest values are taken at the measured peaks rather than using values at a fixed magnetic latitude. An equatorial density is defined as the minimum value seen within 6° of the magnetic equator. The GTIM simulations revealed a clear correlation between increases in the value of the ratio of average crest density to equatorial density and the value of the effective vertical drift scaling value.

As mentioned earlier, there are not always crests in SSIES measurements at 840km, especially at solstitial months when pre-reversal enhancements are typically small, and at low and moderate levels of solar activity when evening prereversal enhancements may be entirely absent. It is worth stressing at this juncture that levels of effective drift derived when the climatological level is small will necessarily be more uncertain. To derive effective drifts at lower drift levels/seasons, a new parameter has been defined; this is the ratio of the equatorial density to the average (northern and southern hemisphere) density in the wings (defined at the same $15 - 35^\circ$ latitude ranges as used above). The use of an average density at middle latitudes largely removes the dependence on wind effects that are revealed in the ratio of the northern and southern average densities.

In summary then, to derive effective vertical drifts:

- take the observations for a given topside density slice and smooth them in latitude
- take the data between magnetic $15 - 35^\circ$ N, and form an average
- take the data between magnetic $15 - 35^\circ$ S, and form an average
- take the average of North and South average densities

- find the minimum density within 6° of the magnetic equator (this serves as both the equatorial value and the trough value)
- find equatorial anomaly crests, and if there are two, take the average of the two peak densities
- parameter 1 is the ratio of average anomaly crest density to the equatorial trough density (if the crests exist)
- parameter 2 is the ratio of equatorial density to the average of N and S wing densities.

4.2 Robustness of Algorithms

This section will review the robustness built into the effective wind and effective drift calibrations. A summary form is preferred here as the reasons for each level of robustness has been described in previous sections.

The algorithms are robust with respect to daily solar flux variations. Daily solar flux variations correlate linearly with absolute densities at DMSP altitudes; this is seen in both measurements and the model runs. Robustness is achieved by only using ratios of densities to derive effective wind and drift levels.

The wind algorithms are robust with respect to effective drift variations. Studies clearly showed that drift effects are concentrated on magnetic latitudes of less than 15° . Robustness is achieved by using a density ratio using only measurements from outside that range. Secondary drift effects are included through the use of additional effective wind calibrations at zero and double the climatological drift levels.

The drift algorithms are robust with respect to effective wind variations. Wind effects manifest in the level of asymmetry in topside densities. Robustness is achieved

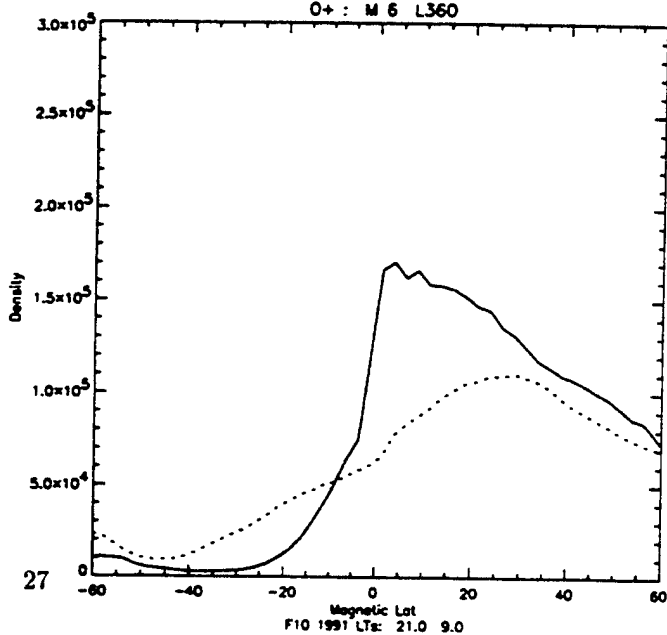
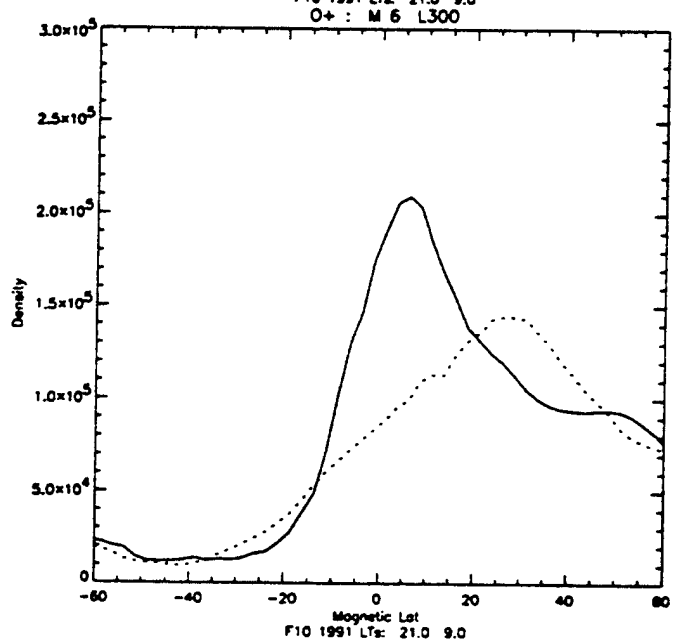
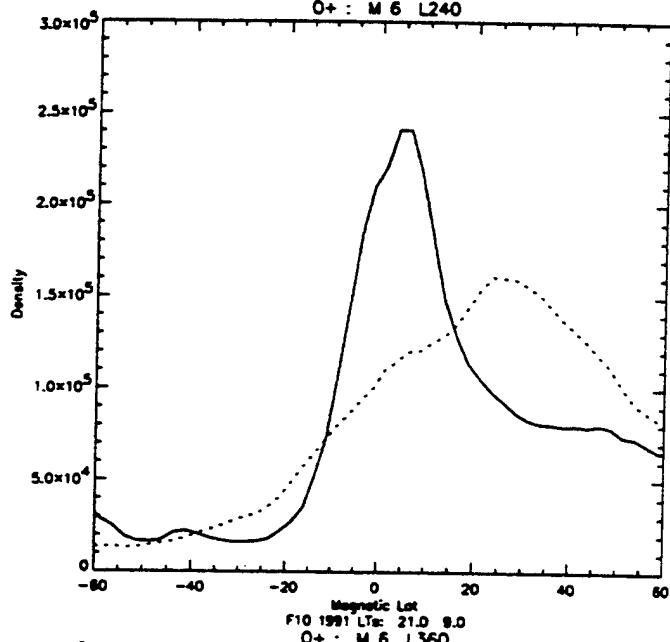
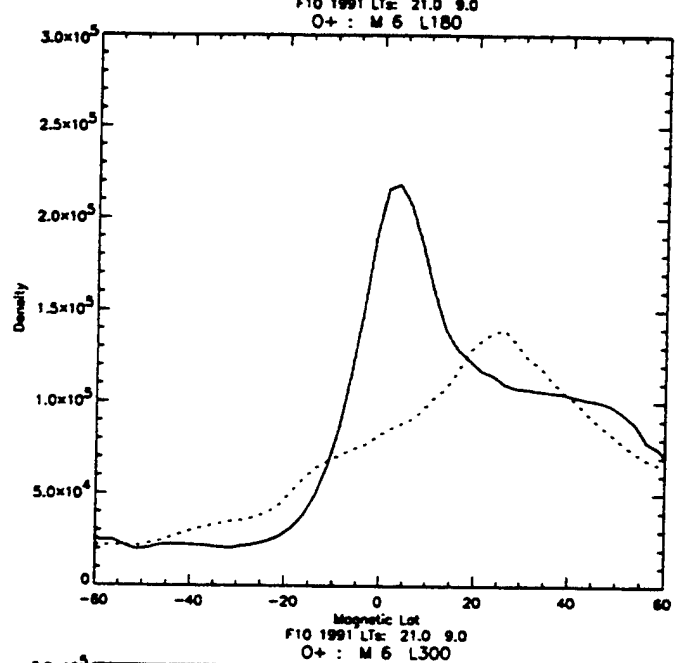
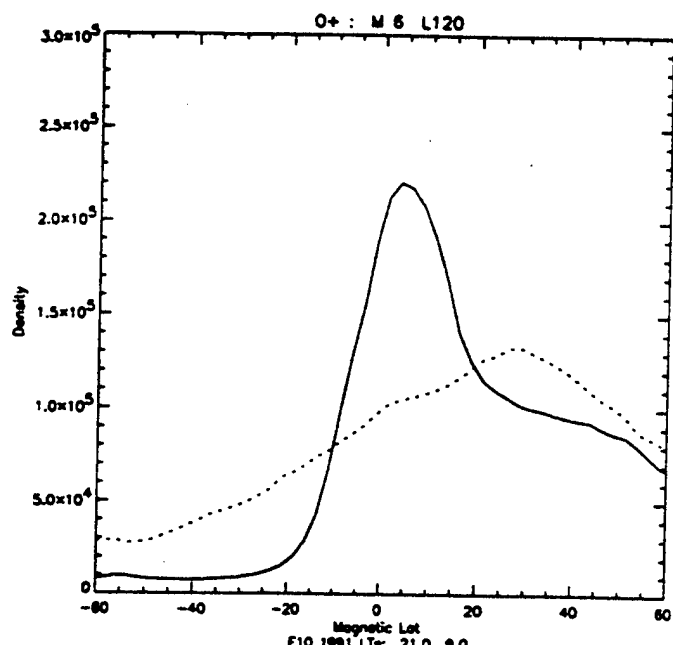
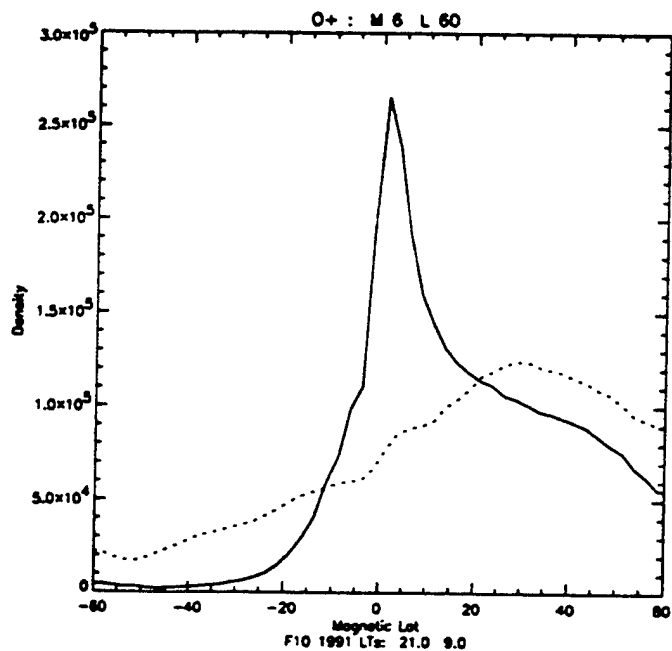
by only using averages of densities in the northern and southern hemisphere, except right at the equator. Secondary wind effects are included through the use of additional effective drift calibrations at zero and double normal wind levels.

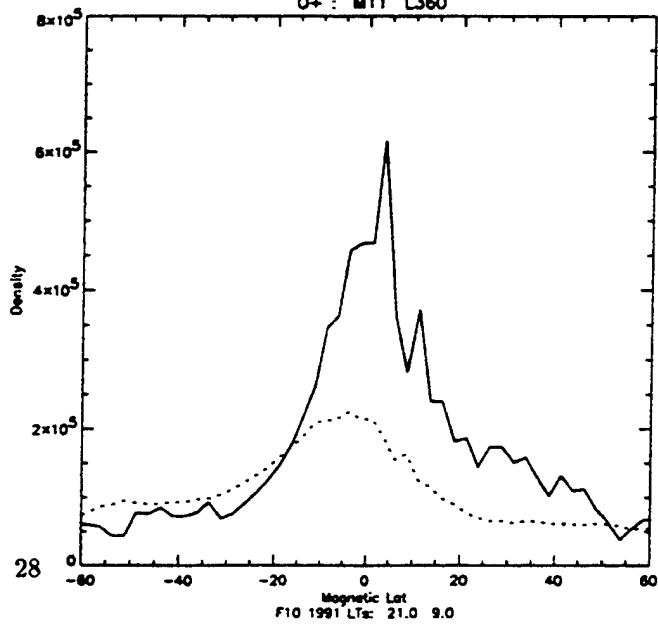
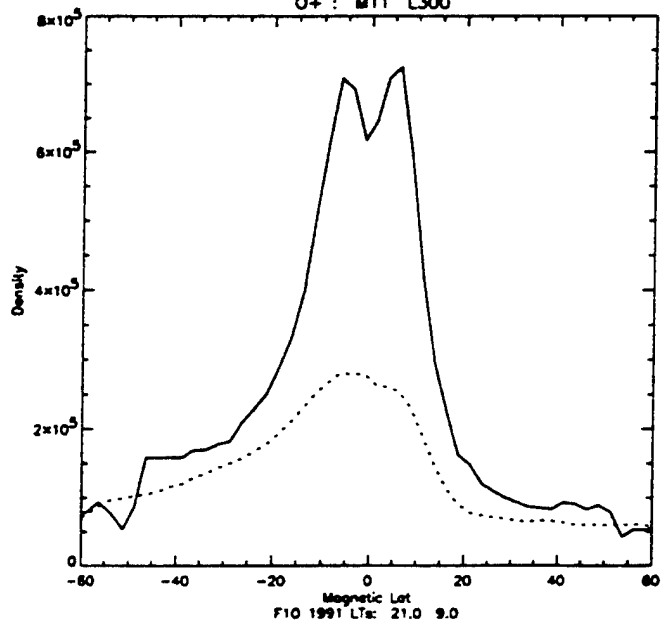
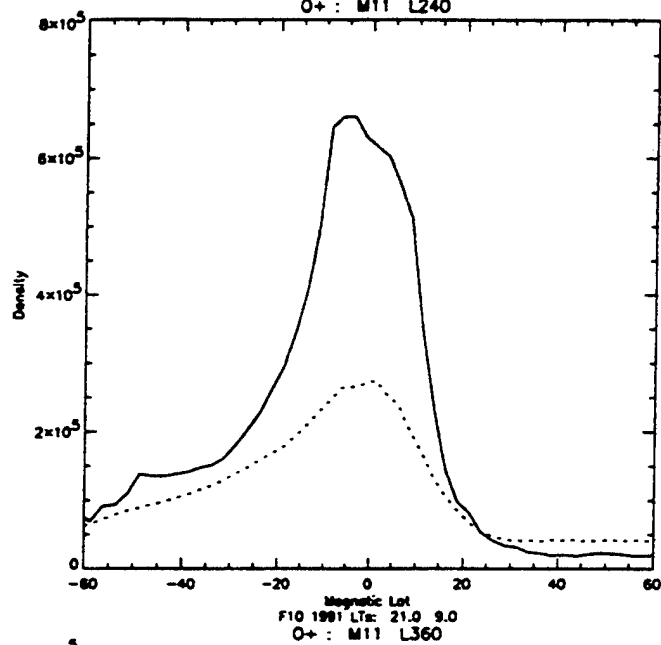
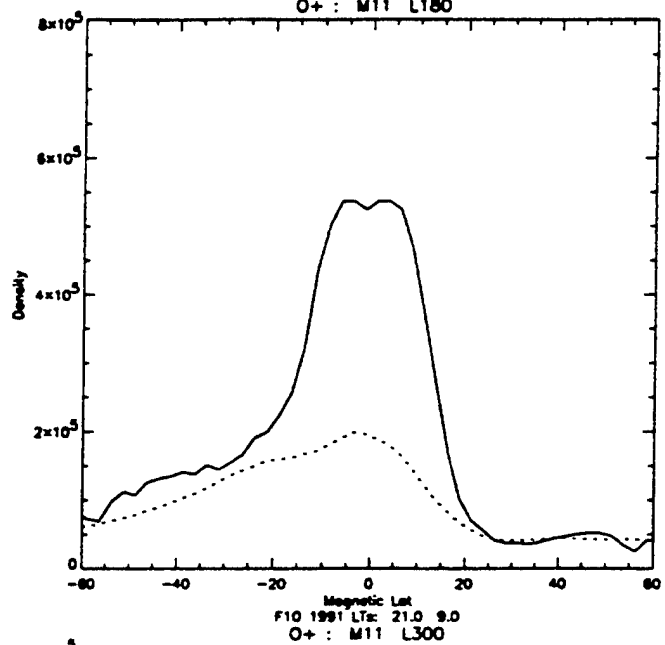
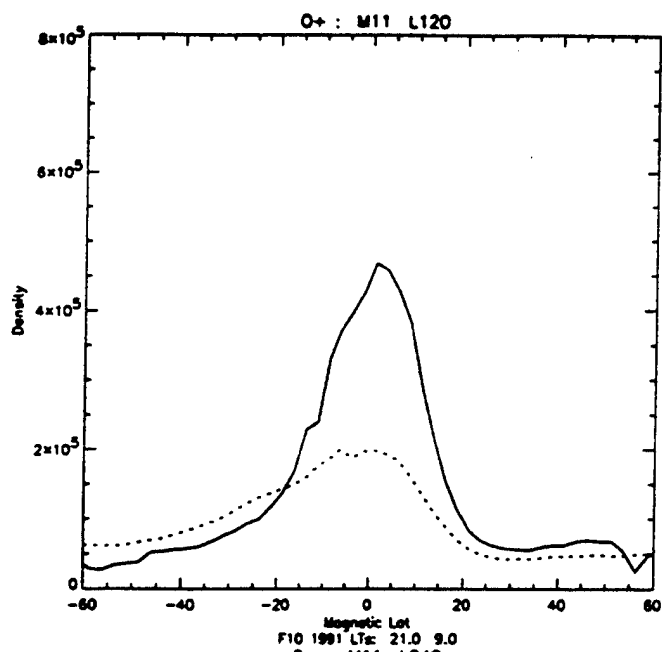
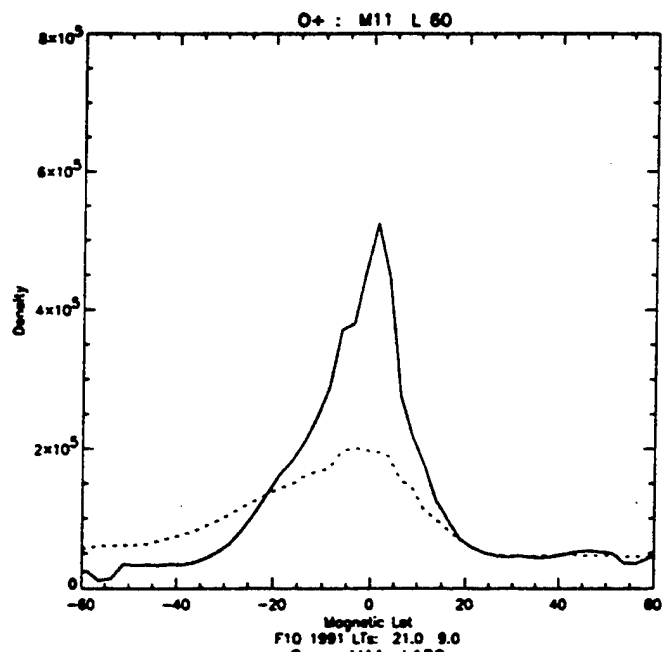
The drift algorithms are robust with respect to altitude-related drift variations. Altitude variations in vertical drifts are revealed by changes in the locations of equatorial anomaly crests (assuming these are visible at all). Robustness is achieved by using actual anomaly crest peak densities, rather than densities at an assumed crest location. Should the altitude dependence result in removal of the crests altogether at DMSP altitudes, then the algorithms will revert to usage of the equator to wing ratio in the derivation of effective drifts. Whenever both parameters (equator to wing and crest to trough) are available to derive effective drifts, consistent values are derived.

4.3 Longitude Dependence

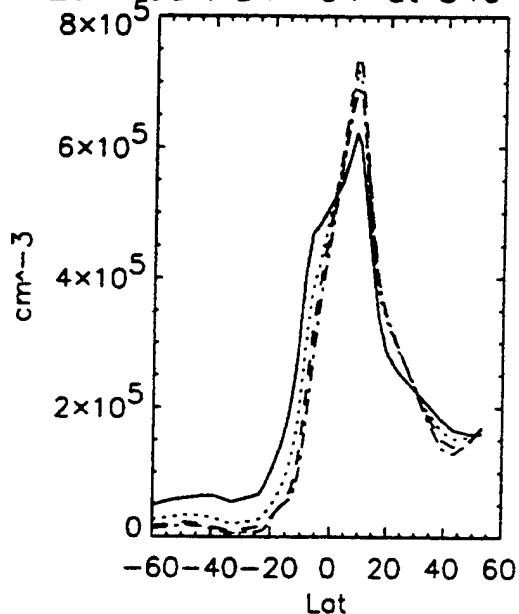
Longitude variations are immediately apparent in the SSIES observations. Figure 11 demonstrates average densities obtained for June 1991 in six different longitude zones (60°E , 120°E , 180°E , 240°E , 300°E and 360°E). Each panel shows the average density versus latitude pattern for the month for O^+ at both 2100LT (solid line) and 0900LT (dotted line) passes. Figure 12 shows the same data plotted using averages for November 1991, and this shows changes even in the morphology of the variations based solely on longitude. It would be clearly desirable to incorporate a longitude dependence in the effective wind and drift coefficient files for use with future DMSP measurements given this level of variation. Because the new GTIM uses a drift model that includes the longitude variations seen in recently published AE-based drift measurements it is immediately available to model longitude effects.

Figure 13 demonstrates an example of the longitude variations predicted by

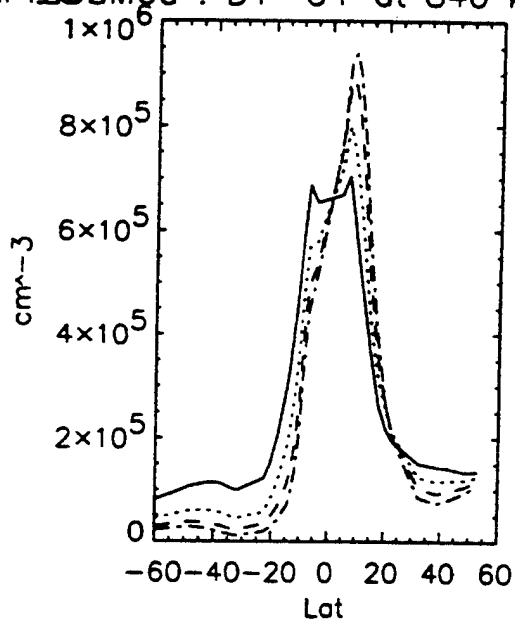




CPI_GTIM6a : D1 O+ at 840 km X60 CPI_X60M6a : D1 O+ at 840 km X120

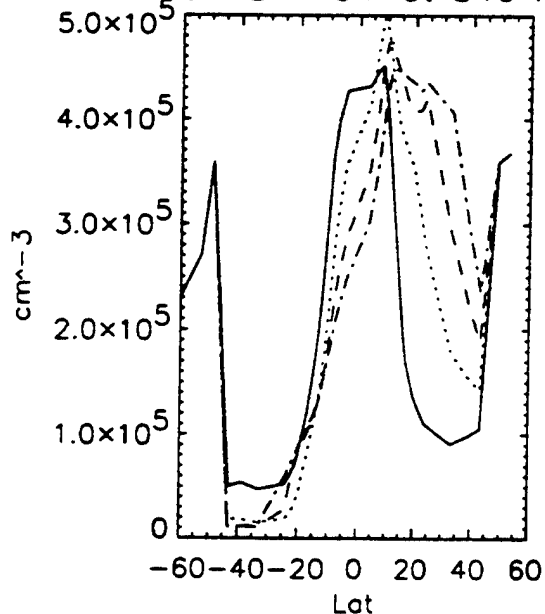


1991 M 6

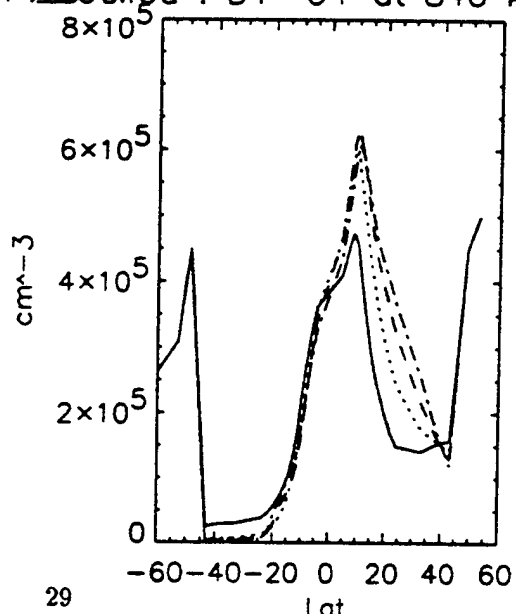


1991 M 6

CPI_GTIM6a : D1 O+ at 840 km X360 CPI_X360M6a : D1 O+ at 840 km X360



1991 M 6



1991 M 6

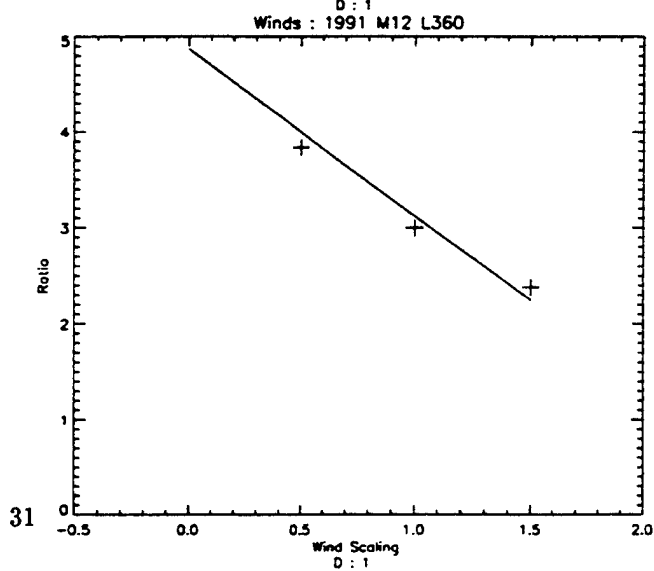
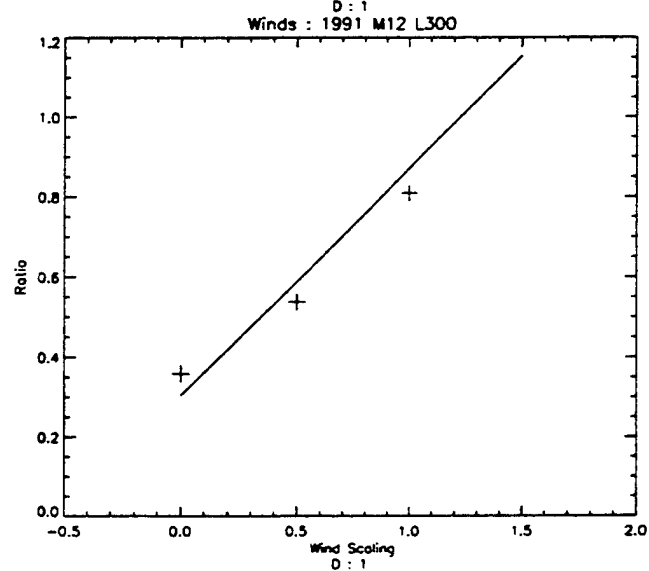
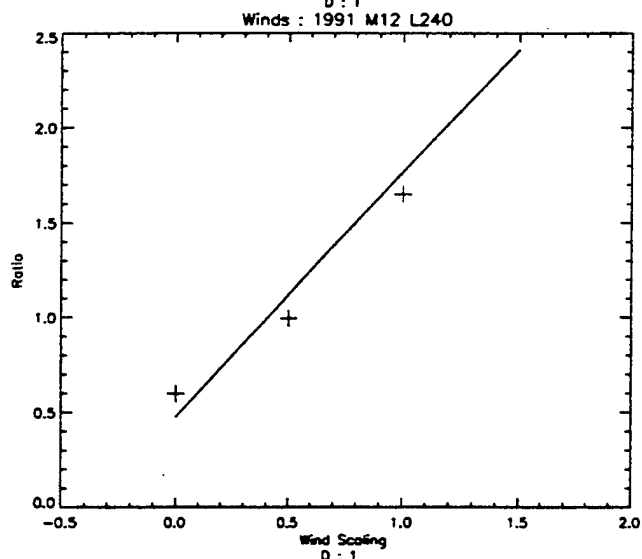
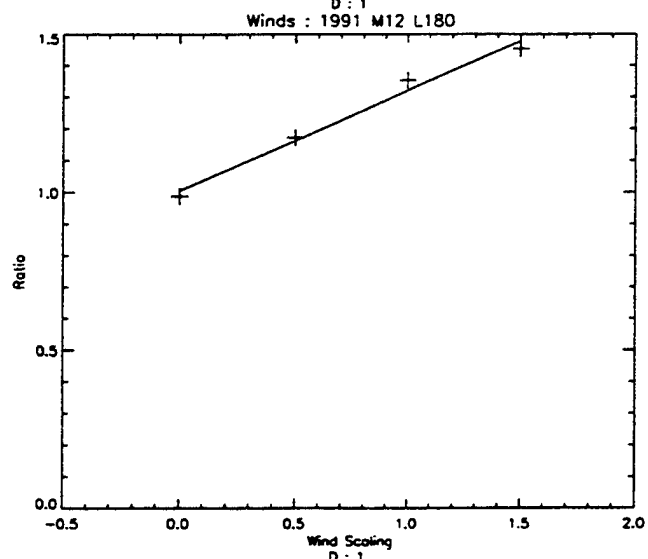
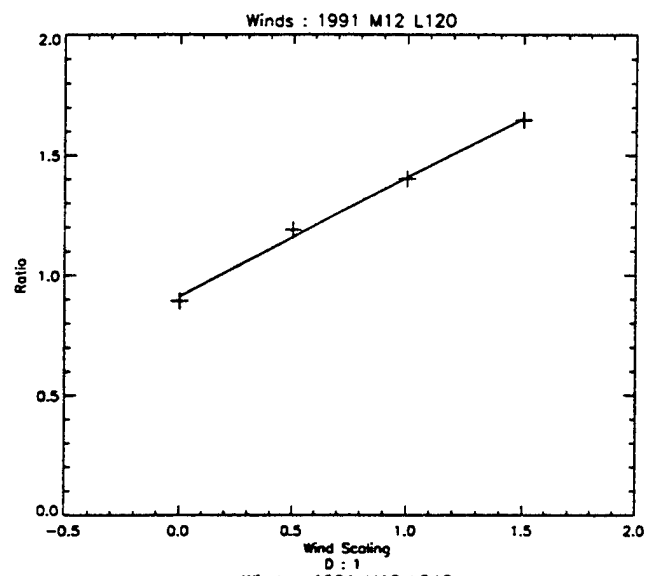
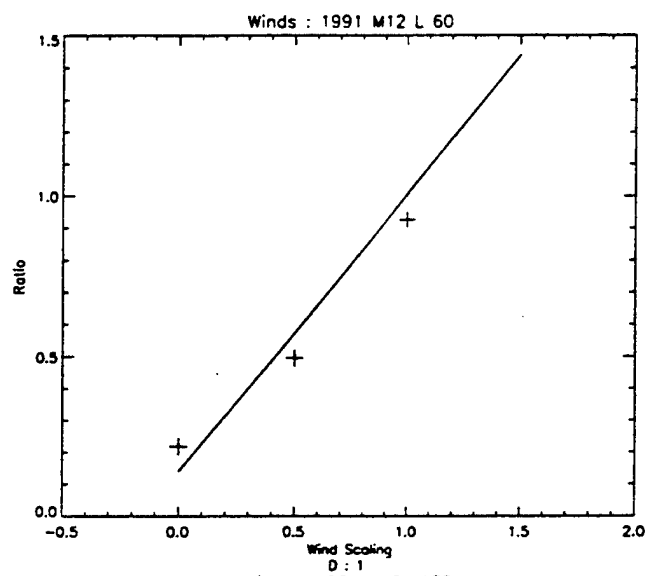
the GTIM. Four panels in the figure correspond to four different longitude sectors (60°E , 120°E , 300°E and 360°E). Each panel shows the predicted O^+ density variations with latitude for June 1991 for a variety of conditions (in this case, various scaling levels of the neutral wind). Clear differences are evident between the panels, especially at middle latitudes.

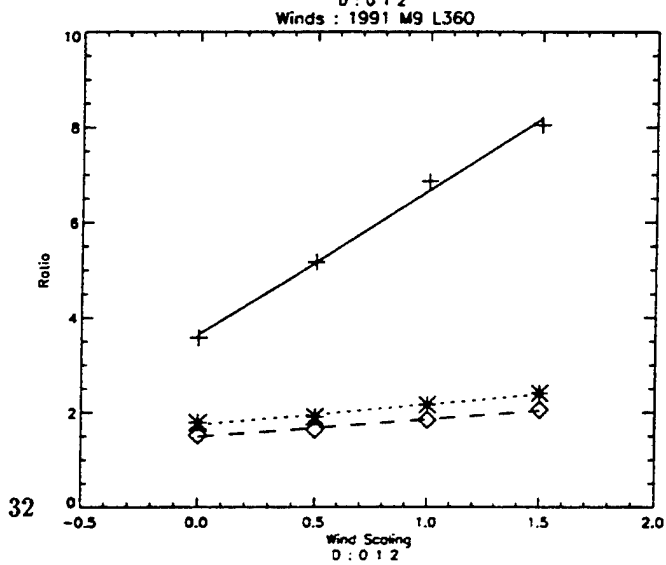
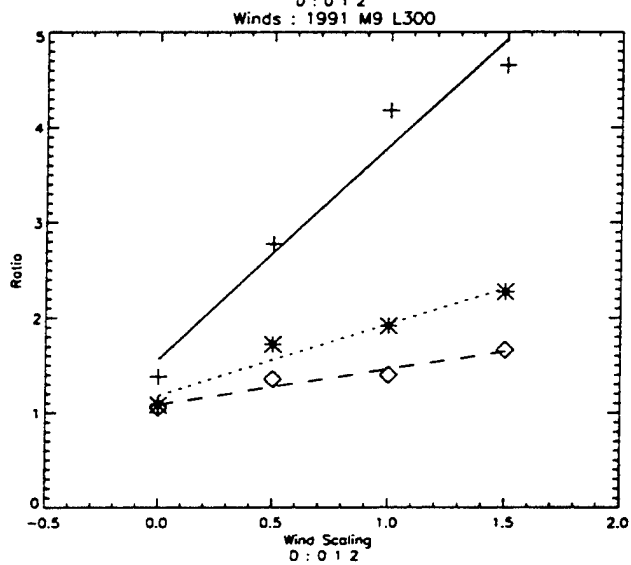
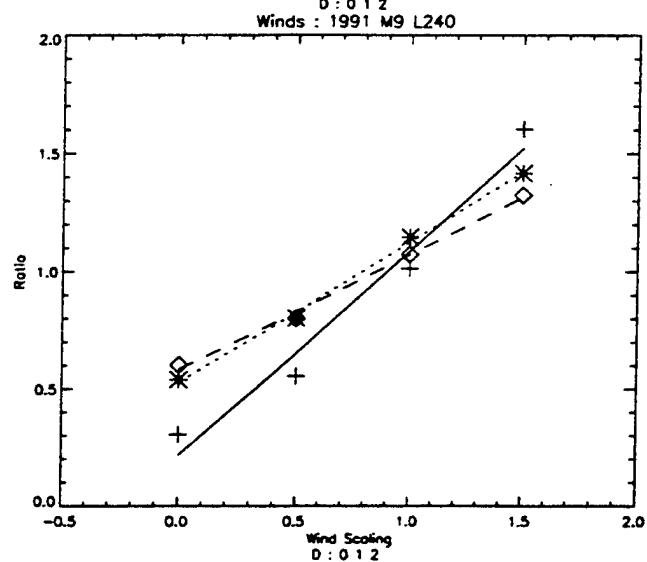
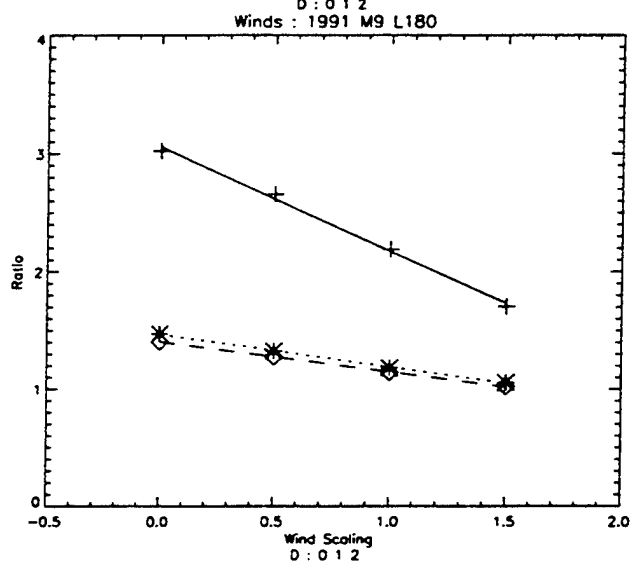
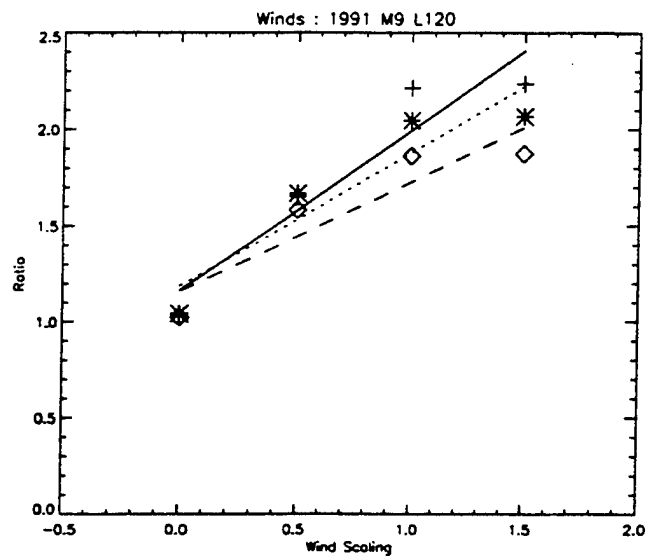
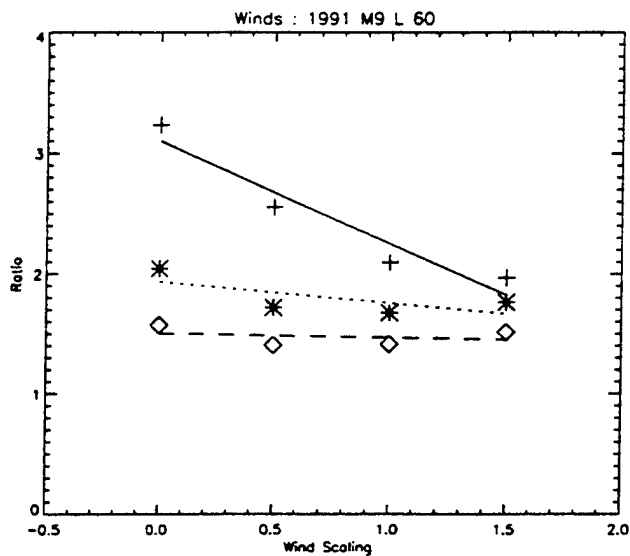
The bigger question, and the resultant larger grid of model runs, is how to define the nature of the longitude variations of the calibrations that define effective wind and drift levels? Instead of simply filling out the GTIM grid of models for all months and all six longitude sectors, a skeletal grid was completed. This expanded grid included:

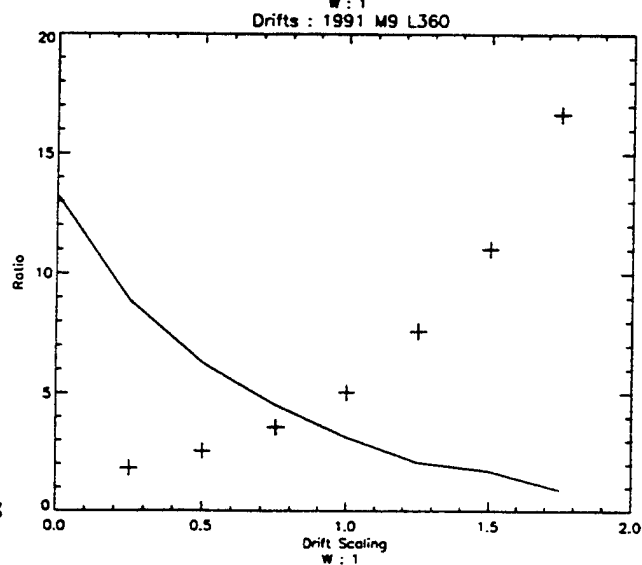
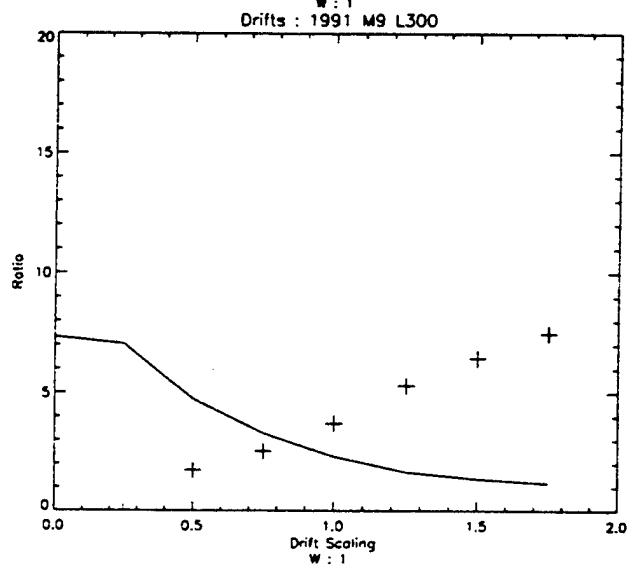
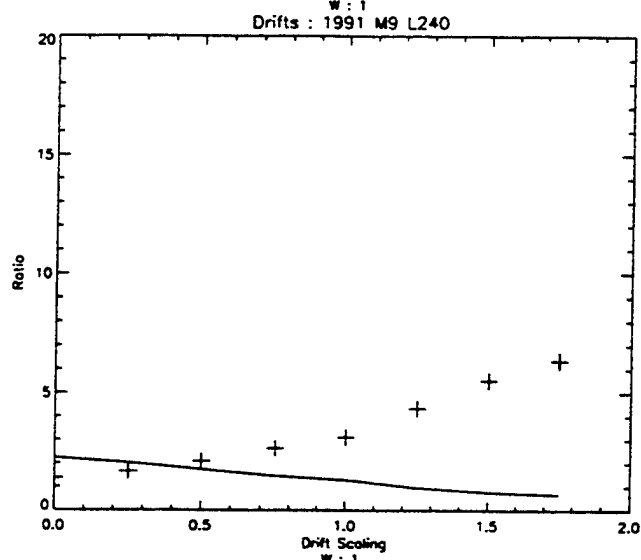
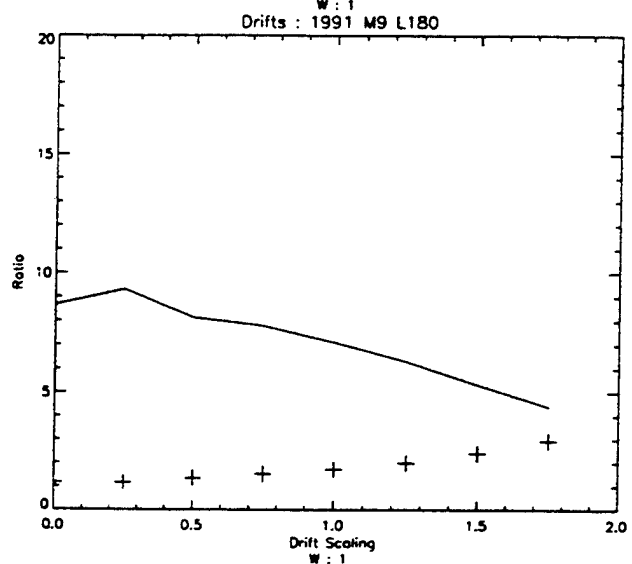
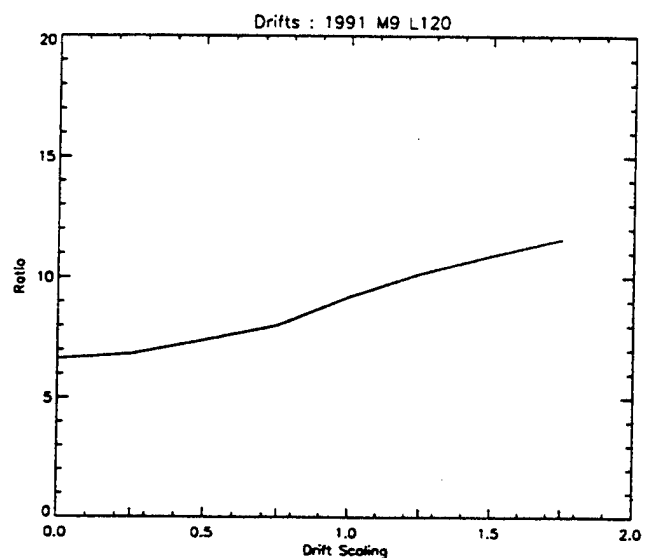
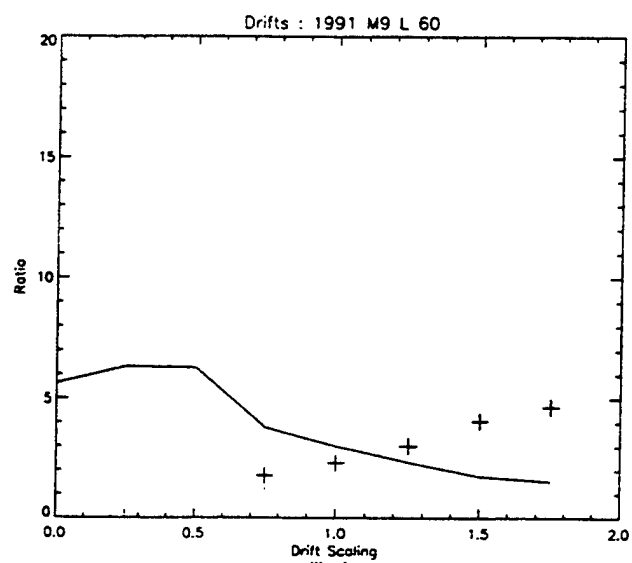
- GTIM runs for all months of the year at a selected longitude (240°E)
- GTIM runs at all longitude sectors at selected additional months (May and November, used to define near-solstice conditions)
- isolated additional GTIM runs as required to fully establish the nature of a given seasonal or longitudinal variation.

Examples of the resulting calibrations between density ratio and effective neutral wind scaling levels are seen in Figure 14 and 15. In the former, where December 1991 results are shown, GTIM asymmetry ratios at each of the six longitude sectors are clearly seen to be strongly linear. Note here that the apparent different type of correlation in the last panel (360°E) is due to the correlation being slightly better for North/South instead of the South/North that was selected as the default at the other longitudes. In Figure 15, the calibrations are shown for all three effective drift levels (0, 1 and 2) for September GTIM runs. This gives some insight as to the drift-related variations in the coefficients.

An example of the resulting calibrations between the two density ratios and effective vertical drift scaling levels is seen in Figure 16. Here, a panel for each of the six longitude sectors shows the GTIM results for how each of the crest/trough ratio (plus symbols) and







equator/wing ratio (solid line) vary with the vertical drift scaling factor, for September 1991 conditions. Note the wide range of variations due to longitude, especially in the crest/trough ratio at longitudes 120E (no crests predicted) and 360E (crest/trough ratios predicted up to a value of 18).

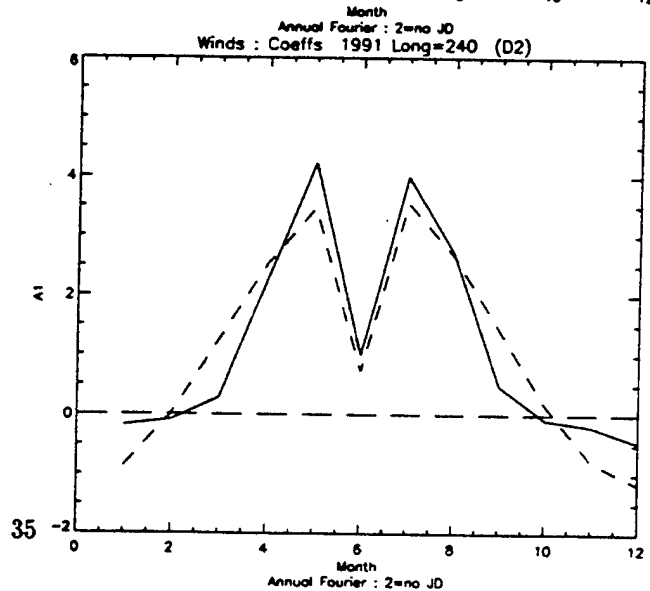
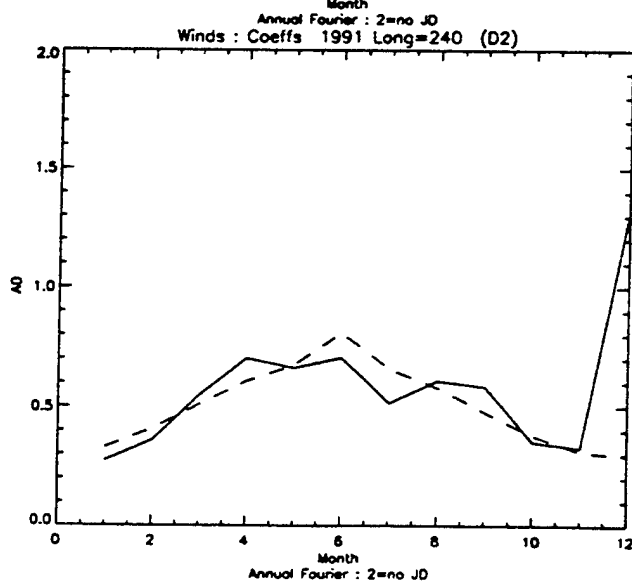
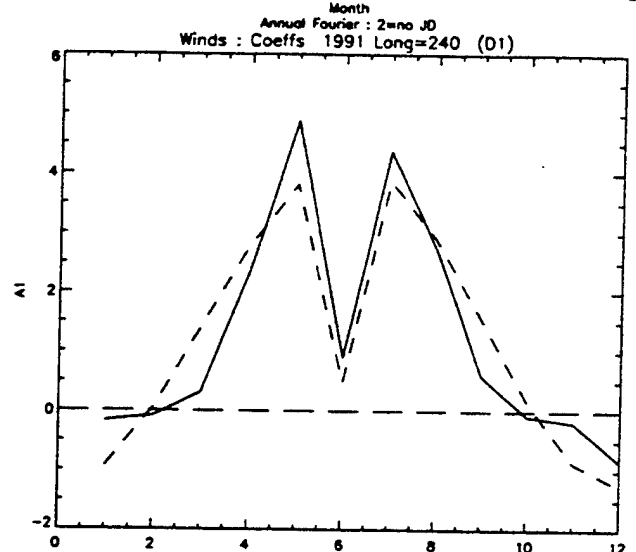
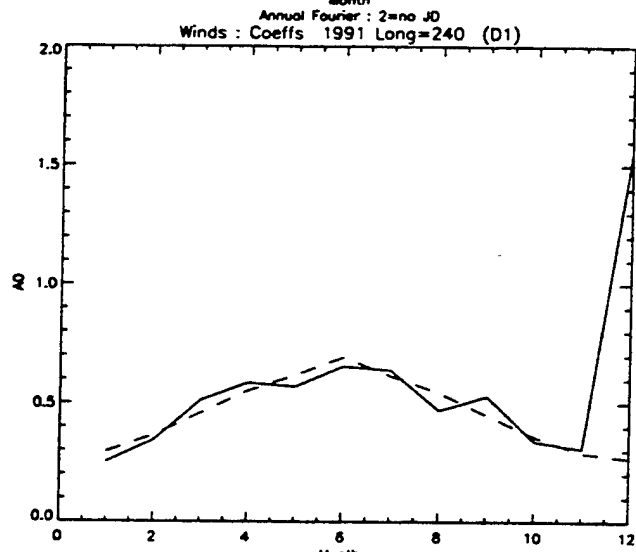
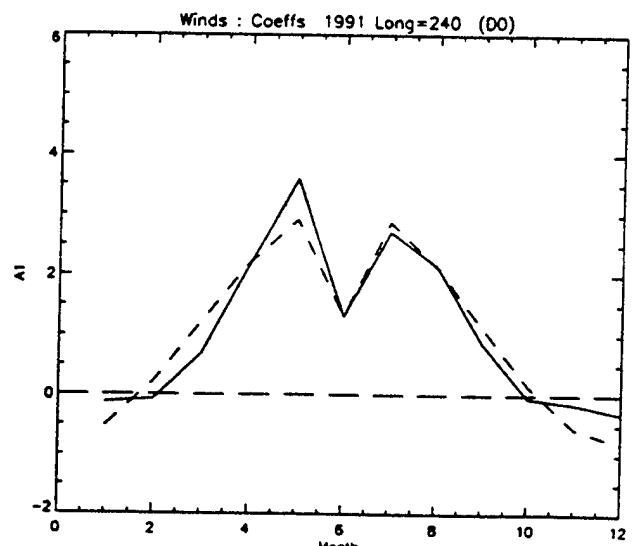
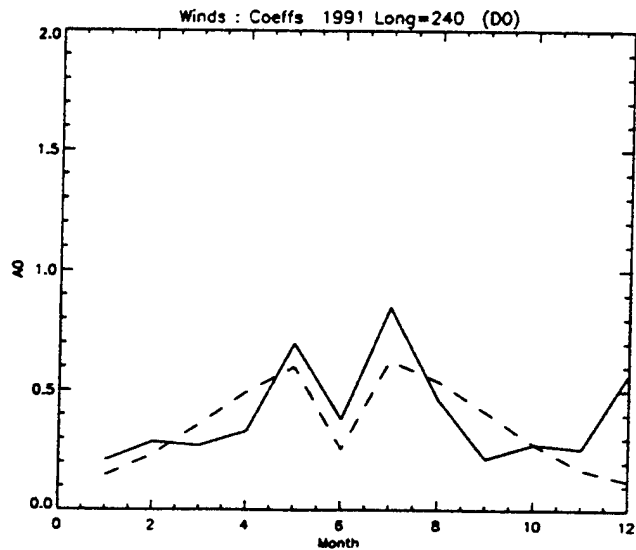
4.4 Algorithms and Coefficients

This section of the report deals with how the best-fit algorithms and coefficients have been developed, and thus, as seen in the following section, how they should be used in a practical sense. While many variations are smooth, the algorithms adopted here utilize both tabular and parametrized forms.

Firstly, we deal with the effective wind scaling factor calibration, as this is the simpler quantity to parametrize. The following list summarizes the breakdown of the calibration into component parts:

- at any month, effective drift level and longitude, there is a linear relation between effective wind level and the ratio of North/South density ratios, as seen in Figures 14 and 15, say. Note that to unify the seasonal variations, all monthly relations have now been converted to North/South.

- at any longitude and effective drift level, the seasonal variations of each of the two above linear-fit coefficients can be summarized in terms of a first-order annual fit, with a June-solstice adjustment. The annual Fourier series coefficients are determined after excluding the two solstitial months, June and December, as hemispheric density ratios are too sensitive to low topside densities in the winter hemisphere. The fitted value at June is then adjusted to better cover the specific June variations. An example of this type of fitting is seen in Figure 17 where results for the 240°E longitude sector are shown. The six panels correspond to the two linear-fit coefficients (left to right), and the three effective drift levels



(top to bottom). The solid lines are the derived GTIM values for each month and drift level and the dashed lines show the modified first-order Fourier fit. Note the smoothing inherent in the fit and the insensitivity to large and probably spurious variations at December.

- the annually fitted coefficients are simply tabulated at each effective drift level and longitude sector.

Next, consider the calibrations involving each of the two parameters used to determine the effective drift scaling factor. As seen in Figure 16, the crest/trough ratio parameter is distinctly non-linear in character. However, inverting this to a trough/crest ratio greatly improves the quality of linear fits. The fit to the equator to wing ratio parameter is linear but it should be stressed that this linear fit frequently changes character (slope) at the effective drift level that marks the beginning of the existence of equatorial anomaly crests (see the 180°E longitude panel in Figure 16). As a result, the two density ratio parameters require seven parameters to describe the variations, specifically:

- a critical value of effective drift, the minimum at which anomaly crests are predicted; above this critical drift value, drifts can be derived using the trough/crest ratio parameter

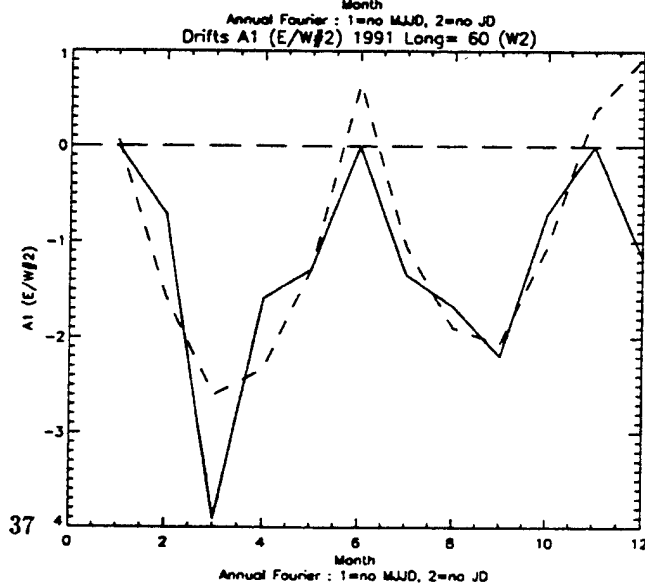
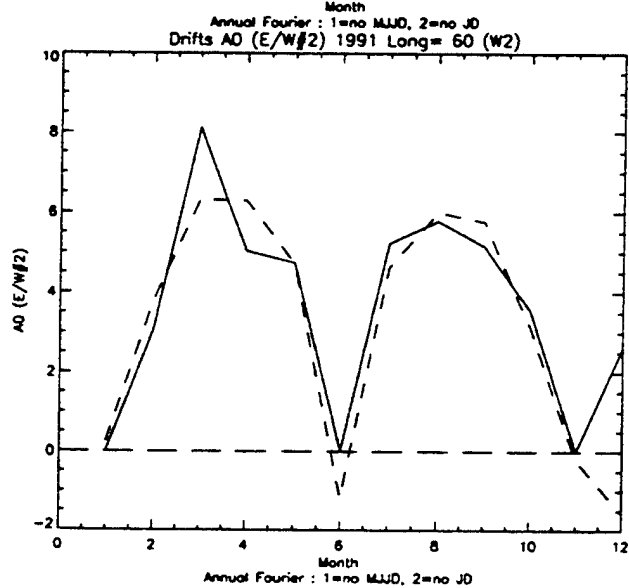
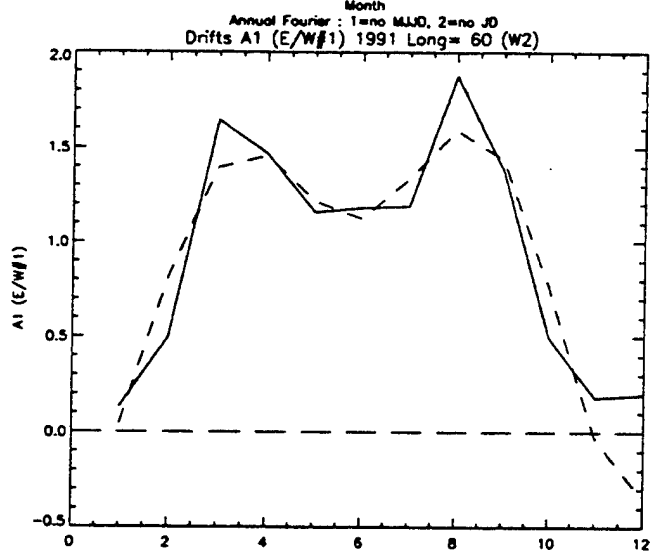
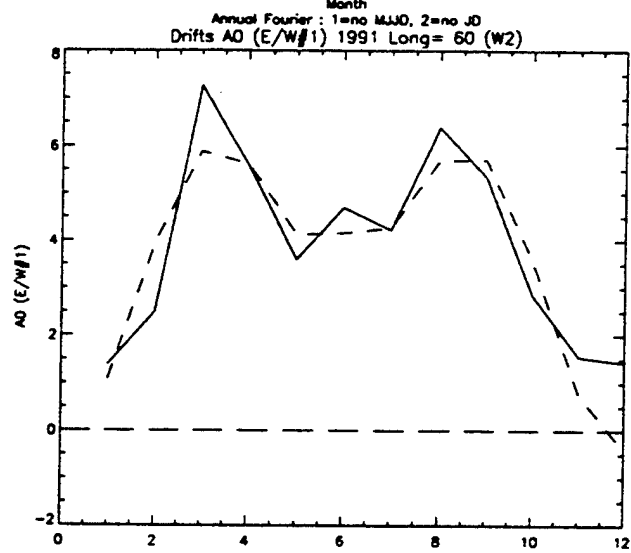
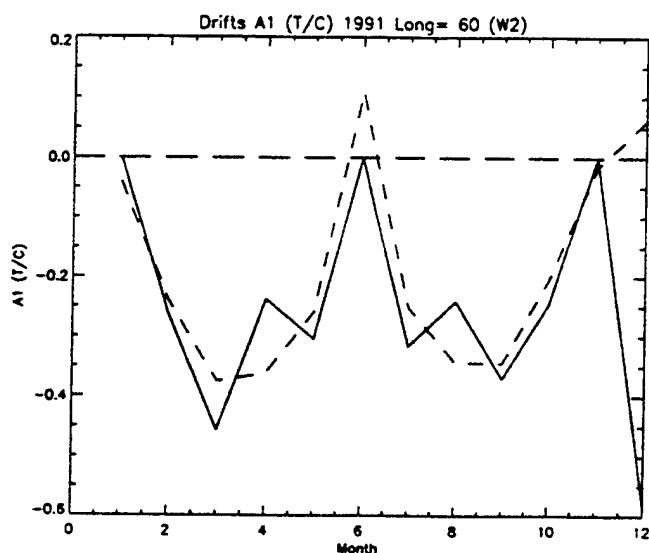
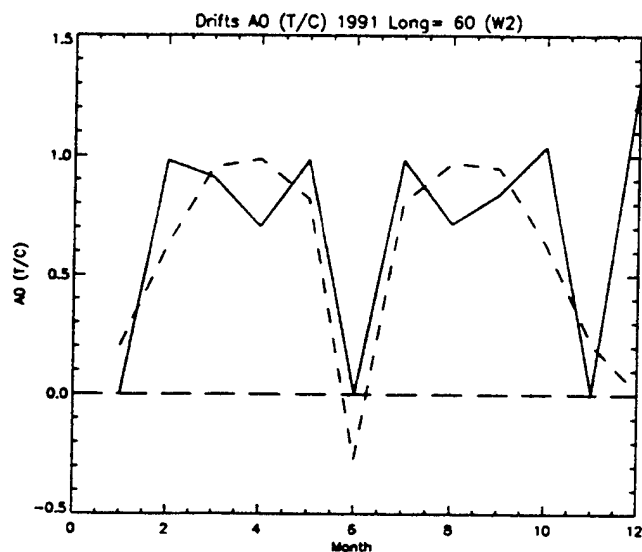
- two parameters, defining the linear relation between the trough/crest ratio and effective drift

- two parameters, defining the linear relation between the equator/wing ratio and effective drift below the critical effective drift

- two parameters, defining the linear relation between the equator/wing ratio and effective drift above the critical effective drift.

These seven parameters form the set that is next to be fit in a seasonal sense, as seen above for the two effective wind linear fit coefficients.

As seen in the example shown in Figure 18, the nature of the annual variations of

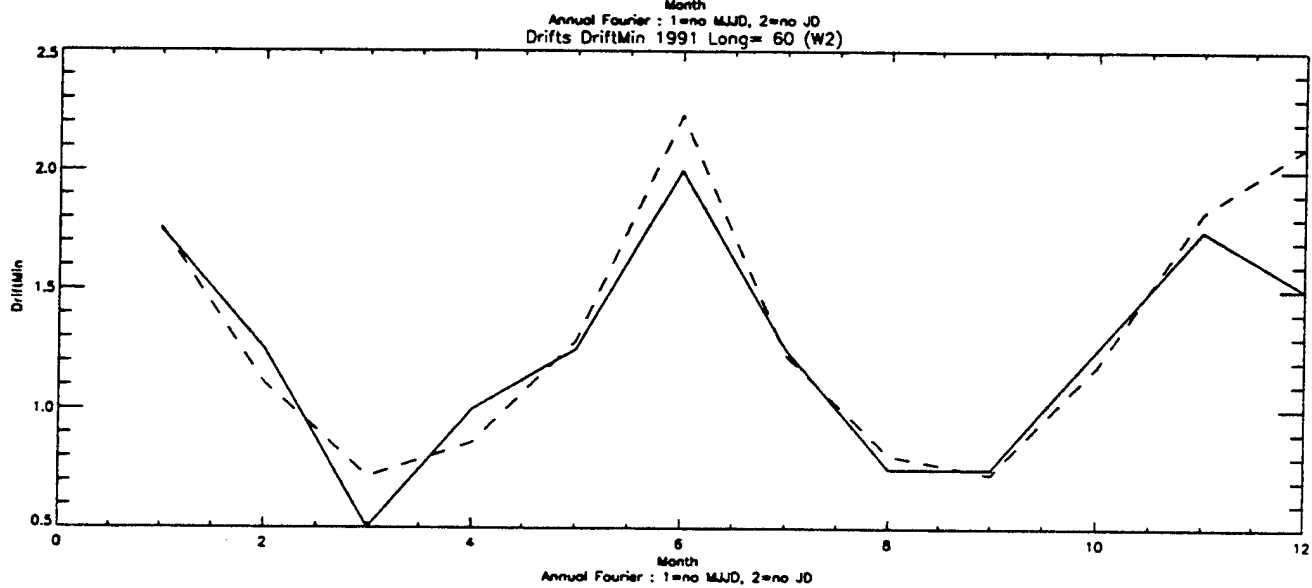
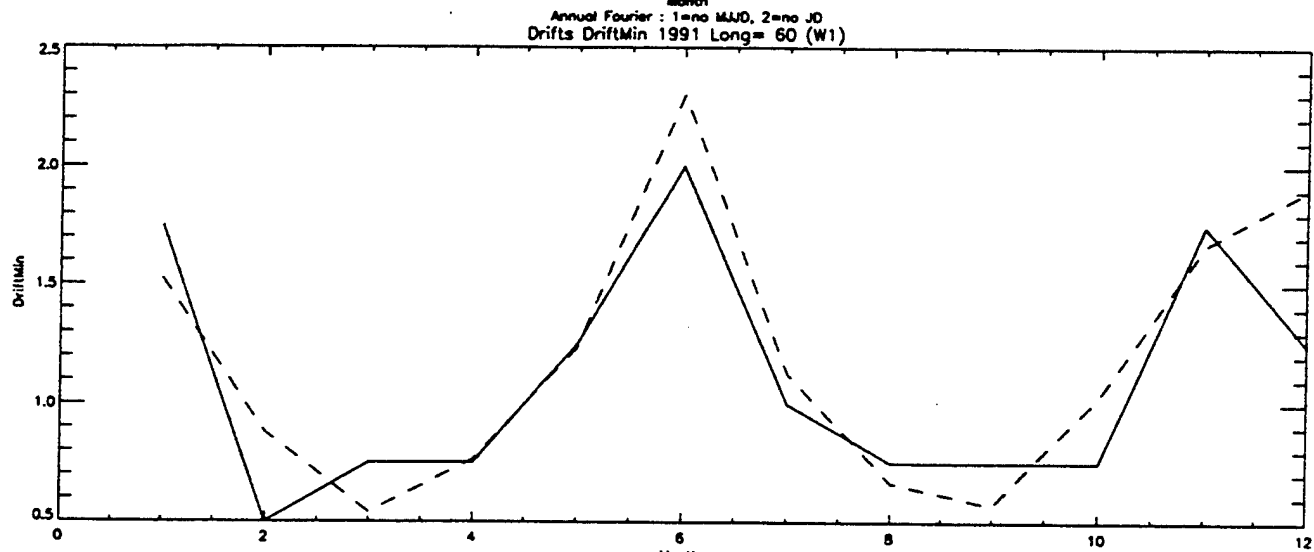
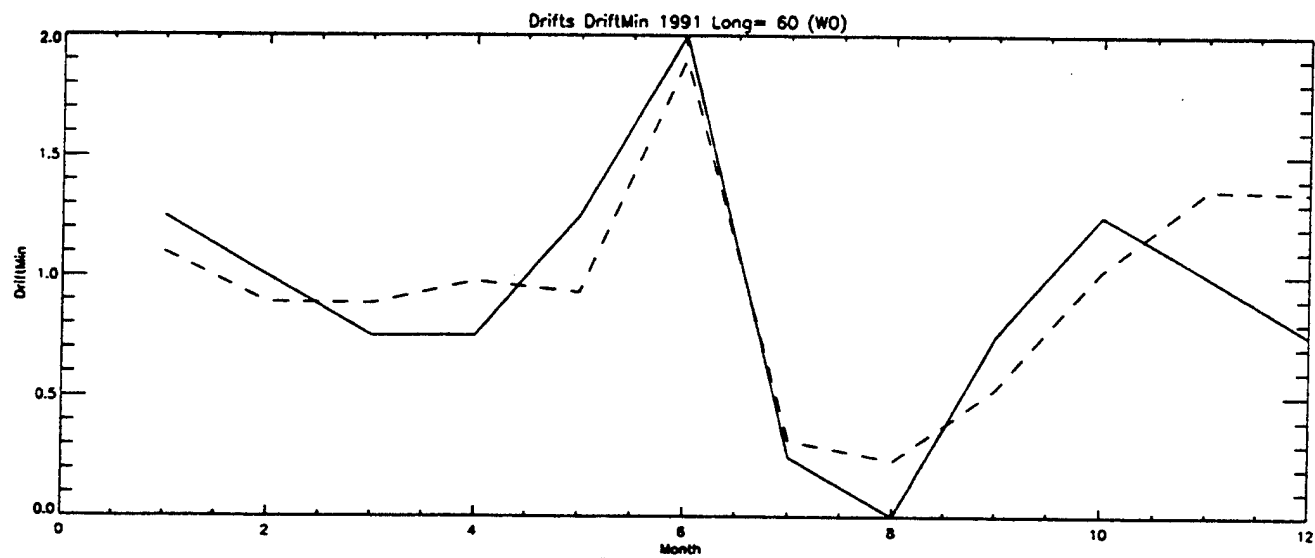


these effective drift coefficients is best described by a second order Fourier series, with again a modification at June solstice. Figure 18 shows six panels, corresponding to the abovementioned parameters excluding the critical effective drift parameter. The panels show the GTIM-derived variations of each parameter for the 60°E longitude, double effective wind level runs, where the solid lines show the fitted coefficients and the dashed lines the results of the second order Fourier fit. Plots such as these can be generated for any longitude or effective vertical drift level. Figure 19 shows an example of the annual variations in the critical effective drift parameter for the same longitude sector, but showing the results from all three effective wind level runs. The seasonal variations here are very recognizable in that the values of effective drift at which equatorial anomaly crests first appear are lower at equinoxes and higher at solstices. This is the variation underscoring the need for a second order Fourier series fit to the seasonal variations, both for this and the other effective drift related parameters.

As was the case for the effective wind parameters, the effective drift parameter coefficients have been simply tabulated on grids of effective wind and longitude sector. The grid has not been fully fleshed out, but only run sufficiently to establish the nature of the underlying variations throughout the grid.

4.5 Use of the Algorithms

Coefficient files have been generated to facilitate the use of these calibrations in determining effective wind and drift levels from in situ DMSP density measurements. Simple Fortran routines have also been prepared that demonstrate their usage. These routines, `drivewind.f` and `drivedrift.f`, are both included as Appendix A of this report, and have been downloaded onto the andersun machine at AFRL where they can be found in the directory `/floor/matthew`. The coefficient files also reside in this directory on andersun.



Note that the routines are to be used iteratively. Specifically, the drivewind routine should be run first. This comes up with an effective wind estimate that is written to a file. This file is read by drivedrift, that uses coefficients appropriate to that effective wind level, to determine an effective drift level that is also written to a file. Then drivewind should be run again if the effective drift level is closer to 0 or 2 than to the 1.0 value assumed in the initial run. This continues until the gridding between the codes is consistent.

In extreme cases, the results may not be an estimate of W or D, but rather an indication such as $W < 0.0$ or $D > 2.0$. The practical application of these algorithms at the next solar maximum will reveal whether or not further grids of model runs (to more extreme wind or drift levels) would be required.

5. MIDDLE LATITUDE VARIABILITY

In this section of the report a series of studies are described. These concern the significance of day to day variability in various parameters of the middle latitude variability, as well as theoretical investigations that attempt to discern the likely underlying cause of the variability.

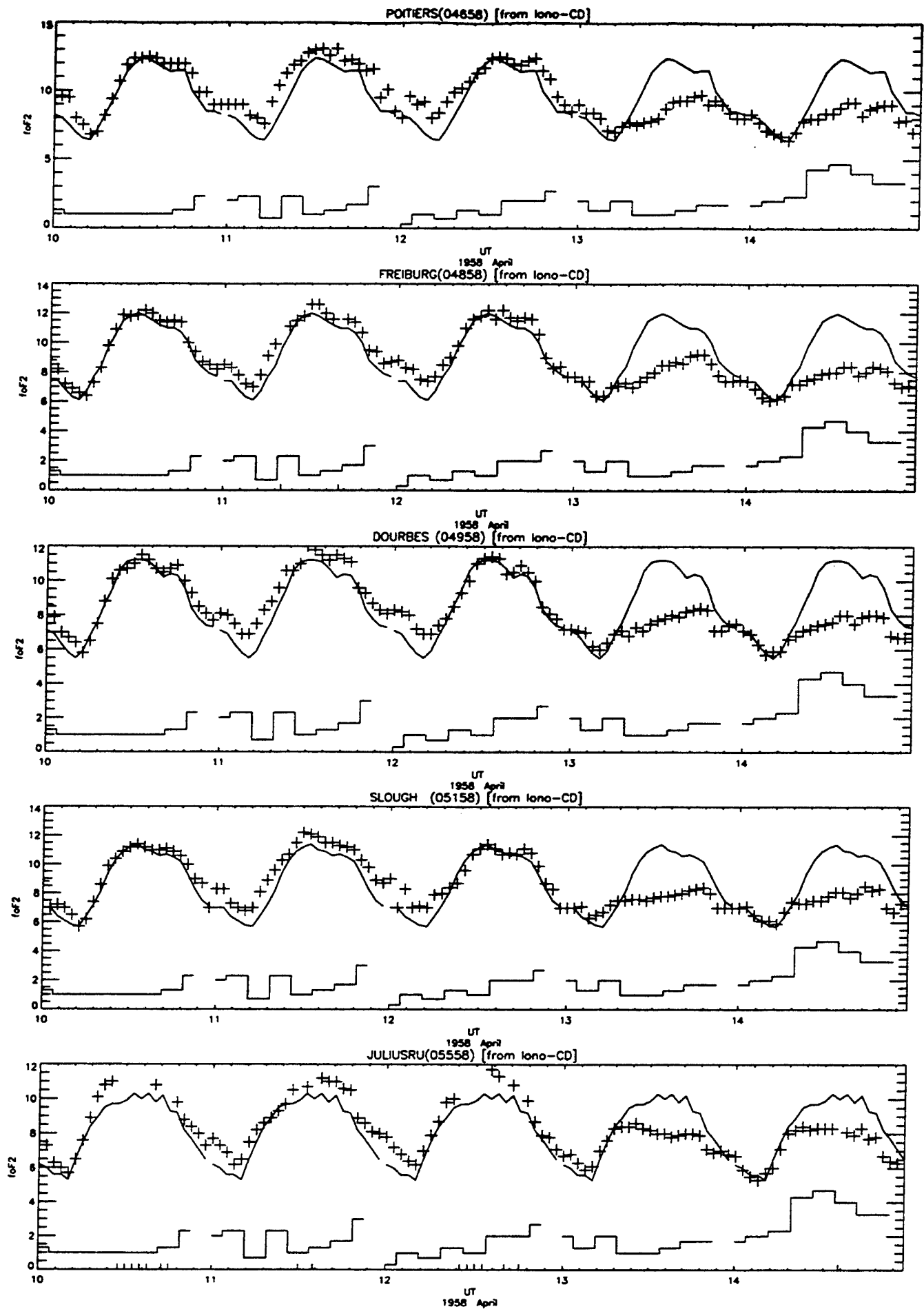
5.1 Dropouts and Quiet-Time Variations

It was proposed in this contracted work to investigate the phenomenon of quiet-time ionospheric "dropouts", these being days when there was a significant depletion in ionospheric densities but no discernible cause (say, geomagnetic activity). Individual cases had been seen in TEC measurements made at a middle latitude station (Hamilton, MA), but no systematic study had been conducted.

Prior to performing a systematic search, it is useful to define what might constitute a "dropout" event. For this, the geomagnetic conditions are required to be truly quiet, so that

an ionospheric event could not be construed as a response to a geomagnetic disturbance. Thus, a search was first made through historical records of Kp (available on the Web at ftp://ftp.ngdc.noaa.gov/STP/GEOMAGNETIC_DATA/INDICES/KP_AP/) to locate the quietest days in each year since 1957 (the earliest foF2 data stored on the NGDC data CDROMs). The software would determine days where for N consecutive days, the maximum Kp attained was no greater than a pre-set value. Different search values were used in order to find the quietest days for years not represented when stricter search criteria were used, and to further augment the sampling. Secondly, for all the stations with data for each of the quiet days, the diurnal maximum of foF2 is compared to the median diurnal maximum for the station-month, and if it is less than 85% of the previous day's value the event is flagged as a possible "dropout". There is subsequently a visual inspection of the daily foF2 records to confirm the significance of the difference. An example is seen in Figure 20, with data from a sample of European stations from several days in April 1958, showing a consistent drop in diurnal maxima on day 13 from a very normal level in day 12. Each panel in the figure shows the monthly median diurnal variation as a solid line, and the individual hourly values as plus symbols. The histogram-like plots along the bottom of each panel denotes the 3-hourly Kp values that is based on the same vertical scale as the foF2 values, and demonstrates the magnetic quietness of the period.

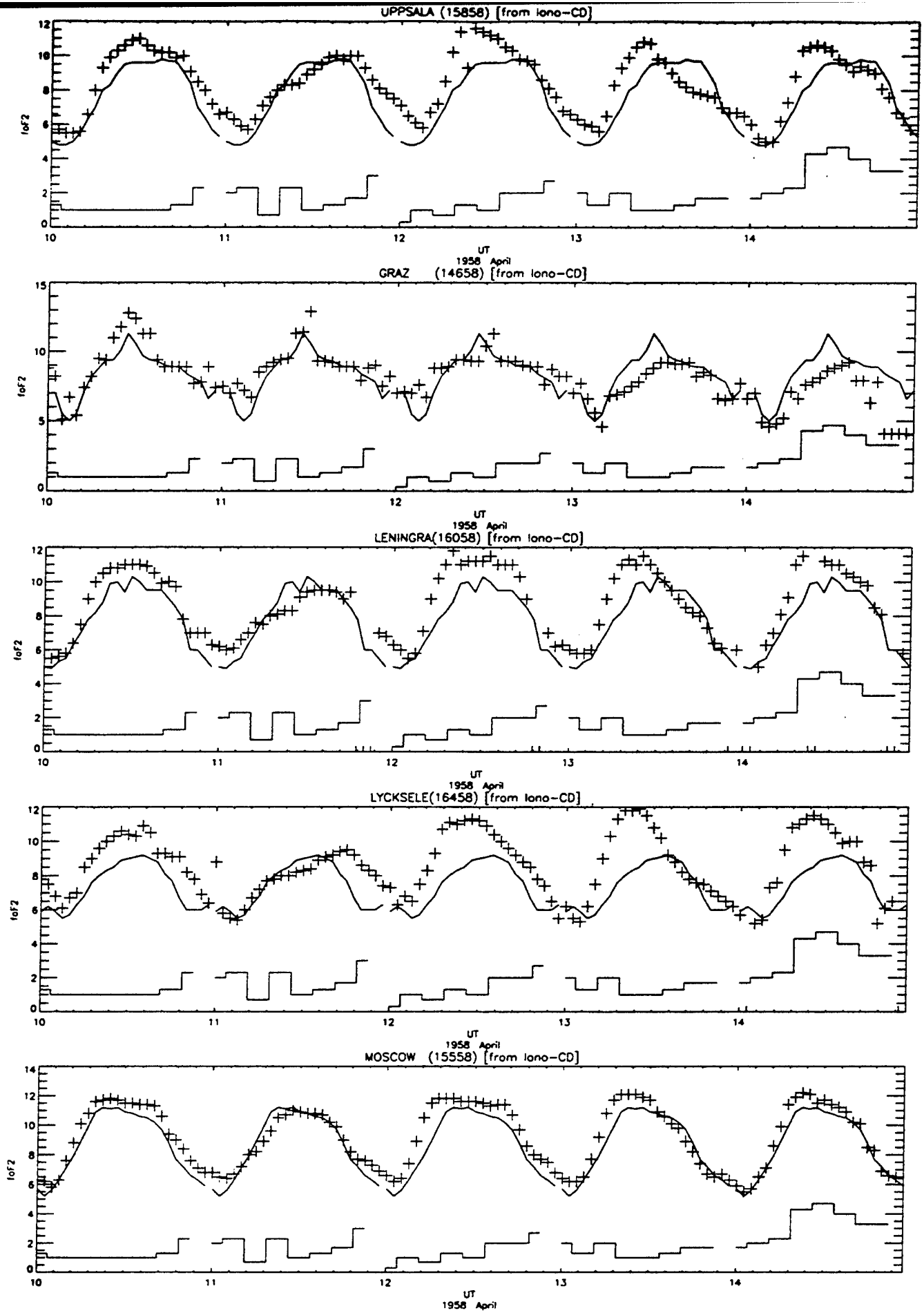
Approximately half the CDROM foF2 database has been searched to date, and a number of events have been catalogued. Preliminary work on this examined the differences between adjacent geomagnetically quiet days in the NGDC CDROM database of foF2 observations, and suggested that dropouts would simply form the tail of a normal distribution of difference values in foF2, and that dropout events seen in TEC may relate more to changes in layer thickness than the layer peak. Later work in fact contradicted those results. Firstly, that true "dropout" events detected via studies of TEC are also seen in the nearby ionosonde data; the ionosonde data being better sampled geographically



establishes that dropout phenomena are regional in nature. That is, dropouts will be visible in a sample of nearby stations, such as shown in Figure 20, but not in all stations in the region, as seen in the Figure 21 example or in other regions (such as stations in the USA or Asian sectors for this example). Indeed, in any given region, there will be ionosonde stations that show either dropouts or enhancements on those dropout days. This observation is strongly suggestive of large-scale wavelike disturbances; scales are implied of one day in time and several thousand kilometers in distance. Table 2 presents a list of events that were found in the NGDC CDRom database, tabulated by year, day of the event and the region affected. Other years are not listed in this table because they showed no such events. As had been seen in TEC dropout studies there is a tendency for the events to occur more often during equinoctial months. The apparent wavelike nature of these disturbances warrants further study.

One additional result of note that impacts on this study related to large numbers of apparently spurious foF2 values in the CDRom database. Filtering of the data is strongly recommended for any statistical studies using this database. Spurious values (including both foF2 values, and dates or other header information) have actually been encountered a significant and surprising number of times overall during this work and caution has been applied in this analysis by simply rejecting data that appears impossible or unlikely or that cannot be properly identified.

Another task planned for the vast foF2 database is to define the level of quiet-time variability in the F region peak. It became apparent that studies of variability of TEC and peak parameters should be conducted in parallel, in order to best present and interpret the results. It should be noted up front that the TEC that is discussed here is the original slant value, to avoid introducing a bias on the sample by assuming a priori that a reliable conversion exists. This would concentrate on the quietest days as defined by Kp, but



will quantify the changes in foF2 at each hour of Local Time, between the current day (quiet) and the previous day (quiet). Trends would subsequently be sought in terms of season, LT, geographic region and so on. It would also be instructive to use the GTIM to determine the level of variation in the MSIS neutral winds required for that level of variability in peak density.

Let us first summarize results from TEC (GPS, Arequipa 1996 only, to date) and foF2 and Hmax (NGDC CDROM, two solar cycles). Overall levels of variability, and variability during quiet periods are listed in Table 3. Note that the values listed in the table have defined variability as the standard deviation of the distribution of difference values that are themselves expressed as a percentage.

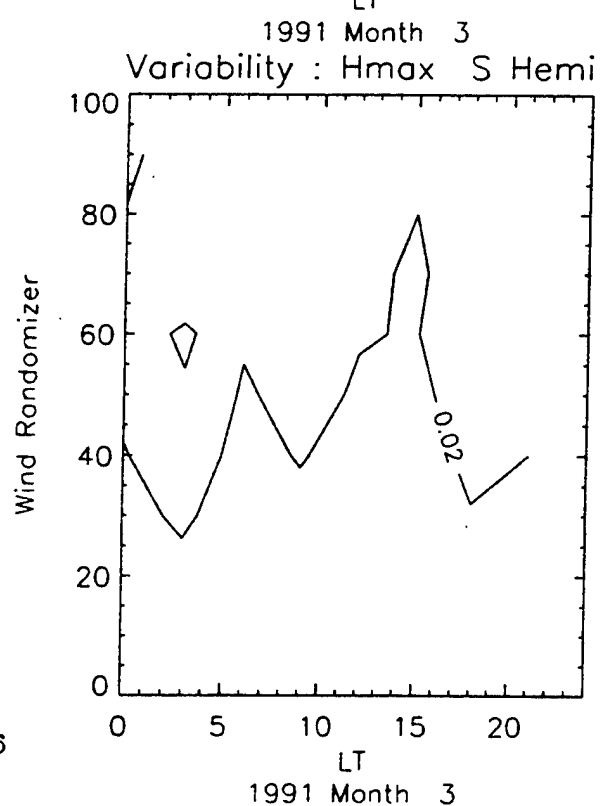
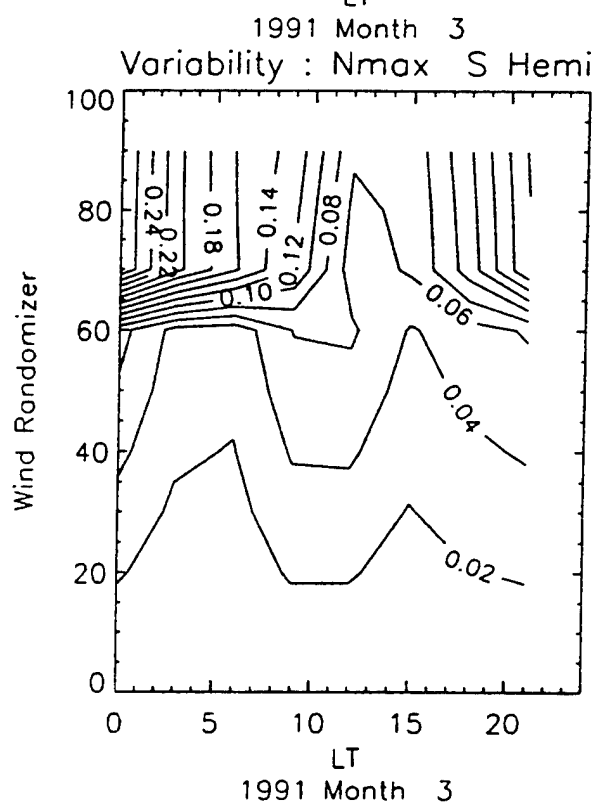
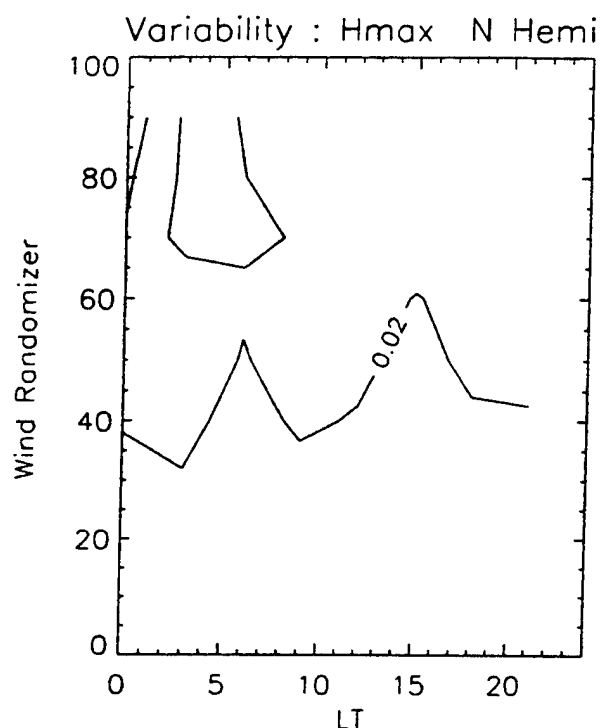
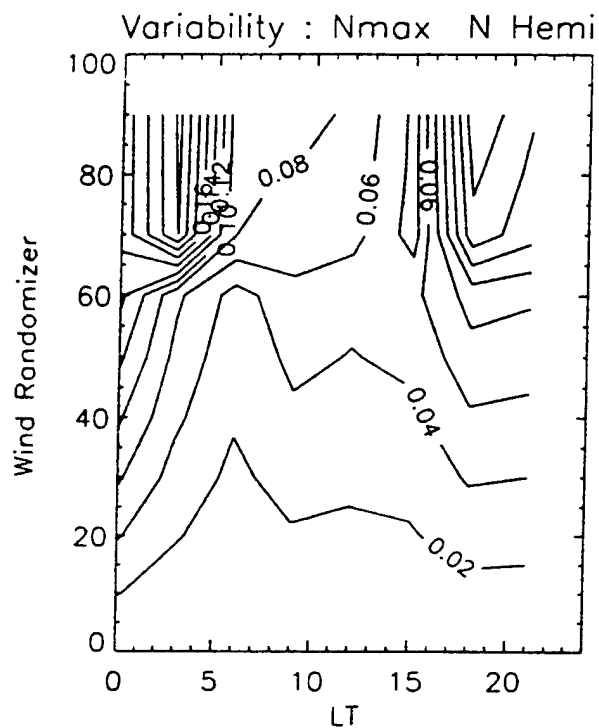
Some additional notes are made on the distribution of day-to-day differences values.

- That quiet-time variations are essentially as large as all variations together, indicating that the distributions of day to day values is not significantly affected by active or storm-like conditions. In other words, variations at middle latitudes are just as significant during quiet periods as active periods.

- Absolute foF2 changes show seasonal and LT variations. Relative changes peak in January with no LT variation. However, there is no peak observed in the distribution during equinoctial months (when geomagnetic activity tends to peak).

- Quiet-time differences showed a very slight tendency to decrease from one day to the next, and indeed, the foF2 values also decreased slightly from one quiet day to the next; the variations are greater for nighttime values and lower latitude stations

- TEC variations show strong LT variations and some seasonal variations.



5.2 Modeling Middle-Latitude Variability

A modeling study has been undertaken to determine the role of neutral meridional wind variations in ionospheric variability. Here, an $L=2.0$ fieldline is modeled using the GTIM for a period of 10 days to ensure convergence. After this period, a random wind is added to the HWM climatological value at each successive time, scaled by a maximum value, and the variations in subsequent days of peak parameters at selected local times is examined. Tests have been conducted at a variety of months and solar minimum, moderate and maximum conditions. Sample results are shown in Figure 22. Panels to the left correspond to N_{max} , while H_{max} is seen to the right. Northern hemisphere results are seen in the top row, and Southern in the bottom. Each panel shows the fractional standard deviation of each parameter as a function of local time (x-axis) and the magnitude of the random neutral wind component in ms^{-1} (y-axis). These solar maximum results show maximum variations of around 10-15% in N_{max} (well short of the 36% seen in observed N_{max}) and only 2% or so in H_{max} resulting from these random neutral wind variations. While the figures at solar moderate and solar minimum conditions are higher (20% and 35%, respectively in N_{max} , 4% and 8% in H_{max}), the facts that values are generally lower than the observed values and that they are strongly solar activity dependent leads to the conclusion that mid-latitude F region variability is **not** a result of random surges in neutral meridional winds.

6. LOW LATITUDE VARIABILITY

Following on from the work in the previous section, our attention is now turned to model-based variability studies of the low latitude ionosphere, considered here to be the region inside and around equatorial anomaly crests. Two particular studies are highlighted:

- a modeling study to investigate the likely impact of a recently devised model the disturbance dynamo that drives vertical motions

- a modeling study to investigate the predicted effects of meridional wind surges on the evening sector equatorial anomaly structure, especially the asymmetry.

6.1 Dynamo Model Driving

The GTIM is an established model at low latitudes that has been shown to provide a good description of the equatorial F region when \mathbf{ExB} vertical drifts are known. As such, it is a good basis from which to attempt to model the ionospheric effects of (geomagnetic) disturbances at low latitudes. The motivation for the study came from a newly-developed empirical description of disturbance vertical drifts from Utah State University (hereafter, USU) driven by the magnetic AE index. A further implication in terms of this contract work is to investigate the nature of ion density changes to impulsive events (i.e. storms), as this will provide constraints on the nature of real-time adjustments that will be of concern when the multiple-ion GTIM begets the next generation of PRISM model.

An adaptation of the GTIM was thus developed, performing normally for a number of days using quiet-time or climatological drifts to allow convergence of the ion densities (filling of the plasmasphere is not a concern here as all the fieldlines considered in these runs are low L values). At storm onset the disturbance drifts are used at each subsequent time step until the drifts have again relaxed to the quiet-time pattern. The model is then run for three additional days to be able to judge the relaxation time for the modeled ionospheric response. At the lowest fieldlines (Mode=2 in GTIM parlance), the model has been modified. Normally the GTIM will generate a low fieldline ($L=1.026$ usually) at a given local time and then terminate the run when the apex altitude reaches a lower limit (physically, the fieldline is then at a low enough altitude that loss will dominate and

thus the ions recombine), and coverage at low latitudes is obtained by starting fieldlines at a number of different local times. In this case, we want to pursue all fieldlines over a period of a number of days (if only to simplify the accounting) for these disturbance drift studies, and so the lowest fieldlines are maintained at the lowest altitude (i.e. fixed at the minimum altitude) until a time when upwards convection has again compensated for the net downward movement. For clarity the modeled response presented is in three-day blocks corresponding to "during" the storm and "after" the storm, concentrating on the difference between the modeled ionosphere and the (converged) ionosphere prior to storm onset.

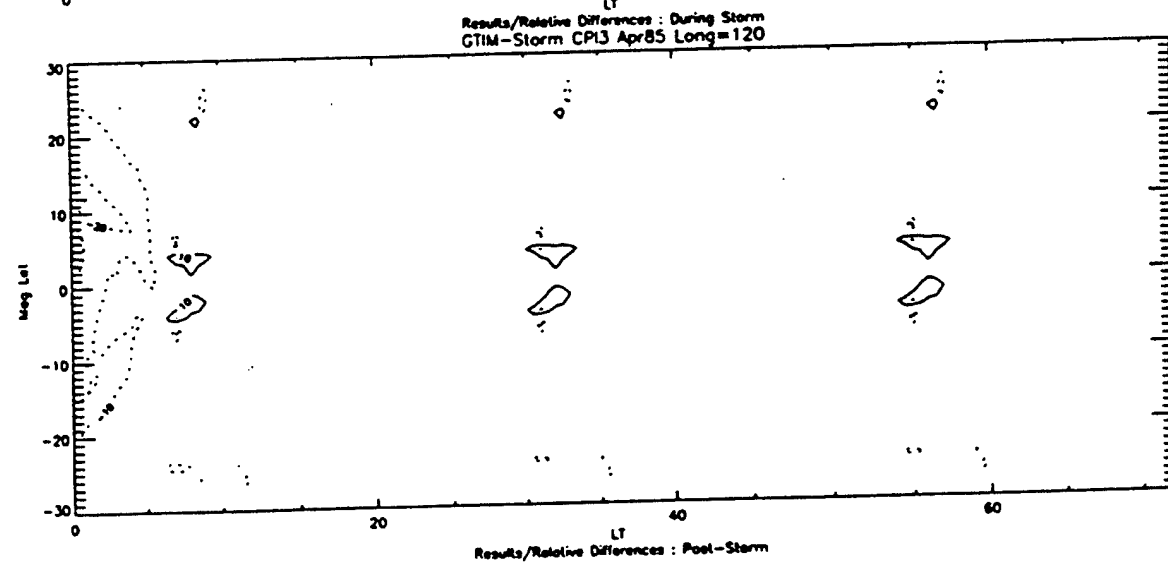
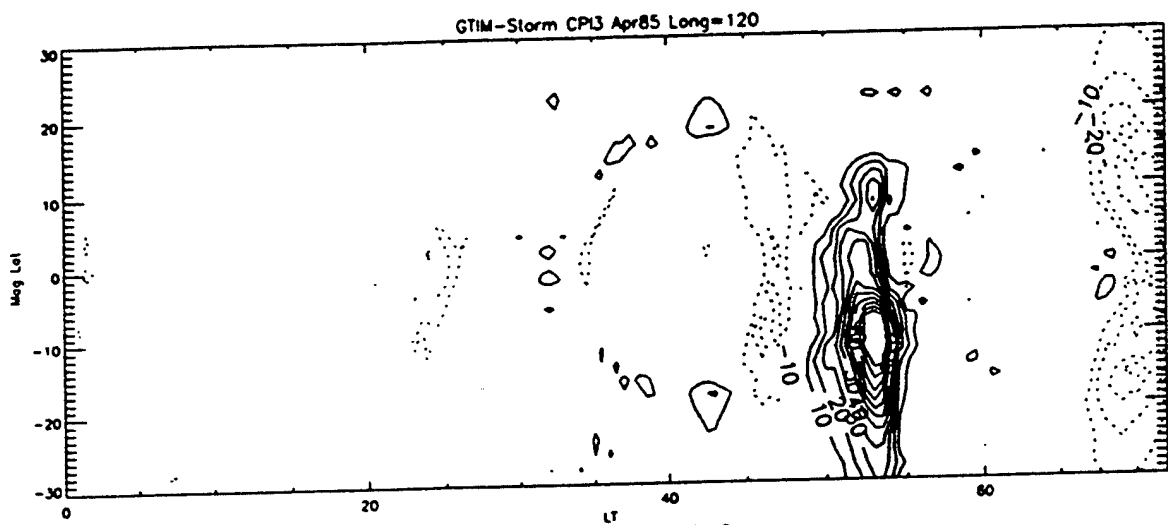
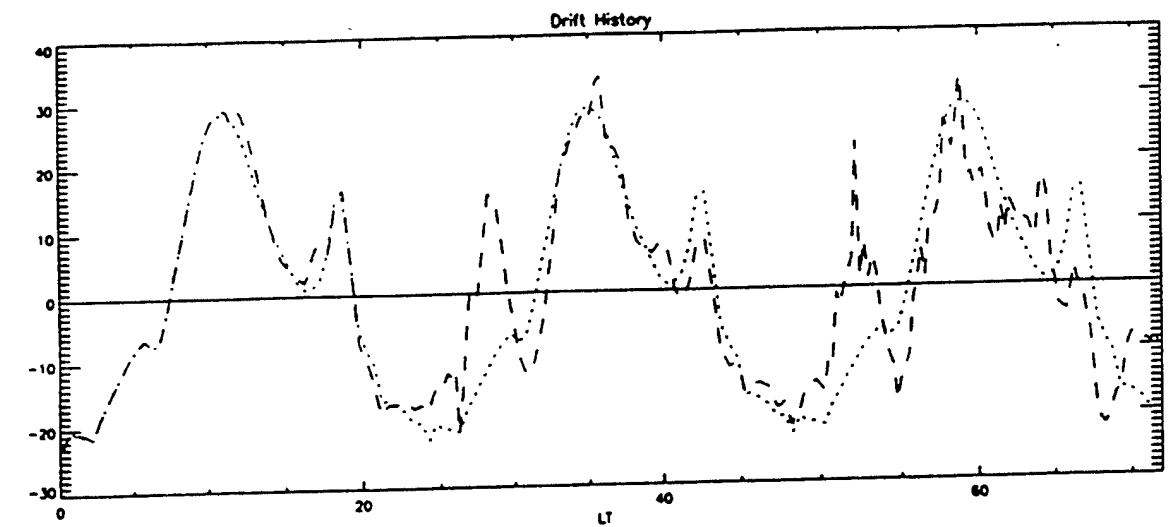
In adapting the GTIM to disturbance modeling, we also enabled thermospheric driving via MSIS and HWM and the use of a storm-time Ap index. Model runs conducted with and without thermospheric driving are used to describe and isolate the thermospheric and drift-based effects.

A sample of disturbance vertical drifts has been provided by colleagues at USU to commence this modeling study. These drift patterns correspond to:

- 1) a sample of ideal storms; these were based upon a simple "event" in AE (the parameter that drives the disturbance drift model) a range of onset local times as well as both solar minimum and solar maximum conditions.

- 2) a case study; a storm in April 1985 met the criteria of having AE values available, being well isolated in time from neighboring geomagnetic storms while still being large enough to be of some interest (in terms of ionospheric response).

The results for the case study are shown in Figure 23. The top panel of this figure shows the drift history over a three-day period where the dotted line is the quiet-time pattern (repeated each day for ease of visual comparison) and the dashed line shows the model disturbance drifts. Storm onset is evident in the middle of the first day. The middle panel shows a contour plot in local time (over three days) and magnetic latitude of



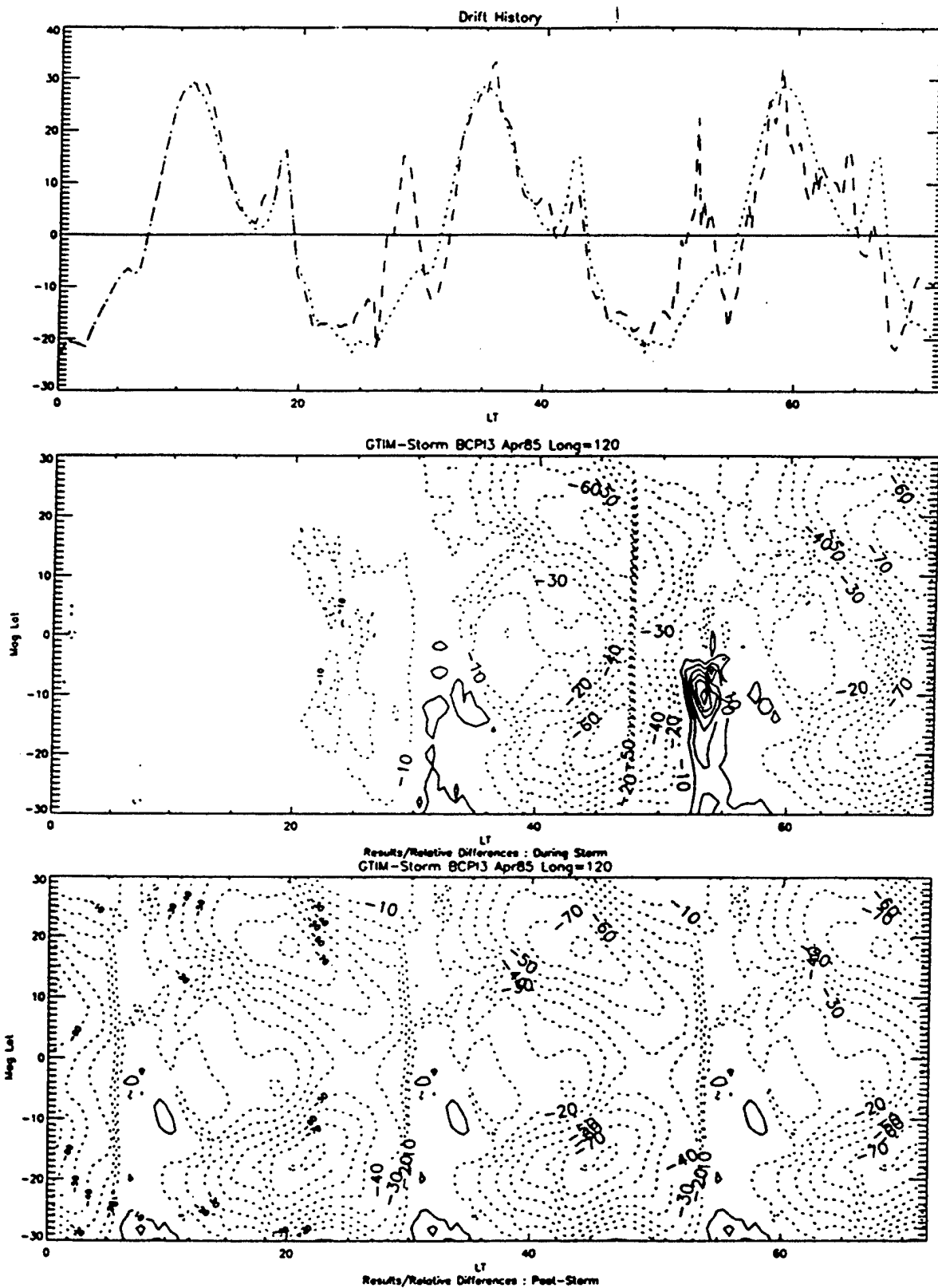
the changes in N_{max} derived using the GTIM with the drifts in the top panel. The changes are plotted as percentage changes in N_{max} compared to the quiet-time values, the contours being spaced at 10% change levels, and where dotted lines show negative phase and solid lines show positive phase. The bottom panel shows the results for the three subsequent days. In this figure, one thus sees

- a strong positive storm phase at low latitudes on the second night
- a smaller negative phase on the following day
- relaxation to quiet conditions by the third day
- some smaller positive and negative phases in the anomaly region on the second day
- little storm response on the day of the storm onset.

The case study storm was then run in the GTIM, including the effects of both disturbance drifts and thermospheric winds. The results of this run are shown in Figure 24. What is immediately apparent here is that the thermospheric effects all point to negative storm phases that can strongly mitigate the dynamo-driven positive phases, and that these negative phases can endure for a number of days after the drift effects have returned to normal. This arises because the A_p histories in MSIS and HWM have a longer timescale than does the USU disturbance drift model, reflecting real timescales in the thermosphere and disturbance dynamo.

A number of runs were made on the grid of conditions for “ideal” storms. Some highlights of these ideal storm runs were:

- typically, the commonest response is a nighttime positive phase (additional upward nighttime drifts helping to maintain ionization at night)
- secondary responses are in the anomaly region, and may be positive or negative in phase



- thermospheric effects are almost invariably negative phase
- evening sector onset times provided the larger disturbance drifts and hence the larger ionospheric responses
- solar minimum (percentage) effects are slightly larger in magnitude than solar maximum.

In the future, it would be most informative to perform modeling studies using this new capability of the GTIM with case studies of the global TEC response that are now being routinely made at the Jet Propulsion Laboratory in Pasadena, CA. Further, as this new observational database becomes larger, the underlying trends in ionospheric response on global scales will become better understood in an empirical sense. This study should commence once the AE data upon which the dynamo disturbance model is based becomes available for the times when the GPS groundstation coverage had become sufficient to justify global empirical TEC and TEC response maps (say, 1997).

6.2 Meridional Neutral Wind Effects

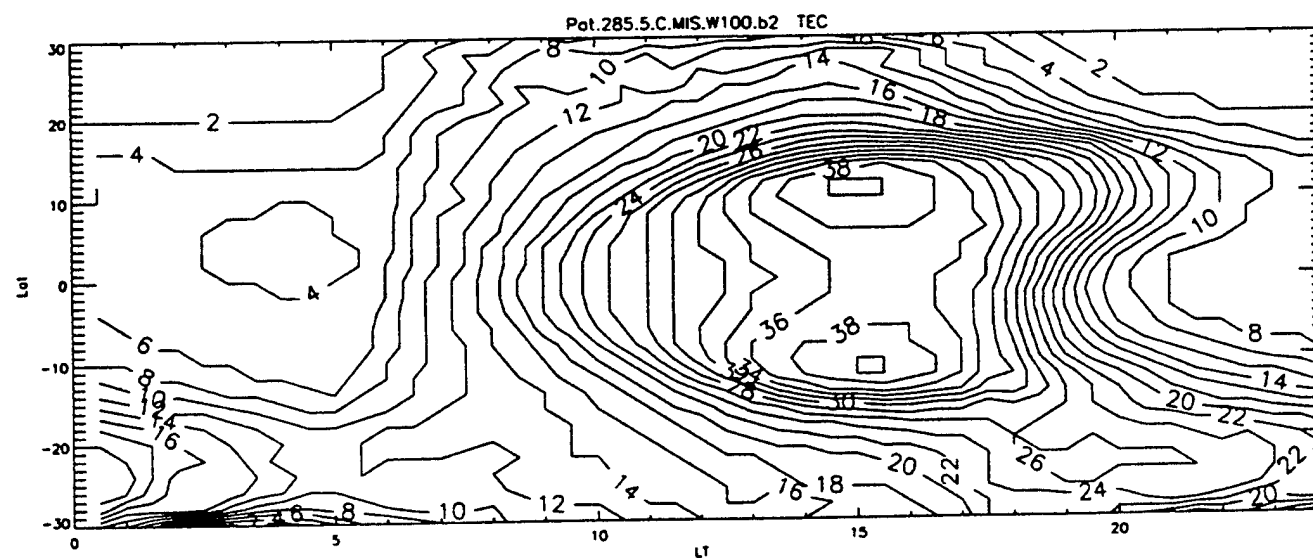
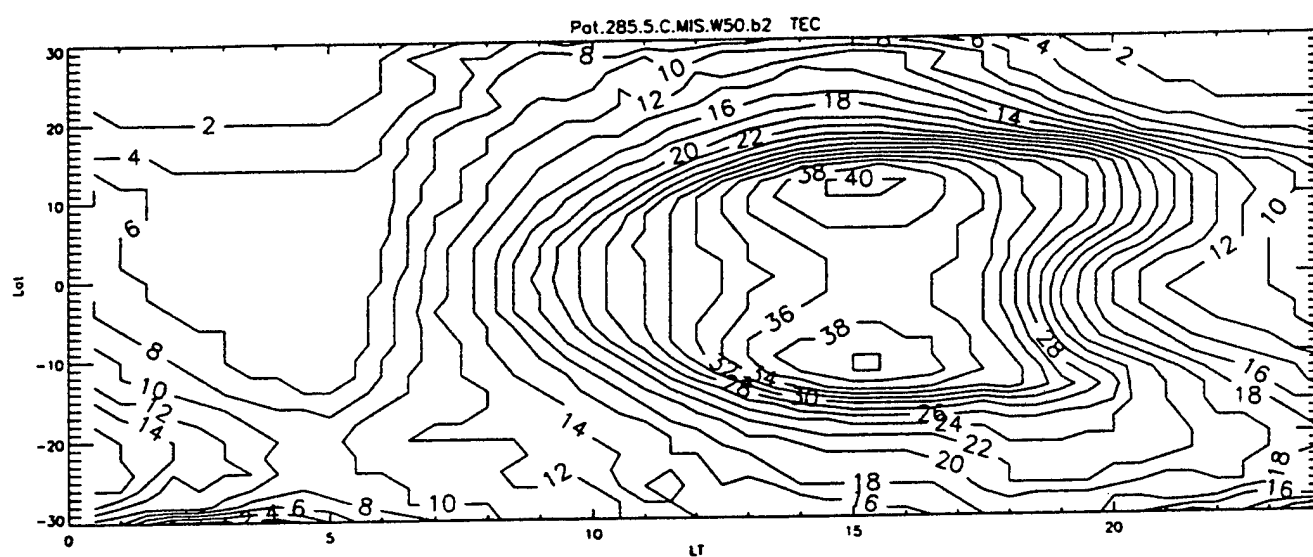
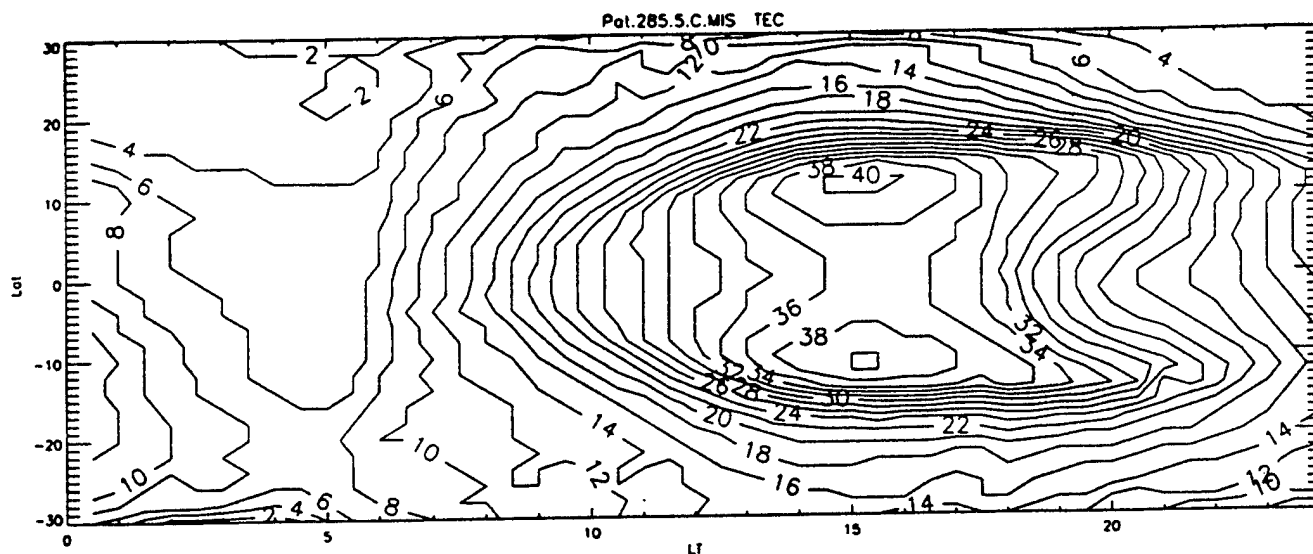
In this section, a project is described that uses an ionospheric model to predict the response of the equatorial ionosphere to shifts or surges in the meridional neutral wind. The basis for the study is the GTIM that in turn uses the HWM wind model (either 1987 or 1990) to specify the climatology of the neutral winds. The goal of the study is to bring together the results of the MISETA campaign (conducted in the equatorial American sector in October 1996), and the generally held view that transequatorial neutral wind surges will lead to asymmetries in the equatorial anomaly (raising plasma in one hemisphere while lowering it in the other). In earlier sections of this report we saw how the topside plasma density does correlate well with neutral wind changes; here, however, we are concerned with the vertical TEC, an integrated quantity that deals with the entire ionospheric profile.

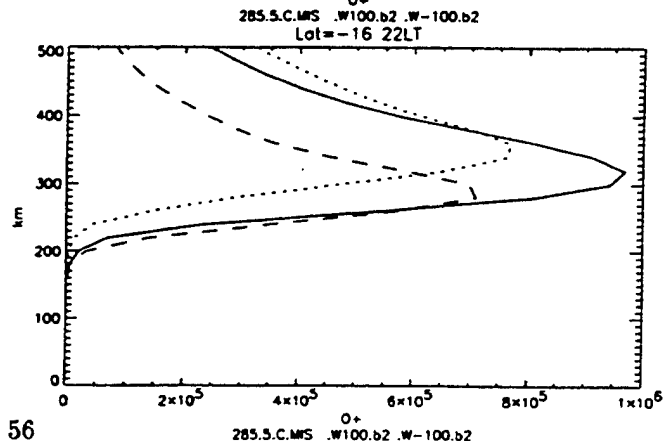
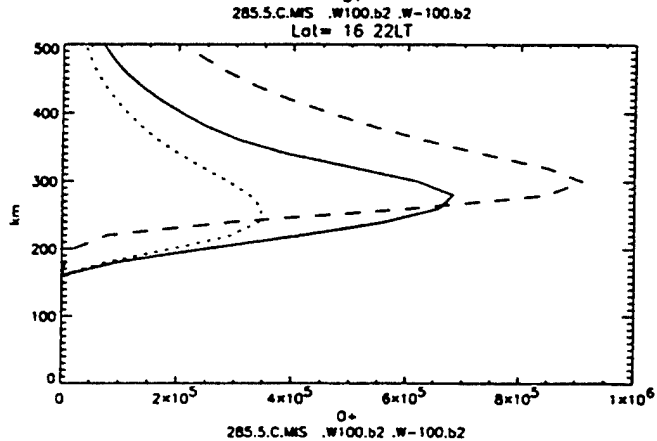
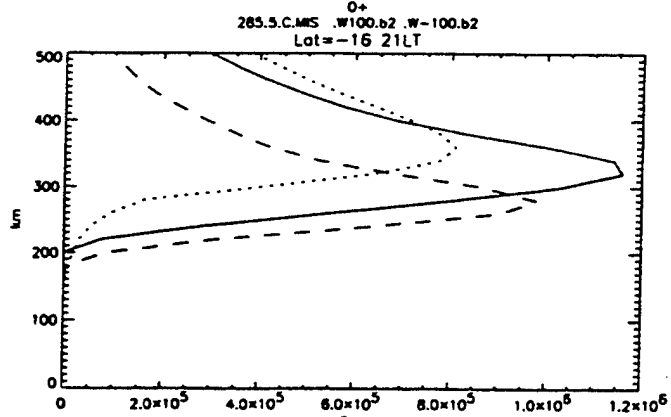
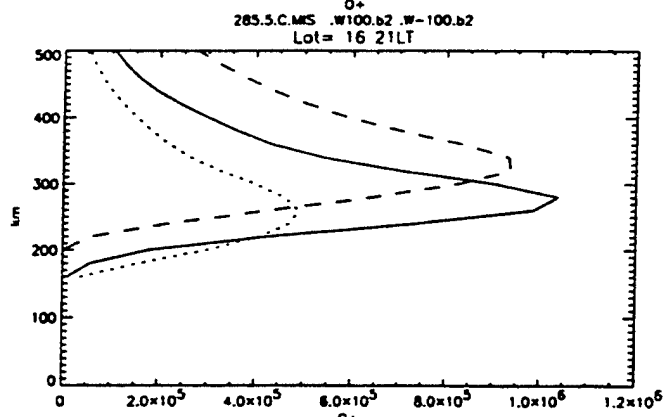
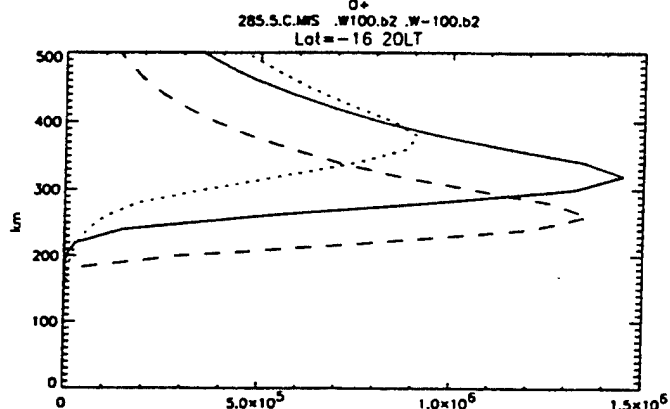
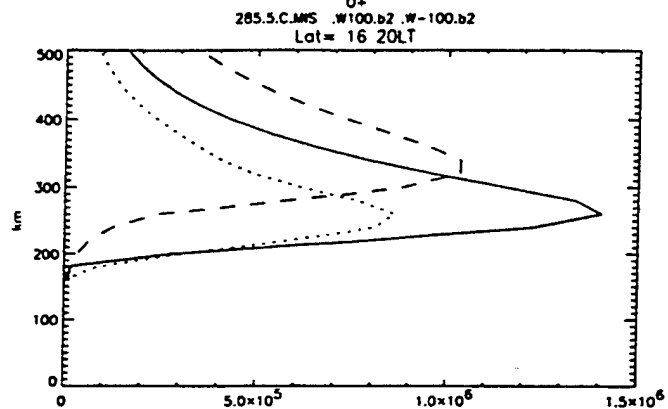
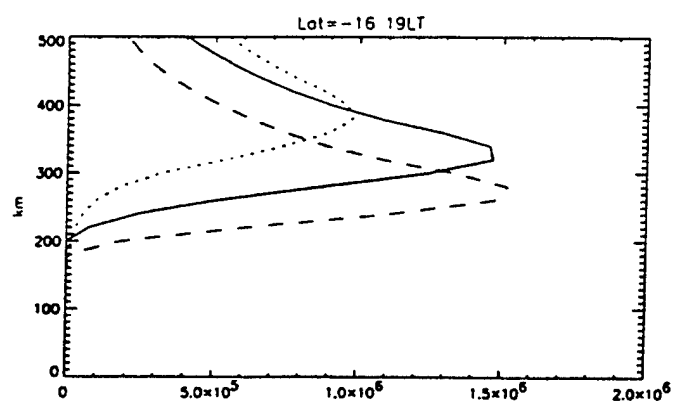
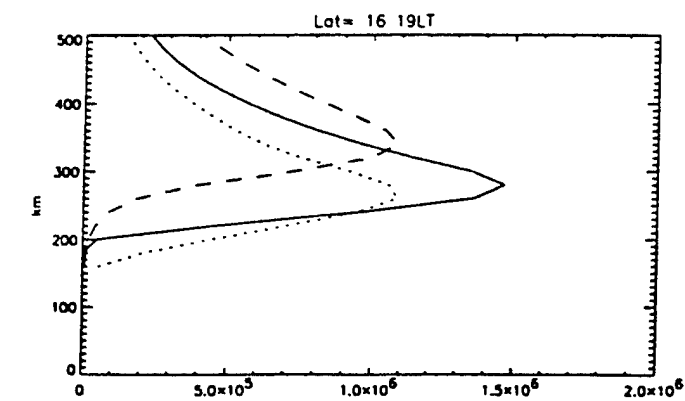
The project began when GPS measurements taken during the MISETA period revealed a significant asymmetry in the equatorial anomaly crests that was not indicated by a GTIM simulation appropriate to this nearly equinoctial time. Interestingly, Topex TEC data consistently shows significant asymmetries in the northern and southern equatorial anomaly crests. This is a feature that theoretical models, especially when run in a climatological sense, do not reproduce.

The original question posed is what level of neutral wind (applied in the afternoon/evening sector, with a peaking distribution centered on 1900LT with an input amplitude) would be required to cause that level of asymmetry?

A sample of GTIM TEC results is seen in Figure 25. There are three panels, each of which shows the variations in TEC plotted against local time and magnetic latitude in the US sector for October 1996 conditions. The top panel is the GTIM climatological estimate, the middle panel has added a (peak) 50ms^{-1} (northward) neutral wind, the bottom panel has added a (peak) 100ms^{-1} (northward) neutral wind. Clearly, the GTIM is predicting little change in TEC anomaly crests or asymmetry as a result of significant wind surges (this has been verified in the model with surges of 100ms^{-1} in both directions).

This apparent non-result is worth looking at more closely. Firstly let us examine the results shown in Figure 26 where electron density profiles are contrasted. The panels in left and right columns, respectively, correspond to magnetic latitudes of $+16^\circ$ and -16° , at the anomaly peak. Reading from top to bottom, the profiles are taken from of 1900LT, 2000LT, 2100LT and 2200LT. Within each panel the solid line corresponds to densities based on simulations including the climatological HWM winds, while the dotted and dashed lines comes from simulations that included evening surges of 100ms^{-1} north and 100ms^{-1} south, respectively. The directionality of the wind surge can be verified by comparing the higher Hmax values in the southern hemisphere in the case of the northward wind surge





(dotted line). However, it is immediately apparent that the response of the peak density, N_{\max} (and equivalently of the modeled TEC values) is not straightforward. By this is meant that the wind does not simply push the plasma around as if it were an incompressible fluid. Let us consider the second row of Figure 26, corresponding to profiles at the time of the maximum anomaly crest. Looking first at the panel on the right, the dotted line does suggest plasma that has been lifted up, whereby the peak has been eroded via transport. However, the dotted line on the left shows that the corresponding plasma has not been simply dumped in the northern hemisphere, but that the wind pushes the peak down, and thus perhaps the plasma has been transported to a region of higher loss (higher molecular density). Thus, while H_{\max} shows a significant asymmetry, N_{\max} shows very little as the anomaly peak in both hemispheres is diminished. This is a typical result in the GTIM runs. Asymmetries in TEC are not induced by evening neutral wind surges because the ionospheric peaks in both hemispheres are changed in the same sense, although they are moved to different altitudes.

7. PROFILE MODEL STUDIES

The final section of this report is concerned with applications development. A recently described simple profile formalism is examined for applications related to the quick and reliable conversions to and from slant TEC values. Firstly, the electron density profiles output from the PIM model are used to test the ability of the profile model to assimilate and describe the profile shapes, and thusly determine TEC along any arbitrary path. Then, the question of converting slant to vertical TEC is addressed, by determining whether this profile can describe the morphology of variations observed in GPS observations of TEC.

7.1 Parametrizing Model Outputs

This section summarizes recent work performed at Boston University that is geared to providing quick and reliable estimates of slant TEC based on an ionosphere generated from the USAF climatological model, PIM. The issue here is that while PIM provides a quick estimate for ionospheric electron densities within a region (likewise, PRISM attempts to describe “weather” conditions), that the vertical profiles generated on a coordinate grid do not lend themselves to an easy evaluation of TEC along arbitrary lines of sight. What has been performed here is a study of the feasibility of one possible solution.

The solution contains the following steps:

1. PIM/PRISM generated electron density profiles are fit with analytic functions. These functions are Chapman-layers in both the topside and bottomside, but where in each layer the scale heights vary linearly with altitude. Each vertical profile fit thusly is summarized by six parameters (two peak, two topside, two bottomside).
2. Each of these six fitted parameters vary smoothly in both location and time, so can at any given time be fit in two dimensions.
3. Electron densities at any location and altitude are rapidly regenerated via profile parameters from fits that are analytic in all dimensions.
4. Slant TECs can be calculated from a ground station by summing regenerated electron densities along the slant path.

The results are listed below, according to the step, as listed above.

Step 1- Running and Fitting PIM.

The first issue here is what size the grid of PIM profiles should be in order to adequately specify TEC. This depends on two factors:

- the minimum elevation angle that we wish to simulate slant TEC
- the accuracy to which TEC is desired.

A sample of ionospheres were used to test the system. These ionospheres are centered on both middle and low latitudes and cover various local time domains and a wide range of morphologies. The comparisons revealed that:

- to simulate elevation angles below 60° , the grid should extend 20° in both latitude and longitude from the "ground station"
- to simulate elevation angles below 30° , the grid should extend 30° in latitude and longitude
- to simulate elevation angles below 10° , the grid should extend 40° in latitude and longitude.

The grid spacing in latitude and longitude has been shown in tests to not be an important factor. Over a range of conditions and a range of resolutions from 10° in longitude and 4° in latitude to 2° in longitude and 1° in latitude there was no appreciable change in the resultant slant TEC. There simply needs to be sufficient resolution in the grid to define the morphology and the fitting will smooth out any low-grade variations.

The above figures are based upon a desired accuracy of 1% for slant TEC. Calculations of TEC have been carried out to a vertical altitude of 10000km to ensure convergence. Note also that the default altitude grid can be used in the PIM runs. The analytic fitting that is done allows for a reliable (see Step 3 discussion for one caveat) extension to arbitrarily high altitudes. In terms of run-time, the longest step (and the most time) is required to simply generate the original PIM profiles. Fitting of the PIM profiles has been performed using a variety of fitting criteria and anchor points on the profiles. Similar results have been obtained for each such fitting scheme.

Step 2- Fitting in 2D.

Because the spatial variations in profile parameters are smooth, polynomial fits have been required to summarize the variations. Existing IDL routines have been used for these fits. It should be stressed here that the fits referred to here have been made in only one-dimension. Purely for simplicity, what was used instead were fits in one dimension along each of both the latitude and longitude directions in the grid with the reconstitution being an average of values obtained in each of the latitude and longitude directions.

Over a range of conditions, fourth-order fits were found to be the most reliable, as they could provide a more faithful rendition of the whole range of morphologies without adding significantly to the runtimes.

Step 3- Regenerating Electron Densities.

Here one begins at a given ground location, and along a given slant path defined by azimuth and elevation angles evaluates electron density. This is carried out as follows:

1. The first point is defined by the slant distance along the given azimuth and elevation
2. The one distance and two angles translates along a curved earth (utilizing spherical trigonometry) to one distance (altitude) and two angles (offsets in latitude and longitude)
3. The six profile parameters are evaluated at the current location (given by the latitude and longitude offsets)
4. The electron density at the desired altitude follows directly from the six profile parameters.

One caveat has arisen. When a fit is made to an individual electron density profiles, the derived parameters always obey the rule $\text{Beta}/\text{Alpha} > -\text{Hmax}$. However, this is not necessarily the case when Hmax, Alpha and Beta values come from polynomial fits in two

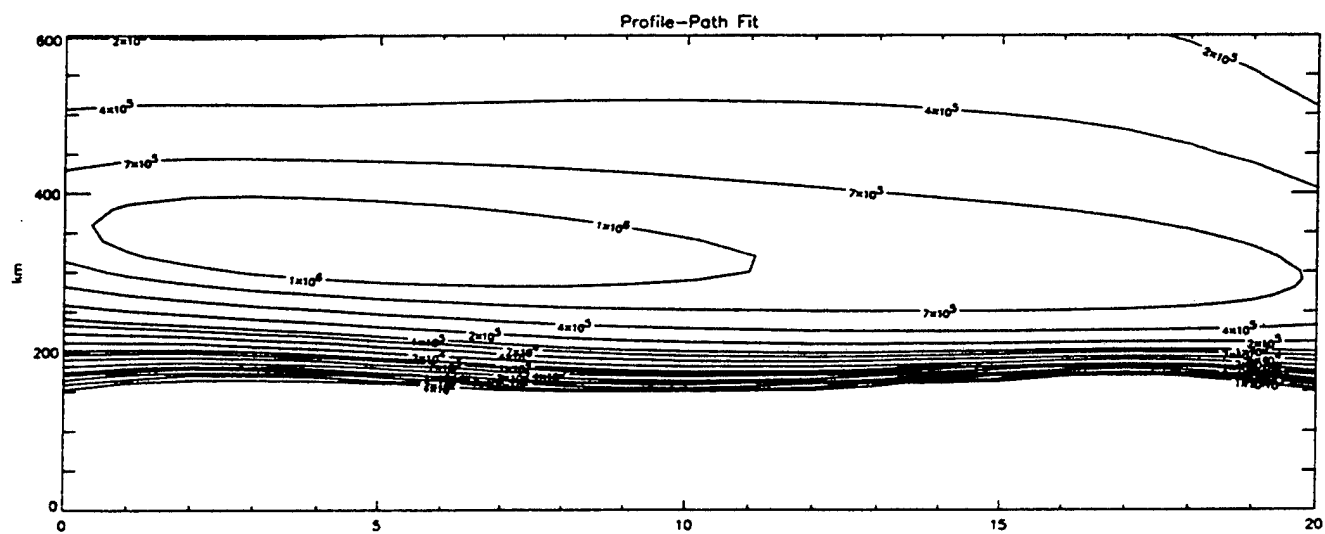
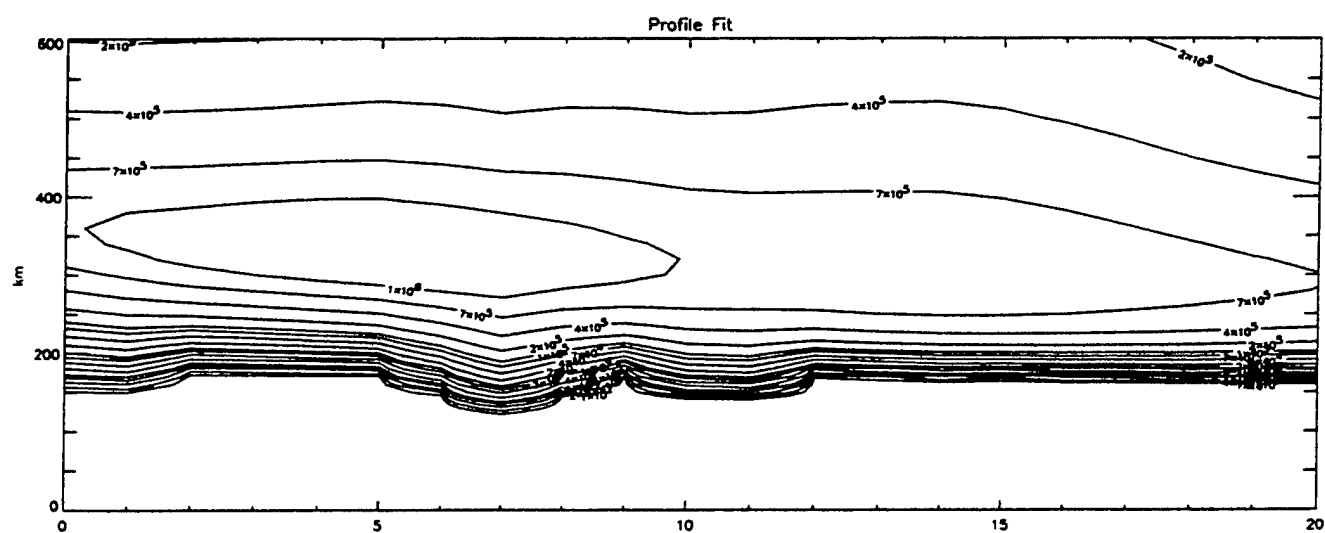
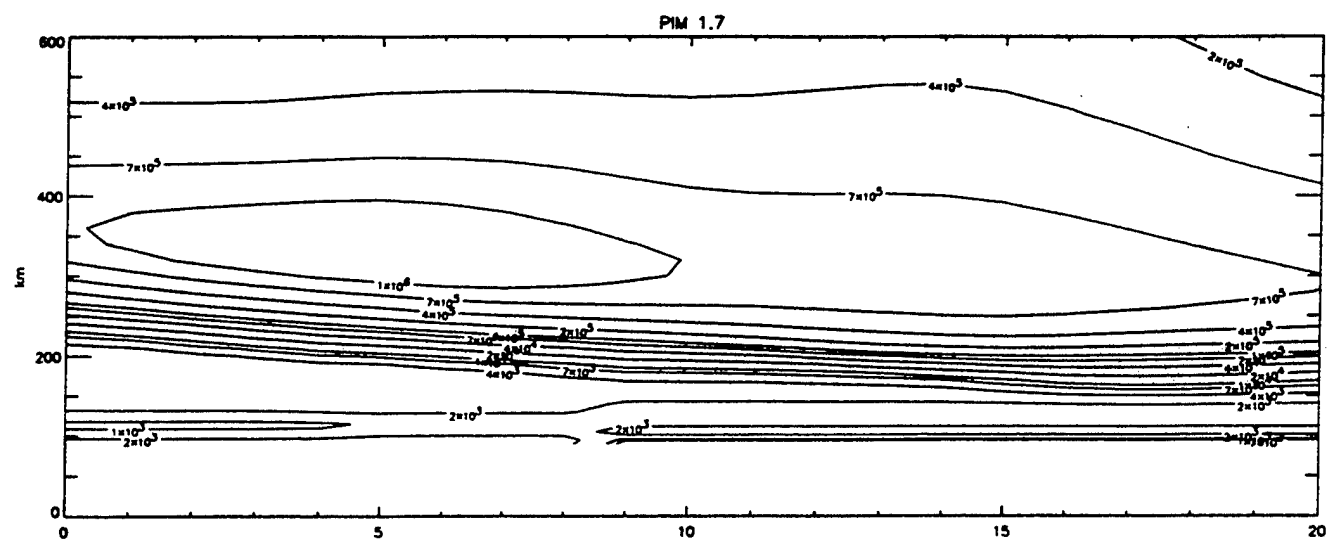
dimensions. For this reason, a watchdog is set in the software whereby a previous value will be used if the current value appears spurious.

Actual run-times (for 408 slant TEC values) were

- fourth order fits, step size 20km, 110sec (0.25 sec/TEC)
- fourth order fits, step size 5, 450sec (1.1 sec/TEC)
- second order fits, step size 20km, 80sec (0.20 sec/TEC)
- second order fits, step size 5km, 320sec (0.80 sec/TEC).

A demonstration of the overall ability of this fitting scheme to describe the “raw” PIM electron densities is given in Figure 27. There are three panels, each showing contours of electron density as a function of horizontal distance (from -20° to $+20^\circ$ latitude at 300°E , in this instance) and altitude. The top panel is the output from a run of PIM, version 1.7. The middle panel shows the electron densities fit using this profile scheme at each location along the path. The lower quality of fit in the bottomside is noted; this profile fitting routine is sensitive to TEC values and will only be influenced by bottomside densities when a significant fraction of the TEC is contained in the bottomside. The bottom panel of Figure 27 shows the reconstructed electron densities when each of the six profile-fitted parameters are further fit along the horizontal path using a simple polynomial. This polynomial fitting is important as it both smoothes the small-scale spurious variations, and permits evaluation of profile parameters and therefore electron densities at any location along the path, not just at the location of known profiles or parameters. The quality of the fitting is clearly seen in Figure 27.

The software that performs these calculations of slant TEC values, SlantPathTEC has been downloaded onto the /floor/matthew/ directory on the andersun machine at AFRL.



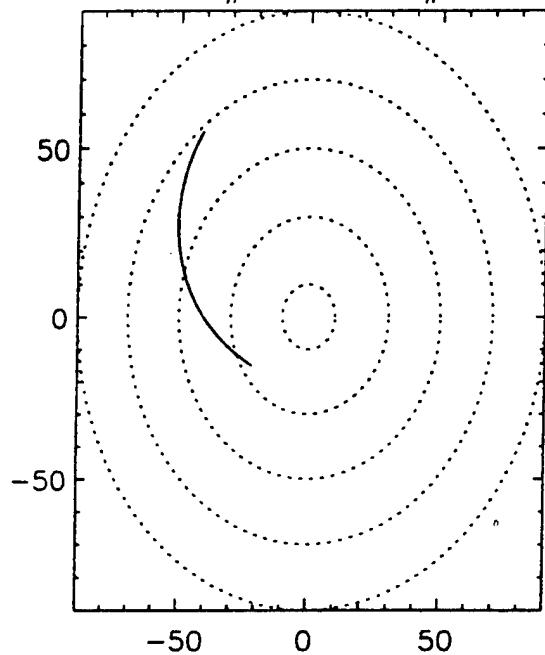
7.2 Describing Slant TEC

An vital component towards establishing that a given profile formalism can be used as a basis for performing slant to vertical TEC calibrations is establishing that the model can indeed span the range of slant TEC variations that are observed.

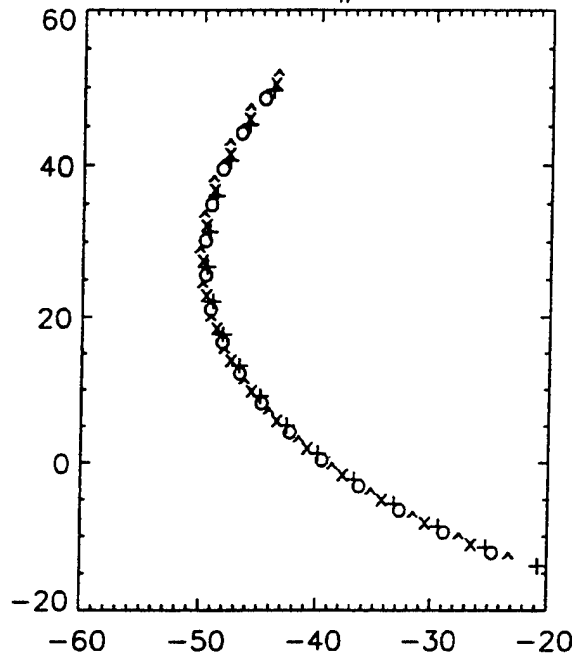
The GPS constellation of satellites is providing a wealth of data that can be a real impetus towards the goal of continuous monitoring of the ionosphere (equivalently, monitoring space weather). Historically, more of the GPS ground stations have operated at middle latitudes where a simple thin shell approximation for converting slant to vertical TEC is reasonably reliable. As more stations are introduced, increasing numbers are at lower latitudes where this approximation breaks down (and roughly half the globe is within the region of influence of the F region equatorial anomaly). The need for a more reliable and realistic means of conversion becomes increasingly pressing.

In the preliminary stages of this project, analysis procedures have been established to deal with the large GPS database in an efficient manner. Initial work has involved (slant TEC) data from Arequipa, a station at a sufficiently low latitude to show the influence of the equatorial anomaly. Firstly, ranges of dates are scanned to determine which GPS tracks recur on a regular basis; these are to form the database of reliable in terms of defining both day to day variations and typical morphology of slant TEC variations. One means of displaying these results is seen in Figure 28. The first panel shows the track on an all-sky plot. The second panel shows a close-up of the track, with different symbols plotted for the (azimuth-elevation) location on each day in the period showing the coincidence of the observations (to justify the overplotting of slant TEC values). The third and fourth panels show overplots of slant TEC for each day in the period, plotted against Elevation Angle, and Azimuth, respectively. Note that although this period of March 6-9 1996 is geomagnetically quiet, the day to day variations of slant TEC show variations of more than

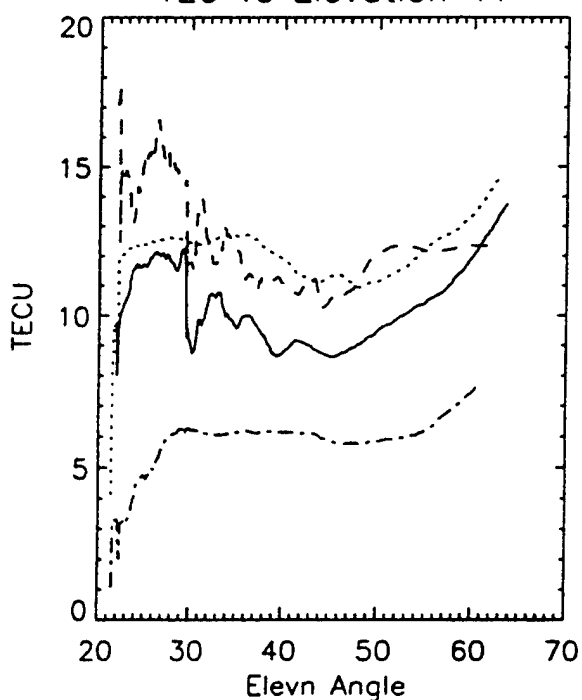
GPS #41 Track #41



GPS Track #41 Sites

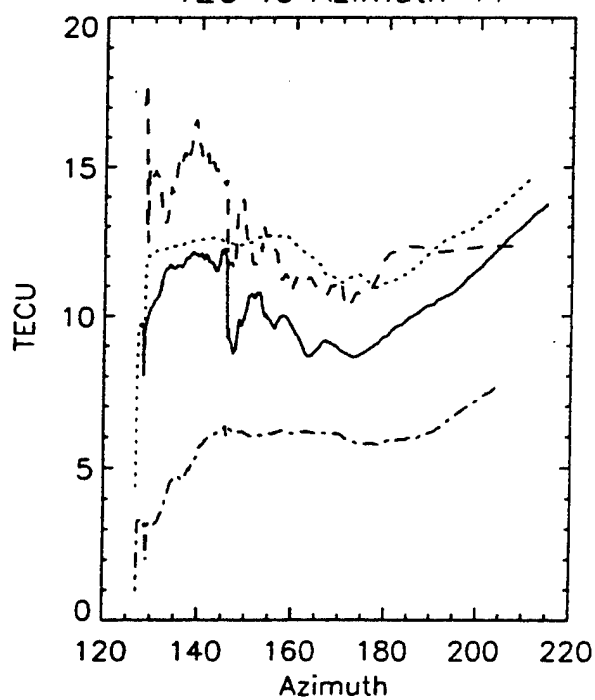


AREQUIPA 1996 March D 6-9
TEC vs Elevation 41



AREQUIPA 1996 March D 6-9

AREQUIPA 1996 March D 6-9
TEC vs Azimuth 41

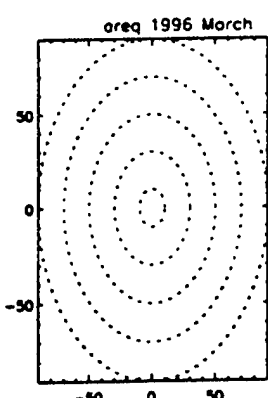


AREQUIPA 1996 March D 6-9

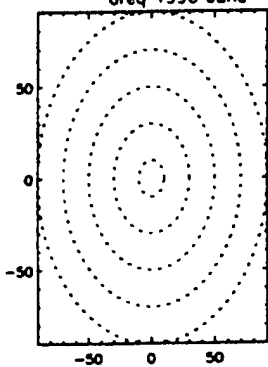
a factor of 2 in magnitude, and show dramatic changes in morphology.

It is useful to examine the range of tracks that are available from any given station i.e. what is the full morphology of tracks (and therefore slant TEC) that a model must span? Sample results are shown in Figure 29. This figure shows overplots of all tracks obtained over Arequipa for March, June, September and December 1996 (reading down), in four UT sectors. We note immediately that the sectors in which data are available are typically well-sampled in terms of elevation and azimuth, but sampling in UT is poor. This will be a typical feature of GPS data from any given location and so groups of similar stations should be studied together.

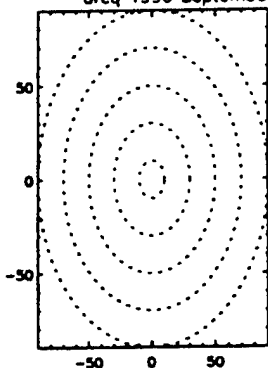
One can then take a closer look at the slant TEC values. Figure 30 shows the GPS TEC data as measured from Arequipa, from January 1996. Four panels across are binned according to UT, while the rows group the data according to the maximum elevation angle achieved during the track. Within each panel, a dial plot (the center is zenith, north is to the top) showing all tracks of sufficient length that appeared in at least two consecutive days in the month. The different lines used in the plot are simply a means of identifying tracks. Figure 31 then shows the slant TEC data taken from each track displayed in Figure 30. The panels are defined in the same sense, and the line styles correspond directly between these two figures. The x-axis here is simply an index that orders the data (note that only every tenth GPS TEC data point is plotted in this set). A figure of this type is useful to provide a quick visual summary of the degree of day-to-day variability and the nature of the spatial variations in the slant TEC database. Figure 32 makes use of the same display format to show the estimates of slant TEC for the tracks shown in Figure 30 but based on climatological parameters of the profile model introduced in the previous section of this report. A visual comparison shows that the model does reproduce the spatial variations of slant TEC data in terms of the character or morphology of the variations



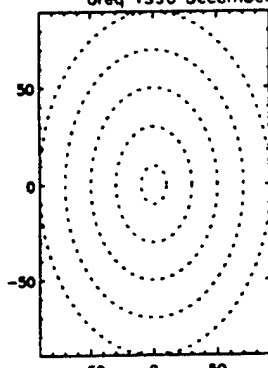
UT: 0.00->6.00
areq 1996 June



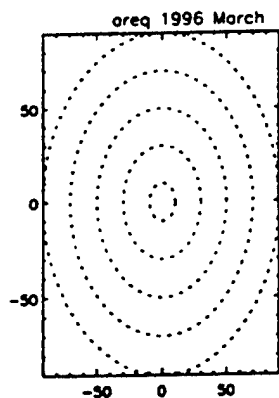
UT: 0.00->6.00
areq 1996 September



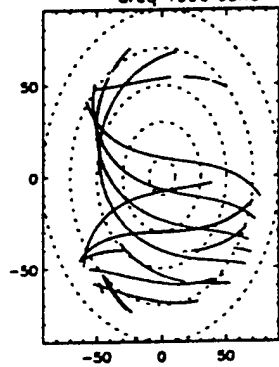
UT: 0.00->6.00
areq 1996 December



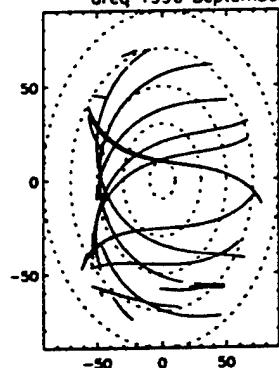
UT: 0.00->6.00



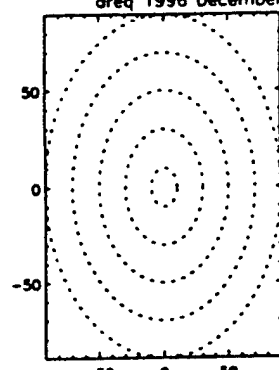
UT: 6.00->12.00
areq 1996 June



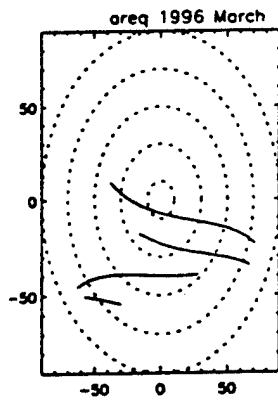
UT: 6.00->12.00
areq 1996 September



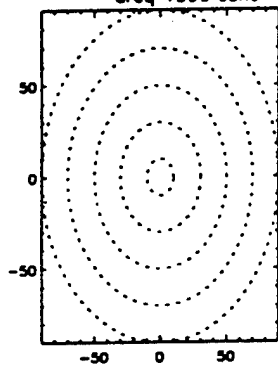
UT: 6.00->12.00
areq 1996 December



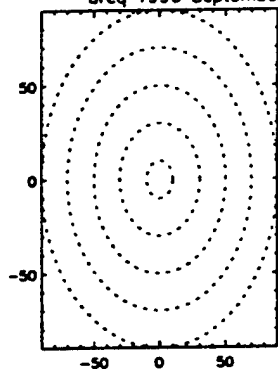
UT: 6.00->12.00



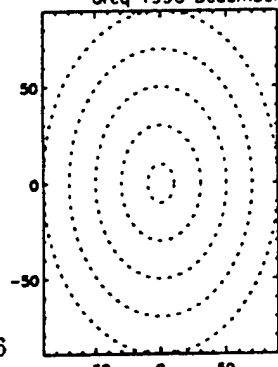
UT: 12.00->18.00
areq 1996 June



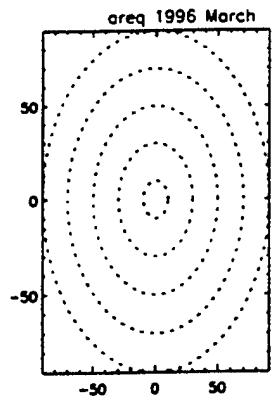
UT: 12.00->18.00
areq 1996 September



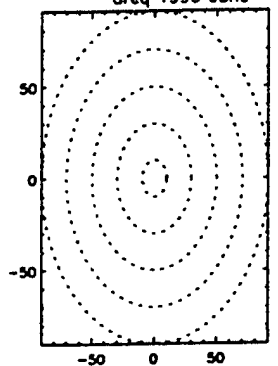
UT: 12.00->18.00
areq 1996 December



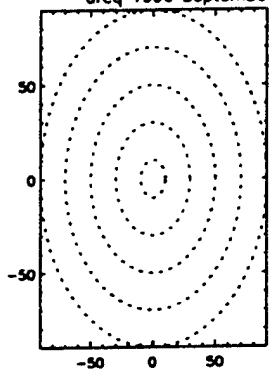
UT: 12.00->18.00



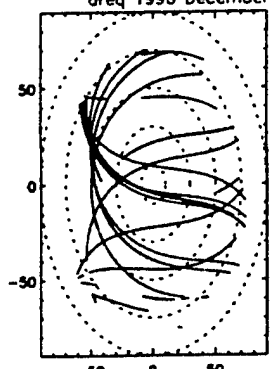
UT: 18.00+
areq 1996 June



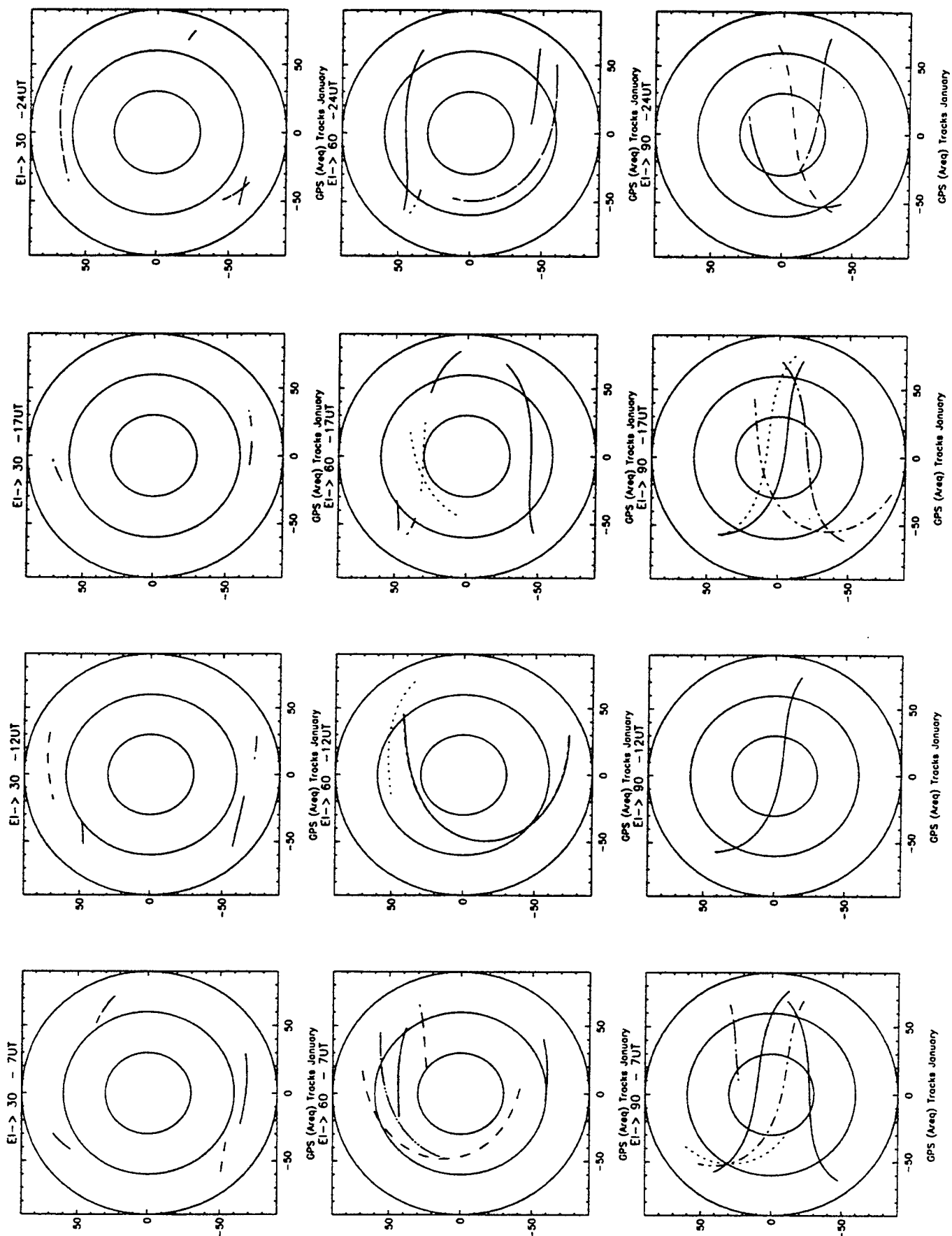
UT: 18.00+
areq 1996 September

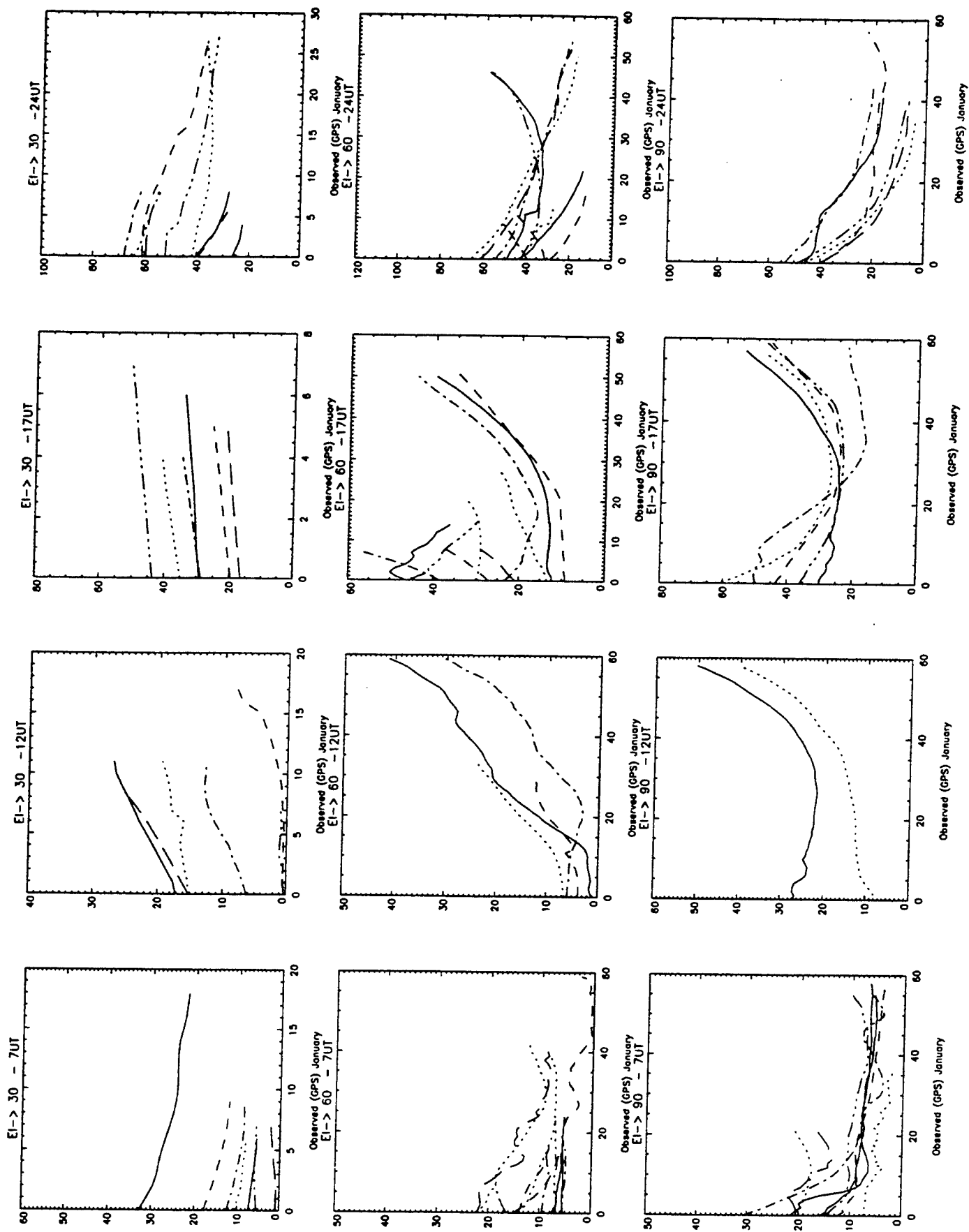


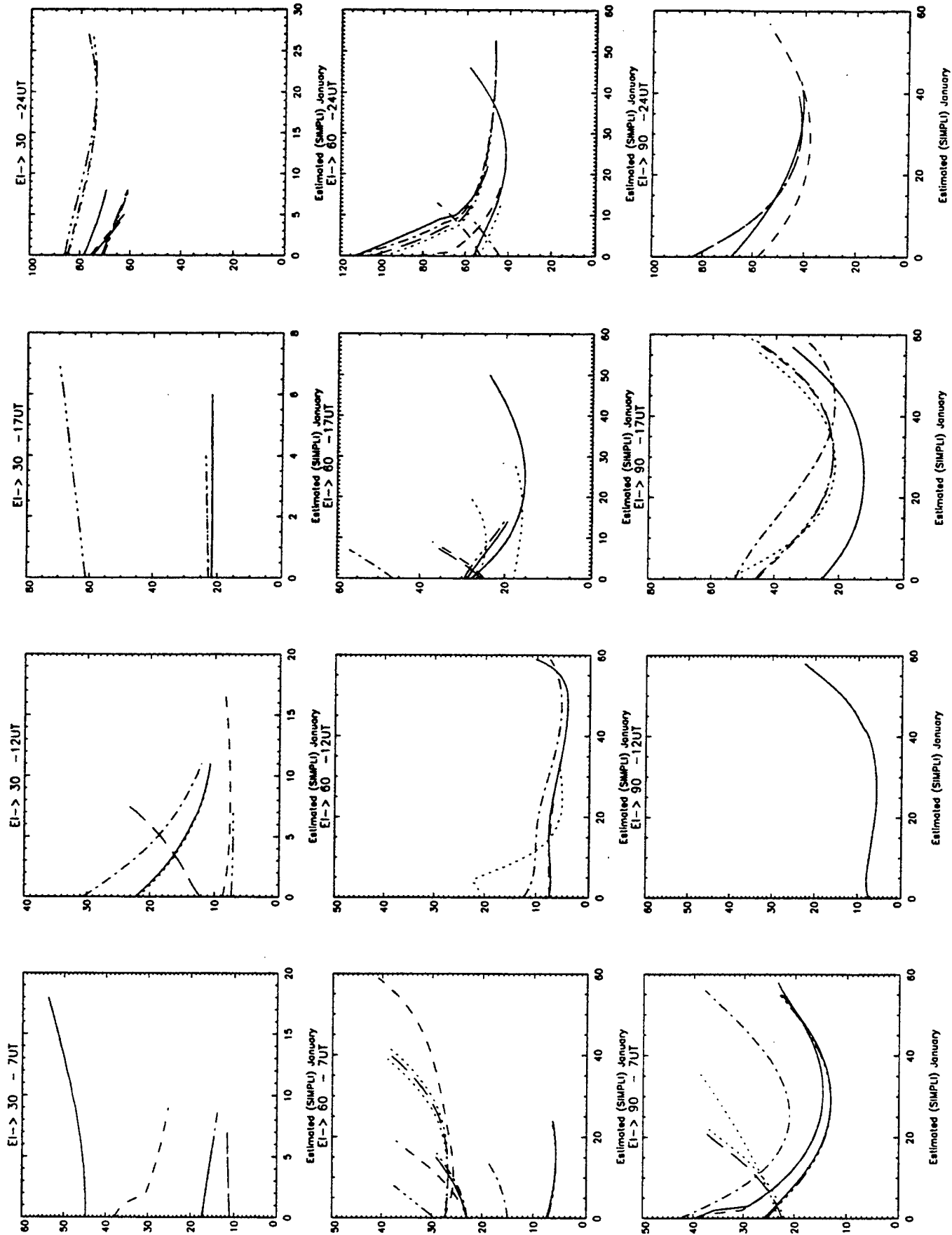
UT: 18.00+
areq 1996 December



UT: 18.00+







(and comparisons made at other months support this conclusion). The individual tracks are not well-described because the model estimates are climatological in nature. For example, in the bottom row, the second panel from the left shows two different TEC data tracks for the data in Figure 31, but identical tracks for the model estimates for those two days in Figure 32. There are also clear indications that the spatial variations of key profile parameters is different between the model and the real ionosphere (such as a scale height increasing to the West rather than the East). Further work would be required to determine how best to update the model climatological specification with independent and near-real time data to perform such updates. The model itself is already geared to data assimilation schemes and thus is well-suited for this purpose.

Additional work would also be required to extend this study to the final goal of determining a reliable slant to vertical TEC correction. The following is a list of the steps that should be performed:

- Accessing the GPS on-line database for station data from the equatorial region, specifically including magnetic latitudes within $\pm 25^\circ$. Sufficient stations should be included to provide an adequate coverage in UT (LT), azimuth and elevation, in addition to solar activity levels and seasons.
- Characterizing the variations in profile parameters that are sufficient to describe the morphology of observed GPS slant TEC variations in the above dataset.
- Determining a simple functional form for the slant to vertical TEC conversion, utilizing the analytic form of the model profile shapes and the apparent nature of the best-fit model shape functions to the low-latitude ionosphere.

Table 1. List of DMSP Observations
Made Available by AFRL to Boston U.

1(a) Daily Average Passes, Longitude-Averaged

Satellite	Year
F10	1991
F12	1994
F12	1995
F13	1995

1(b) Daily Average Passes, Sector Averages (each 60 degrees)

Satellite	Year
F10	1991
F10	1992
F10	1993
F11	1992
F11	1993
F11	1994

1(c) Additional Data From Selected Magnetically Quiet Days

Year	Month
1994	September
1994	December
1995	March
1995	April
1995	June

Table 2. List of Middle Latitude Ionospheric Events
Located Using the NGDC CDROM Database.

Year	Month	Day	Region/Country
1958	April	13	Europe
1961	November	24	Asia
	December	16	S. Africa
1962	July	14	Asia
1963	March	20	Europe
1965	September	3	Asia
1966	April	21	Russia
1967	February	14	Australia
	May	10	Japan
1969	August	22	Russia
	December	4	Canada
1970	January	6	Europe
	September	9	Russia
1971	March	7	Australia
	November	6	Russia,Australia
1972	February	6	Australia
	March	23	Europe
	May	27	Russia
	September	9	Russia, Canada
	September	28	Australia
	November	14	Europe

Table 3. Day-to-day variability of ionospheric parameters

	Overall Variability	Quiet-Time Variability
foF2	18%	17%
Hmax	12%	12%
TEC	31%	28%

```

c
c Simple driver program to demonstrate use of the coefficients
c that derive effective wind-scaling levels from in situ DMSP
c measurements. The basic principle is that these MERIDIONAL
c winds effect the asymmetry of the densities as measured by the
c satellite. The results are based on a series of GTIM simulations
c covering a large grid of geophysical conditions, run by
c Matthew Fox at Boston University.

c Software written by Matthew Fox, June 1999 and provided to AFRL

c Other notes:
c 1. These coefficients are based on simulations for the 19LT
c (evening) pass of DMSP
c 2. Asymmetry levels in densities, though primarily affected
c by winds, do see some influence of the effective vertical
c drift level. Therefore, drivewind, and the equivalent routine
c drivedrift, should be run ITERATIVELY to converge to a
c consistent solution. The software below reflects this.
c 3. Asymmetry levels in the GTIM also vary with season and longitude.
c Longitude and drift level variations are tabulated, whereas
c the annual variations are described by a 1st-order Fourier series
c with an adjustment at June solstice (more highly varying asymmetry).
c These coefficients are used to derive 2 coefficients for a linear
c relation between North/South density ratio and effective wind.
c 4. This is demonstration software. The final application will include
c known files and formats containing the actual data and ephemeris,
c that are not currently available to the author. However, it will
c show what's needed and how it's used.
c
c real coefficients(6,3,4,2)
c real current(4,2), final(2)
c real xmlats(100), xdens(100), sdens(100)

c
c prompt for inputs- the quantities that determine which coefficients
c should be used
c NB: Wind correlations are not affected by solar flux level
c but the input is included here for completeness
c
c write(0,*)' Enter longitude, f10.7 cm flux (East) and month '
c read(5,*) ilong, F10p7, month

c so what sector are we in ?? In order: 60, 120, 180, 240, 300, 360
c isector = (ilong + 30)/60
c if(isector.eq.0)isector=6

c also, from the prior (iteratively) run of drivedrift, what is the
c latest drift level estimate ?
c NB!!!!!! We need this file to exist
c It's written by drivedrift, value should be initialised to 1.0
c open(unit=10,file='Drift.Eff',status='old')
c read(10,*) EffDrift
c close(10)

c and thus, the coeffs to use are
c idrift = 2
c if(EffDrift.lt.0.5) idrift = 1
c if(EffDrift.gt.1.5) idrift = 3

c
c then use the coefficients and the measurements to derive the
c effective meridional neutral wind level
c
c open(unit=10,file='WindCoeffs',status='old')

```

```

        do 10 jsector = 1, 6
        read(10,*) jlong
        do 10 jdrift = 1, 3
        do 10 iorder = 1, 2
        read(10,100) (coefficients(jsector,jdrift,j,iorder),j=1,4)
10      continue
        close(10)
100     format(4f10.3)

c save the ones we want
        do 20 iorder = 1, 2
        do 20 iparam = 1, 4
        current(iparam,iorder) = coefficients(isector,idrift,iparam,iorder)
20      continue

c reconstruct for the month to get the final linear fit coefficients
        scale = acos(-1.0)/6.0
        angle = float(Month) * scale
        do 30 iorder = 1, 2
        final(iorder) = current(1,iorder) + current(2,iorder)*sin(angle) +
1      current(3,iorder)*cos(angle)
        if(Month.eq.6)final(iorder) = final(iorder) + current(4,iorder)
30      continue

c
c OK - Read the data, and SMOOTH it. If there are multiple passes in a given
c longitude sector for the day in question smooth with those too.
c
c NB: !!!!!!! Use magnetic latitudes
c
        open(10,file='DMSP.Data',status='old')
        do 40 i = 1, 100
        read(10,*) xmlats(i), xdens(i)
40      continue
        close(10)

c smooth 3-wise
        sdens(1) = xdens(1)
        sdens(100) = xdens(100)
        do 50 i = 2, 99
        sdens(i) = (2.0*xdens(i) + xdens(i-1) + xdens(i+1))/4.0
50      continue

c derive the north and south middle-latitude averages
        nnorth = 0
        nsouth = 0
        sumnorth = 0.0
        sumsouth = 0.0
        do 60 i = 1, 100
        if(xmlats(i).ge.15.0.and.xmlats(i).le.35.0)then
            nnorth = nnorth + 1
            sumnorth = sumnorth + sdens(i)
        endif
        if(xmlats(i).le.-15.0.and.xmlats(i).ge.-35.0)then
            nsouth = nsouth + 1
            sumsouth = sumsouth + sdens(i)
        endif
60      continue

        if(nnorth.eq.0.or.nsouth.eq.0)then
            write(0,*)' Insufficient Data ',nnorth,nsouth
            goto 1000
        endif

        xnorth = sumnorth/nnorth
        xsouth = sumsouth/nsouth

```

```

c and the ratio is
    Ratio = xnorth/xsouth

c so that, given Ratio =  A0 + A1 * Scaling (Effective Wind)

    EffWind = (Ratio - final(1))/ final(2)
    if(EffWind.lt.0.0) EffWind = 0.0
    if(EffWind.gt.2.0) EffWind = 2.0

c
c finally, write the derived effective wind to file, for use by drivedrift
c
    open(unit=10,file='Wind.Eff',status='old')
    read(10,*) EffWind
    close(10)

1000    continue
c all finished
    stop
    end

```

```

    program drivedrift
c
c Simple driver program to demonstrate use of the coefficients
c that derive effective drift-scaling levels from in situ DMSP
c measurements. The basic principle is that these vertical
c drifts effect the equatorial (crest and trough) densities as measured by the
c satellite. The results are based on a series of GTIM simulations
c covering a large grid of geophysical conditions, run by
c Matthew Fox at Boston University.

c Software written by Matthew Fox, June 1999 and provided to AFRL

c Other notes:
c 1. These coefficients are based on simulations for the 19LT
c    (evening) pass of DMSP
c 2. Crest and trough densities, though primarily affected
c    by drifts, do see some influence of the effective neutral
c    wind level. Therefore, drivedrift, and the equivalent routine
c    drivewind, should be run ITERATIVELY to converge to a
c    consistent solution. The software below reflects this.
c 3. Crests/Troughs in the GTIM also vary with season and longitude.
c    Longitude and drift level variations are tabulated, whereas
c    the annual variations are described by a 2nd-order Fourier series
c    with an adjustment at June solstice (more highly varying densities).
c    These coefficients are used to derive 7 coefficients for the
c    linear relations between various equatorial density ratios
c    and effective drift.
c 4. This is demonstration software. The final application will include
c    known files and formats containing the actual data and ephemeris,
c    that are not currently available to the author. However, it will
c    show what's needed and how it's used.
c
    real coefficients(6,3,6,7)
    real current(6,7), final(7)
    real xmlats(100), xdens(100), sdens(100)

c prompt for inputs- the quantities that determine which coefficients
c should be used
    write(0,*) ' Enter longitude (East), solar f10.7cm flux, and month '
    read(5,*) ilong, fl0p7, month

c so what sector are we in ?? In order: 60, 120, 180, 240, 300, 360
    isector = (ilong + 30)/60
    if(isector.eq.0) isector=6

c so what solar activity level are we in ??
    ilevel = 2
    if(fl0p7.lt.100) ilevel = 1
    if(fl0p7.gt.170) ilevel = 3

c also, from the prior (iteratively) run of drivewind, what is the
c latest wind level estimate ?
c NB!!!!!! We need this file to exist
c It's written by drivewind, value should be initialised to 1.0
    open(unit=10,file='Wind.Eff',status='old')
    read(10,*) EffWind
    close(10)

c and thus, the coeffs to use are
    iwind = 2
    if(EffWind.lt.0.5) iwind = 1
    if(EffWind.gt.1.5) iwind = 3

c
c then use the coefficients and the measurements to derive the
c effective vertical drift level

```



```

c
    open(unit=10,file='DriftCoeffs',status='old')
    do 10 jsector = 1, 6
    read(10,*) jlong
    do 10 jdrift = 1, 3
    do 10 iorder = 1, 7
    read(10,100) (coefficients(jsector,jdrift,j,iorder),j=1,6)
10    continue
    close(10)
100    format(4f10.3)

c save the ones we want
    do 20 iorder = 1, 7
    do 20 iparam = 1, 6
    current(iparam,iorder) = coefficients(isector,idrift,iparam,iorder)
20    continue

c reconstruct for the month to get the final linear fit coefficients
    scale = acos(-1.0)/6.0
    angle = float(Month) * scale
    do 30 iorder = 1, 7
    final(iorder) = current(1,iorder) +
1    current(2,iorder)*sin(angle) + current(3,iorder)*cos(angle) +
1    current(4,iorder)*sin(2.*angle) + current(5,iorder)*cos(2.*angle)
    if(Month.eq.6)final(iorder) = final(iorder) + current(6,iorder)
30    continue

c
c OK - Read the data, and SMOOTH it. If there are multiple passes in a given
c longitude sector for the day in question smooth with those too.
c
c NB: !!!!!!! Use magnetic latitudes
c
    open(10,file='DMSP.Data',status='old')
    do 40 i = 1, 100
    read(10,*) xmlats(i), xdens(i)
40    continue
    close(10)

c smooth 3-wise
    sdens(1) = xdens(1)
    sdens(100) = xdens(100)
    do 50 i = 2, 99
    sdens(i) = (2.0*xdens(i) + xdens(i-1) + xdens(i+1))/4.0
50    continue

c derive the north and south middle-latitude average
c the equator/trough value and the values of any crests
    nnorth = 0
    nsouth = 0
    sumnorth = 0.0
    sumsouth = 0.0
    xeq = 1.0e12
    crnorth = 0.0
    crsouth = 0.0
    do 60 i = 2, 99
    if(abs(xmlats(i)).le.6.0)then
        if(sdens(i).lt.xeq) xeq = sdens(i)
    endif
    if(abs(xmlats(i)).gt.10.0.and.abs(xmlats(i)).lt.20.0)then
        if(sdens(i).gt.sdens(i-1).and.sdens(i).gt.sdens(i+1))then
            if(sdens(i).gt.crnorth.and.xmlats(i).gt.0.)then
                crnorth = sdens(i)
            endif
            if(sdens(i).gt.crsouth.and.xmlats(i).gt.0.)then
                crsouth = sdens(i)
            endif
        endif
    endif

```

```

endif
endif
endif
if(xmlats(i).ge.15.0.and.xmlats(i).le.35.0)then
    nnorth = nnorth + 1
    sumnorth = sumnorth + sdens(i)
endif
if(xmlats(i).le.-15.0.and.xmlats(i).ge.-35.0)then
    nsouth = nsouth + 1
    sumsouth = sumsouth + sdens(i)
endif
60 continue

i1 = 0
i2 = 0
c can the equator/wing ratio be done ??
if(xeq.lt.1.0)then
    write(0,*)' No Equator Data '
    goto 10000
endif
if(nnorth+nsouth.eq.0)then
    write(0,*)' No Wing Data ',nnorth+nsouth
    goto 1000
endif
xwing = (sumnorth+sumsouth)/(nnorth+nsouth)
Ratio2 = xeq/xwing

c OK, Critical effective drift is
DriftCrit = final(1)
EffDrift2a = (Ratio2 - final(4))/ final(5)
EffDrift2b = (Ratio2 - final(6))/ final(7)
if(EffDrift2a.lt.0.or.EffDrift2a.gt.2.
1 or.EffDrift2a.gt.DriftCrit)then
    EffDrift2 = EffDrift2b
else if(EffDrift2b.lt.0.or.EffDrift2b.gt.2.
1 or.EffDrift2b.lt.DriftCrit)then
    EffDrift2 = EffDrift2a
else
    EffDrift2 = (EffDrift2a+EffDrift2b)/2.0
endif
i2 = 1

1000 continue
c can the equator/crest ratio be done ??
if(crnorth.lt.1.0.or.crsouth.lt.1.0.or.ilevel.eq.1)then
    write(0,*)' Not 2 crests, or solar min '
    goto 2000
endif
Ratio1 = xeq/((crnorth+crsouth)/2.0)

c so that, given Ratio1 = A0 + A1 * Scaling (Effective Drift)

Drift1 = (Ratio1 - final(2))/ final(3)
c this defines the drift velocity
c if we're at solar max, this is the Effective Drift
c if not at solar min, scale up the effective drift factor accordingly
c The correction has two parts:
c 1. Annual, a 1st order Fourier
c 2. Solar activity, a gradual scaling from min to max
c (chosen to be zero at min, and 1 at max)
c
factor = 1.0
if(ilevel.gt.1)then
    scale = acos(-1.0)/6.0
    xmon = float(Month)
    factor = 3.0-0.335*sin(xmon*scale)+1.417*cos(xmon*scale)

```

```

        solfactor = (f10p7-100.0)/70.0
        if(solfactor.gt.1.0)solfactor=1.0
        factor = factor * solfactor
    endif
    EffDrift1 = Drift1 * factor
    i1 = 1

2000    continue

c the average of any available value is thus
    EffDrift = (i1 * EffDrift1 + i2 * EffDrift2)/(i1+i2)
    if(EffDrift.lt.0.0) EffDrift = 0.0
    if(EffDrift.gt.2.0) EffDrift = 2.0

c
c finally, write the derived effective drift to file, for use by drivewind
c
    open(unit=10,file='Drift.Eff',status='old')
    read(10,*) EffDrift
    close(10)

10000    continue

c all finished
    stop
    end

```